**Defining the Role of the Hexosamine Biosynthesis Pathway in Pancreatic Cancer**

by

Peter K. Kim

A dissertation submitted in partial fulfillment
of the requirements for the degree of
Doctor of Philosophy
(Cancer Biology)
in the University of Michigan
2023

Doctoral Committee:

Professor Marina Pasca di Magliano, Chair
Associate Professor Benjamin L. Allen
Professor David B. Lombard
Associate Professor Costas A. Lyssiotis

Peter K. Kim

petekkim@umich.edu

ORCID iD:

0000-0001-9382-7223

## Dedication

To my family, for all the support and love you have given me.

To friends, peers, and professors from the University of Michigan, for shaping me into the scientist I am today and making science fun.

**Acknowledgments**

To my mentors Costas Lyssiotis and David Lombard, thank you for your unwavering support and patience. Thank you for creating an engaging and enjoyable work environment. Thank you for your patience and understanding during stressful moments. I would not be the scientist I am today without your amazing mentorship.

To my thesis committee members Marina Pasca di Magliano and Ben Allen, thank you for your continued guidance and support. Your help and advice were invaluable in my research and career.

To all the members of PanTERA, thank you for creating a collaborative and supportive environment. It was unlike anything I have experienced. You have helped me realize just how important collaboration and camaraderie are in science.

To the Cancer Biology Program faculty, students, and staff, thank you for being so readily available and helpful. My time at the University of Michigan would not have been so fun and fulfilling without you.

Finally, to my family, I am forever grateful for your love and support. Words cannot describe how much you mean to me.

## Table of Contents

## List of Figures

## Abstract

Metabolic rewiring is a hallmark of pancreatic ductal adenocarcinomas (PDA), a lethal disease that is notoriously resistant to therapies. This is due in part to the tumor microenvironment, which is largely composed of a dense fibrotic stroma and extracellular matrix. Hyaluronic acid (HA), a linear, carbohydrate polymer and a key component of the extracellular matrix, is a major contributor to the elevated interstitial pressure, resulting in vascular collapse that impedes drug delivery and creates an aberrant nutrient landscape. To survive and proliferate in this environment, pancreatic cancer cells rewire their metabolism and scavenge from the tumor microenvironment. Nearly all pancreatic tumors harbor mutations in oncogenic Kras, which increases the glycolytic flux into the hexosamine biosynthetic pathway (HBP). As such, the HBP potentially represents a metabolic vulnerability that could reveal novel targets for disease treatment.

The underlying goal of this thesis is to define the role of HBP in pancreatic cancer. This dissertation provides a comprehensive review on pancreatic cancer metabolism, tumor microenvironment, and the role of HBP in other cancers (Chapter 1). Testing for PDA dependence on the HBP revealed HA as a novel nutrient source that fuels the HBP via the *N*-acetyl-glucosamine salvage pathway (Chapter 2).

Furthermore, future work stemming from preliminary findings will investigate whether inhibition of cell-intrinsic HBP is sufficient to sensitize pancreatic cancer to anti-PD-(L)1 therapy, an immune checkpoint blockade immunotherapy that has not been successful in PDA, despite demonstrating revolutionary success in other cancers (Chapter 3). Finally, this dissertation

proposes several future directions: the elucidation of the GlcNAc salvage pathway in more physiologically relevant models, further mechanistic delineation of HA fueling the HBP, and testing whether other non-cancerous cells populating the tumor microenvironment and components of the extracellular matrix can regulate the HBP in cancer cells (Chapter 4).

# Chapter 1

## Introduction: Pancreatic Cancer, Altered Metabolism, and the Role of the Tumor Microenvironment

### 1.1 Disease Overview

Pancreatic ductal adenocarcinoma (PDA), the most common form of pancreatic cancer, is one of the deadliest solid cancers despite its relatively rare diagnosis[1]. In the United States in 2023, PDA is the third leading cause of cancer-related deaths despite being the eleventh most commonly diagnosed cancer. At 12%, the five-year survival rate for PDA is the lowest among major cancer types, with a median survival of approximately nine months for late stage patients[2]. Although the five-year survival rate of patients gradually improved since the 1970s (2.5%), PDA is slated to become the second leading cause of cancer-related mortalities by 2030[3]. This clinical reality for PDA is in stark contrast to other major cancers such as melanoma, breast, and lung cancer, which have benefited significantly from breakthroughs in screening, early detection, or novel therapies.

Several challenges underlie the extremely poor outcome of PDA. First, the location of the pancreas, deep in the abdomen, and the lack of symptoms in the early stage of the disease make early detection difficult. Second, PDA is aggressive and metastasizes early, resulting in 80-85% of patients being diagnosed when the disease is locally advanced or metastatic[4]. This leads to 10-20% of patients being eligible for surgical resection, which is currently the only potentially curative option. However, approximately 80% of these patients will ultimately relapse and die post-surgery. Third, PDA severely weakens patients and limits their ability to tolerate aggressive treatments. While increasing the overall survival is paramount, quality of life for

patients is an important factor to be considered when designing new treatment strategies. Finally, there are currently no effective treatment options for PDA. For most patients, chemotherapy is the primary treatment modality, and despite the ongoing effort to optimize adjuvant and neo-adjuvant approaches, patients' overall median survival has only increased by several months[4]. The lack of reliable molecular and genetic biomarkers represents a roadblock for optimally stratifying and guiding treatment options for patients. Numerous cell-intrinsic and cell-extrinsic factors contribute to therapeutic resistance, which will be discussed later in this chapter.

### 1.2 Risk Factors

PDA is associated with several significant environmental risk factors including age, tobacco consumption, chronic pancreatitis, and type 2 diabetes mellitus. Most patients are diagnosed after 50, and 70% are older than 65 years of age[1]. Tobacco smokers are two- to three-times more likely to develop PDA compared to non-smokers[5]. Smokeless tobacco consumption is another preventable risk factor[6]. Multiple studies link low physical activity, obesity, and "Western diet" – high intake of saturated fat and processed red meat, and low intake of fruits and vegetables – to PDA[7-10]. Chronic pancreatitis, which can be caused by heavy alcohol consumption, increases the risk by more than ten-fold[11]. Long-term diabetes mellitus almost doubles the risk of PDA, but it can also be caused by pancreatic cancer at early stages[12]. This sporadic onset of pancreatic cancer-associated diabetes mellitus, known as type 3c diabetes mellitus, can potentially be used for early PDA diagnosis[13].

PDA has several genetic risk factors which, combined with the environmental risk factors, can potentially provide in-roads for early screening and prevention. A family history of PDA lacking germline mutations and genetic syndromes with known germline mutations account for 7% and 3% of patients, respecitvely[14]. An example of such genetic syndrome is familial atypical multiple mole melanoma syndrome, which is caused by a germline mutation in cyclin-dependent

kinase inhibitor 2A. Familial atypical multiple mole melanoma syndrome increases PDA risk by 13-fold[15]. Other germline mutations of interest include genes involved in DNA damage response (*BRCA1*, *BRCA2, PALB2, FANCC, FANCG*, and *ATM).* Patients with inherited mutations in these genes are high-risk and are monitored for screening. While identifying and screening high-risk patient groups is an attractive strategy, 90% of patients lack a familial basis. Therefore, reliable biomarkers are critical to improve early diagnosis and prevention.

**1.3 Biomarkers and Early Detection**

Late-stage diagnosis, which occurs in over 80% of patients, is one of the major driving forces behind PDA lethality. PDA can take over 10 years to metastasize, providing a potential window for early detection[16]. Thus, sensitive and specific biomarkers that can detect early stage pancreatic cancer, as well as accurately measure therapy response will be instrumental in the fight against PDA.

Serum cancer antigen 19-9 (CA 19-9) is the only biomarker approved by the U.S. Food and Administration for PDA management[17]. However, CA 19-9 is not an optimal marker for several reasons. CA 19-9 is ineffective in early detection or screening asymptomatic patients because of its low positive predictive value[18]. 5-10% of the population lacks 1,4-fucosyl transferase, an enzyme necessary for synthesizing CA 19-9[19]. Furthermore, different types of cancers, as well as benign diseases such as pancreatitis and jaundice, can elevate CA 19-9 serum level[20]. Despite these limitations, CA 19-9 is used in the clinic for monitoring treatment response and detecting possible tumor recurrence.

Novel strategies to finding more specific and sensitive biomarkers are areas of active investigations. These alternative approaches involve identifying and analyzing dysregulated miRNAs[21-23], exosomes[24,25], and circulating tumor DNA[26-28]. These tools can potentially complement or replace CA 19-9 in the future to improve early detection and treatment response.

All three approaches have their advantages, but they also have obstacles that must be addressed. While miRNAs are stable in blood, they are hard to accurately detect because they are small molecules that can be protein-bound or can be incorporated into vesicles. Isolating cancer exosomes from patients is difficult and time-consuming because of the lack of markers that can distinguish cancer from non-cancer exosomes. Similarly, identification and isolation of circular tumor DNA from circulating tumor cells remain as major challenges. Finally, all these studies require further validation in larger cohorts before they are ready for application.

### 1.4 The Therapeutic Landscape

The lack of effective therapies is a major obstacle to improving overall survival. In 2023, the five-year overall survival is at 12%[2]. A cure would require an accurate early detection of pre-invasive PDA and surgery, but the majority of PDA patients are diagnosed at advanced stages. Only 10-20% of patients have a resectable disease and are therefore eligible for surgeries such as Whipple procedure and distal pancreatectomy, which removes the tumors in pancreatic head and tail, respectively. For these particular patients, recent progress in chemotherapy regimens have resulted in improved outcomes[29]. For these reasons, surgery, when eligible, is the best option, and is associated with a five-year survival rate of 20%[1]. For the vast majority of patients diagnosed with advanced or metastatic PDA, cytotoxic chemotherapies are the primary treatment option. Currently, the standard of care is a chemotherapy cocktail consisting of 5-fluoracil, leucovorin, irinotecan, and oxaliplatin (FOLFIRINOX), which has led to a median overall survival of approximately 1 year. It is important to note that chemotherapy modestly increases survival by a few months.

A critical gap exists between the current understanding of PDA biology and translating it into the clinic to improve survival and quality of life. Compared to other tumor types, recent multiple large-scale phase III trials have been unsuccessful for PDA[30-32]. Major therapeutic challenges include a desmoplastic stroma that impedes drug delivery, an immunosuppressive

tumor microenvironment, and intratumoral crosstalk amongst different non-cancer and cancer cells that can contribute to chemotherapy resistance. Despite these challenges, there have been recent, promising leads in targeted therapy and immune therapy, which may inform future treatment options.

**Targeted Therapy**

The genomic landscape of PDA has been known for many years due to several large-scale genomics efforts and next-generation sequencing studies from resected PDA tumors[33,34]. Notably, oncogenic *KRAS* mutations occur in over 90% of human PDA cases, with different incidence rate of mutated sites: G12D (41%), G12V (34%), G12R (16%), Q61H (4%), and G12C (1%)[35]. Despite the high frequency, targeting mutant KRAS isoforms has been notoriously challenging due to their high affinity to GDP and GTP substrates[36].

Recent advances in drug development have led to allele-specific mutant KRAS inhibitors. The first iteration was ARS-1620, which covalently binds to the GDP-bound, inactive $KRAS^{G12C}$, preventing its activation[37]. Although the $KRAS^{G12C}$ mutation constitutes approximately 1% of PDA cases, ARS-1620 became the first, pre-clinical, proof-of-concept evidence for mutant-specific KRAS inhibition. Identification of a pocket in $KRAS^{G12C}$ (H95/Y96/Q99) by X-ray crystallography studies led to the development of the first potent clinical-grade $KRAS^{G12C}$ inhibitor, AMG-510 (Sotorasib)[37,38]. In 2021, Sotorasib became the first FDA fast track-approved RAS inhibitor after demonstrating durable clinical benefits[39]. In 2022, MRTX1133, a small molecule inhibitor specific for $KRAS^{G12D}$, has demonstrated tumor regression in xenograft and patient-derived xenograft models[40]. $KRAS^{G12D}$ inhibitors have the potential to make a significant impact on PDA treatment because it is the most common mutant KRAS in human PDA.

Approaches beyond allele-selective KRAS inhibition are being actively investigated. RMC-6236, which forms a complex with active KRAS to prevent downstream signaling,

demonstrated anti-tumor effects across *KRAS* genotypes in a preclinical setting[41]. BI-3406 is a selective oral small molecule that targets SOS1, a key nucleotide exchange factor for KRAS. Across *KRAS*-driven cancer models, BI-3406 significantly reduced tumor growth[42]. It is currently undergoing a phase I clinical trial in advanced *KRAS*-mutated solid tumors as a single agent or in combination with MEK inhibitor trametinib (NCT04111458). Several groups employed the same lipid nanoparticle-encapsulated mRNA vaccine strategy against SARS-CoV-2 to develop vaccine targeting the four major KRAS mutations. Currently, there are two phase I clinical trials ongoing (NCT03948763 and NCT03608631).

Although there have been encouraging results, especially in the last five years, it is important to elucidate the compensatory mechanisms that decrease the efficacy of KRAS inhibition. In pre-clinical settings, increased EGFR and AURKA signaling led to ARS-1620 resistance[43]. Clinical acquired mutations that led to $KRAS^{G12C}$ inhibition were also identified[44]. Future clinical trials involving KRAS small molecule inhibitors should apply the combination therapy approach to target escape pathways.

**Immune Therapy**

Cancer immunotherapy has revolutionized cancer treatment, significantly improving patient overall survival and quality of life. A major aspect of immunotherapy arose from understanding immune surveillance, in which innate immune cells recognize and eliminate cancer cells. Here, we refer to immunotherapy as immune checkpoint blockade, although other therapeutic modalities exist. T cell immune checkpoints, PD-1 and CTLA-4, maintain the fine balance between immune surveillance against foreign abnormal cells, such as cancer cells, and autoimmunity. Immune checkpoint blockade therapies, notably monoclonal antibodies targeting PD-1/PD-L1 and CTLA4, have made significant impacts in cancer treatment across numerous solid tumors, such as melanoma, lung cancer, and renal cell carcinoma[45]. However, these established immune checkpoint inhibitors have been ineffective in PDA[46,47].

PDA has been resistant to immunotherapy for several reasons. A high mutational burden can promote cancer neoantigen formation, facilitating tumor-specific killing by $CD8^+$ T cells[48]. PDA has a low tumor mutation burden compared to response solid tumors. The most significant challenge for effective immunotherapy is the tumor microenvironment. The dense fibrotic stroma acts as a physical barrier to cytotoxic T cells, and stromal cells secrete factors that inhibit $CD8^+$ T cell function and survival. Other immunosuppressive cells, such as regulatory T cells and myeloid derived suppressor cells, present further challenges for eliciting $CD8^+$ T cell-mediated anti-tumor response.

Despite the major challenges conferred by the low immunogenicity and the profound, immunosuppressive microenvironment, there have been some encouraging results that can be instructional to shaping immunotherapy approach in PDA patients. Several studies reported that patients with microsatellite instability high status demonstrated prolonged survival rate[49]. One possible explanation for this is that tumors high in microsatellite instability are typically more likely to have high mutational burden[50]. Several clinical trials are currently testing whether high microsatellite instability status can act as a valid predictor of response to immunotherapy[51]. Recent efforts are focused on overcoming immunotherapy resistance by employing combination therapy with immunotherapy and cytotoxic approaches.

### 1.5 The Tumor Microenvironment

The tumor microenvironment (TME) is an integral component of tumors, which are pseudo-organs that exhibit unique pathophysiology. A hallmark of PDA is a desmoplastic reaction that is present in both primary and metastatic tumors. Pancreatic tumors have a low percentage of neoplastic cells. The majority of the tumor bulk content consists of fibroblasts and immune cells[52]. Activated fibroblasts deposit a significant amount of extracellular matrix, causing immense interstitial pressure that results in vasculature collapse, impaired perfusion, hypoxia, and aberrant nutrient availability. Elucidating the role of the TME in tumorigenesis and therapy

resistance is critical to identifying and improving novel therapeutic strategies and targets. Here, we briefly describe the major cell populations of the TME that impact tumor phenotype and therapeutic resistance (**Fig. 1-1**).

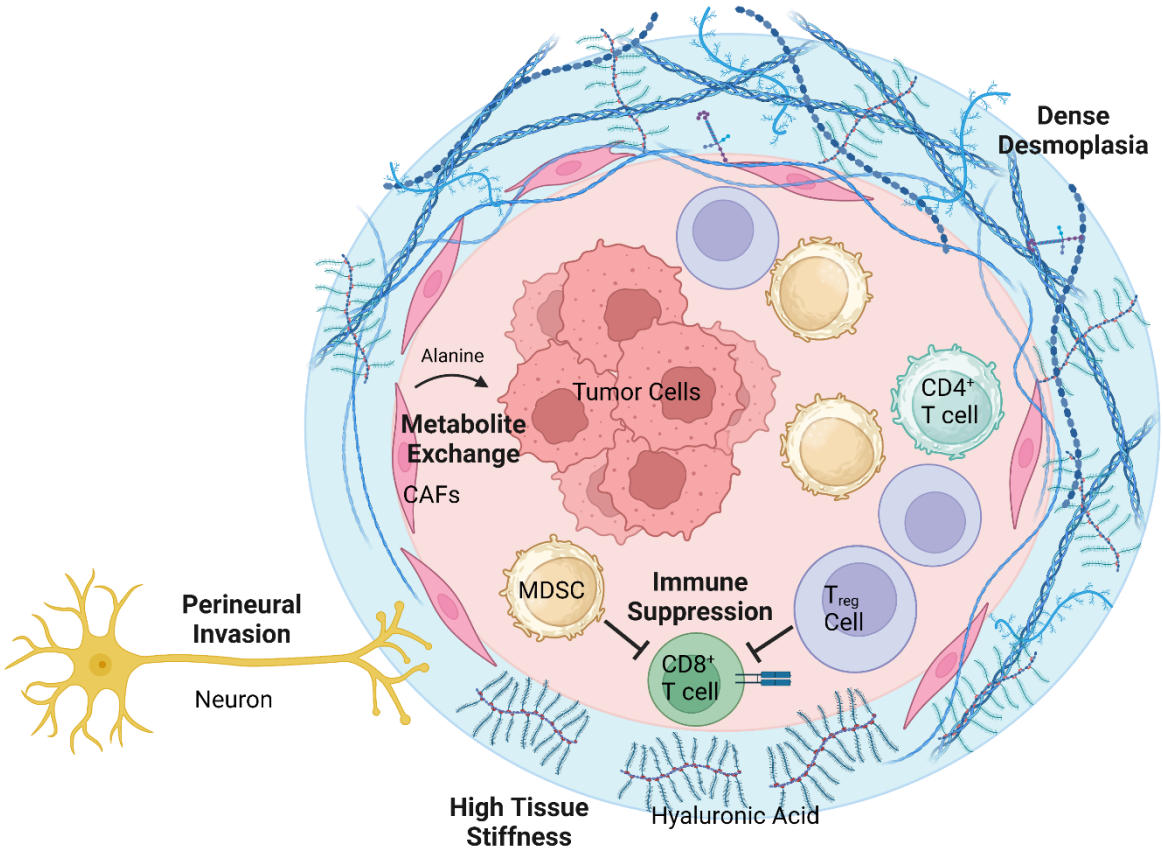


**Figure 1-1 Key characteristics of the pancreatic tumor microenvironment represent therapeutic challenges.**

The pancreatic tumor microenvironment presents a therapeutic obstacle for PDA treatment. The dense desmoplasia and high tissue stiffness caused mainly by hyaluronic acid impede drug delivery. Perineural invasion is high in PDA, and studies done in genetically engineered mouse models point to their direct role in promoting tumorigenesis. The vast majority of the total cellularity in the tumor microenvironment is not cancer cells. Instead, they consist of cancer associated fibroblasts (CAFs) and immune cells. The supraphysiological intratumoral pressure caused by hyaluronic acid and the dense stroma leads to metabolic rewiring within cancer cells. Cancer cells scavenge from the tumor microenvironment to meet their metabolic demands. For example, CAFs provide the metabolite alanine to cancer cells to support their anabolism. Immune cells such as myeloid-derived suppressor cells (MDSC), regulatory T cells ($T_{reg}$), and $CD4^+$ T cells suppress anti-tumor $CD8^+$ T cells. Furthermore, the lack of infiltration by $CD8^+$ T cells is a notable feature of PDA.

Leukocytes

Leukocyte infiltrate in human PDA is remarkably heterogenous, both functionally and spatially, and include multiple subsets of T cells, NK cells, B cells, macrophages, neutrophils, and other granulocytes[53,54]. These different cell types impact PDA biology in a context-dependent manner. For example, regulatory T cells, which are well-established as immunosuppressive cells, reduced vaccine efficacy in a mouse model[55]. However, depleting regulatory T cells failed to relieve immunosuppression, and instead, led to inflammatory fibroblast differentiation, myeloid cell infiltration, and disease progression[56]. $CD4^+$ T cells blocked the activity of anti-tumor $CD8^+$ T cells to contribute to carcinogenesis in mice[57]. Myeloid cells are more often associated with having tumor-supporting activities, enabling tumor growth, survival, metastasis, and immune evasion[58,59]. However, myeloid cells can have antitumor roles, such as enhancing chemotherapy efficacy by degrading fibrosis, and contributing to productive T cell immunity[60,61]. Elucidating the various spatial, functional, and microenvironmental contexts will be critical to improving immune therapy strategies.

Peripheral nerves

Autonomic innervation is a critical regulator of hormone secretion by pancreas[62]. As such, the normal pancreas is highly innervated. During tumorigenesis, innervation significantly increases, a phenomenon called perineural invasion (PNI). PNI incidence is particularly high in PDA (>80%) compared to other tumor types[63]. Furthermore, a recent analysis of long-term survivors who underwent surgical resection identified absence of PNI as the only favorable predictor of survival greater than 5 years[64].

PNI is also observed in genetically engineered mouse models. The neuroplastic changes and PNI occur as early as premalignant lesions[65]. In invasive PDA, the large nerve bundles were located near cancer cells and vasculature. Another study demonstrated that

sensory denervation led to a decrease in neoplastic, neuroendocrine cell population and impaired tumorigenesis[66]. These studies suggest that the peripheral nerves in the TME may play a direct role in disease progression. Interestingly, a recent study suggests that neurons may be involved in a metabolic cross-talk with cancer cells[67]. The group demonstrated that in a nutrient-deprived environment, neurons secrete amino acids, such as serine, to support growth and survival *in vitro.*

The studies above point to the complex and functionally heterogeneous nature of nerves found in different stages of PDA. Further investigation in elucidating these questions can reveal new therapeutic targets and strategies.

Cancer-associated fibroblasts

Cancer-associated fibroblasts (CAFs) play a critical role in development, homeostasis, and tumorigenesis. Spatial heterogeneity of CAFs suggests distinct functional roles based on their proximity to cancer cells[68,69]. CAFs that are near cancer cells exhibit a classically activated, myofibroblast-like phenotype. CAFs in the surrounding stromal tissue display an inflammatory phenotype. While single-cell genomics was instrumental in identifying different CAF subtypes, their precise functions and effects of their transcriptional programs on PDA remain areas of active investigation.

A well-characterized role of CAFs is the deposition of extracellular matrix, which has been demonstrated to have both tumor supporting and suppressive roles. Major components of the extracellular matrix include proteoglycans and hyaluronic acid. Hyaluronic acid is one of the major drivers of the supraphysiological interstitial pressure that impedes drug delivery and creates a nutrient-aberrant environment[70]. Another factor hindering drug delivery is the hypovascular nature of PDA. More specifically, PDA vascularization is characterized by a

heterogeneous distribution of high microvascular density, but with impaired integrity and poor perfusion[71].

Extracellular Matrix

The extracellular matrix (ECM), which is present in all tissues, is a non-cellular component that provides biochemical and biomechanical cues, and the essential physical scaffolding to the surrounding cellular components. In many cancers, malignant cell transformation can change the ECM architecture[72-74].

A key characteristic of PDA that is thought to contribute to therapy resistance is the dense fibrotic stroma intertwined with the ECM. The PDA ECM is primarily composed of collagens, hyaluronic acid, integrins, proteoglycans, glycoproteins, and proteases[75]. Numerous pre-clinical studies have identified the dichotomous role of the ECM in PDA. Tumor-promoting roles may include integrin, TGFβ/SMAD, DDR-1 signaling, and collagens as a nutrient source for cancer cells[76-78]. Tumor-suppressive roles may include providing a barrier against metastases and restraining tumor growth[79,80]. Elucidating how the tumor stroma and ECM interact with PDA cells and other non-cancerous cell populations in the tumor microenvironment is an area of active investigation, and has the potential to reveal new targets for therapy.

### 1.6 Metabolic Adaptations

#### The Warburg Effect

Deregulated metabolism is a hallmark of cancer, and elucidating it can reveal potential metabolic vulnerabilities that can be leveraged therapeutically[81]. Proliferating cells such as cancer cells require different metabolic requirements than those of quiescent, differentiated cells. Although the need for ATP generation is similar, cancer cells require an ample supply of nutrients to generate biosynthetic precursors to sustain their growth and proliferation.

A well-established phenomenon of cancer metabolism is a process known as aerobic glycolysis or the Warburg Effect[82]. In most non-transformed cells, glucose, a major carbon source, is broken down to pyruvate via glycolysis. Pyruvate fuels the tricarboxylic acid (TCA) cycle and oxidative phosphorylation to generate ATP. If oxygen levels are not sufficient to maintain oxidative phosphorylation, fermentation occurs, converting pyruvate to lactate. In contrast, cancer cells, driven by oncogenes, convert glucose to lactate despite having sufficient oxygen levels. This process is called the Warburg Effect, and this metabolic phenotype is found in approximately 80% of human cancers[83].

A complex interplay amongst several factors can contribute to metabolic rewiring – oncogene activation, loss of tumor suppressors, altered signaling pathways, interaction with the components of tumor microenvironment, and hypoxia. Here, we summarize these factors in the context of PDA, and discuss the reprogrammed metabolism of key nutrients and scavenging pathways PDA employs to fuel its anabolism (**Fig**. **1-2**).

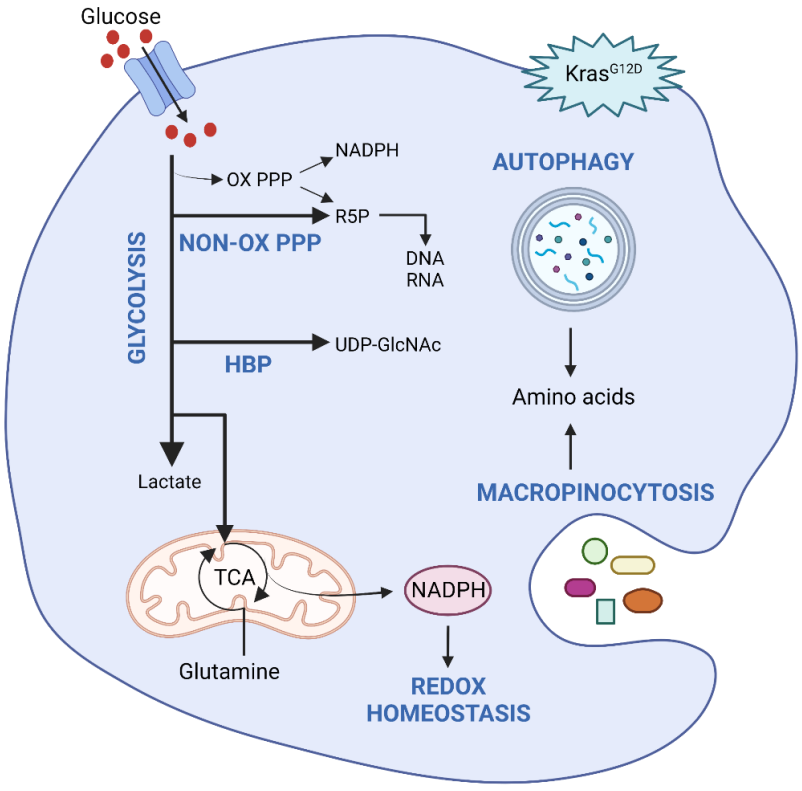

**Figure 1-2 Mutant KRAS-mediated metabolic reprogramming in pancreatic cancer supports proliferation and survival.**

Mutant KRAS ($Kras^{G12D}$) increases glucose uptake and flux into the non-oxidative branch of the pentose phosphate pathway (Non-ox PPP) and the hexosamine biosynthetic pathway (HBP) to generate ribose-5-phosphate (R5P) and UDP-GlcNAc, respectively. R5P is the precursor molecule to RNA and DNA synthesis. Mutant KRAS reprograms glutamine metabolism to generate NADPH to maintain redox homeostasis. Pancreatic cancer cells employ macropinocytosis and autophagy for acquisition of amino acids to support growth and proliferation.

## Pancreatic Cancer Metabolism

Pancreatic cancer metabolism is influenced by key genetic alterations and the tumor microenvironment (TME). Oncogenic *KRAS* leads to increased glucose uptake and flux through anabolic pathways, glutamine reprogramming, and reactive oxygen species regulation[84]. In mouse models, oncogenic *KRAS* upregulates cytokines and promotes immune cell infiltration, leading to tumor metabolic reprogramming[85]. The tumor suppressor *TP53*, which is frequently mutated in PDA, induces autophagy and controls ROS to affect metabolism[86]. *MYC*, a transcription factor that is frequently amplified, is a master regulator of metabolic processes and contributes to tumorigenesis via intrinsic and extrinsic factors[87,88]. *PTEN*, a tumor suppressor that is commonly deleted, regulates the PI3K-AKT pathway, which regulates redox control, glucose metabolism, and de novo lipid synthesis[89]. In multiplate mouse models, PTEN deletion cooperates with mutant KRAS to promote PDA tumorigenesis[90-92]. Furthermore, as previously stated, the supraphysiological intratumoral pressure imparted by the stromal desmoplasia leads to hypoxia and aberrant nutrient levels in the TME. To survive and proliferate in this austere environment, cancer cells rewire their cell-intrinsic metabolism. Below, we discuss the reprogrammed fuel source metabolism and lysosomal nutrient scavenging that cancer cells utilize to meet their anabolic demands.

### Glucose

Glucose, a major source of energy for cells, is in high demand for cancer cells. PDA cells, mediated by oncogenic KRAS, increase glucose uptake and flux through glycolysis by

upregulating glucose transporter GLUT1 and hexokinase[93]. The KRAS4A isoform also contributes to the increased glycolytic flux *in vitro* and *in vivo* by directly interacting with hexokinase 1[94]. Furthermore, glucose is diverted from glycolysis into side branches to generate key precursors for biomass[84]. Examples of these branching metabolic pathways include the pentose phosphate pathway (PPP) and the hexosamine biosynthetic pathway (HBP). PPP is responsible for production of the cofactor NADPH and ribose-5-phosphate. NADPH combats oxidate stress and is required for fatty acid synthesis. Ribose-5-phosphate is an essential intermediate for ribose synthesis. The HBP is the only de novo pathway to synthesize uridine diphosphate-*N*-acetylglucosamine, a key substrate for two essential post-translational modifications – glycosylation and O-GlcNAcylation. The glycolytic intermediates can feed into the serine, glycine, and one-carbon metabolism, supporting nucleotide and lipid syntheses.

Glutamine

Glutamine, a non-essential amino acid, is found in high levels in human plasma and has numerous roles in cellular metabolism[95]. Cancer cells use precursors from the TCA cycle to support growth and proliferation. Glutamine can enter the TCA cycle by glutaminolysis, and the glutamine carbon skeleton is an important contributor to TCA cycle intermediates. In addition, mitochondrial glutamine metabolism is important for maintaining mitochondrial integrity and functions.

Glutamine has important biosynthetic roles outside of the TCA cycle. The amine portion of glutamine is a nitrogen donor for synthesizing other amino acids and hexosamines. Glutamine is a required substrate for *de novo* synthesis of purines and pyrimidines. Importantly, glutamine contributes to production of glutathione and NADPH to regulate redox homeostasis, which is important for tumorigenesis and proliferation[96,97].

In PDA, glutamine regulates redox homeostasis via a non-canonical pathway[98]. Canonically, most cells fuel the TCA cycle by using glutamate dehydrogenase to convert glutamine-derived glutamate to α-ketoglutarate in the mitochondria. In PDA cells, mitochondrial aspartate aminotransferase (GOT2) converts glutamate into α-ketoglutarate and aspartate. Aspartate is transported to the cytoplasm and is metabolized by cytosolic GOT1, malate dehydrogenase 1 (MDH1), and malic enzyme 1 (ME1). These metabolic reactions ultimately result in pyruvate and NADPH formation. Indeed, glutamine deprivation or genetic inhibition of any enzyme on this non-canonical pathway led to an increase in reactive oxygen species. Importantly, this non-canonical pathway was Kras-regulated, and knockdown of any of these enzymes led to a significant decrease in PDA growth *in vitro* and *in vivo*[98]. Further studies targeting enzymes involved in glutamine metabolism – mitochondrial uncoupling protein 2, glutamate ammonia ligase, and a novel variant of glutamine transporter SLC1A5 – reinforced the concept that glutamine metabolism is an attractive therapeutic target[99-101].

Despite the promising results listed above, the pleiotropic effects of glutamine metabolism and the rapid compensatory metabolic rewiring offer challenges that necessitate further investigation. For instance, glutamine deprivation led to induction of epithelial-mesenchymal transition *in vitro* and *in vivo*[102]. Clinal-grade inhibitors of glutaminase, which converts glutamine to glutamate, lost its efficacy in prolonged *in vitro* treatment and *in vivo*[103]. An integrated metabolic and proteomic platform revealed rapid metabolic rewiring upon glutaminase treatment. The group observed impaired tumor growth in a nude mouse model, only after identifying a potential adaptive response and designing rational combinatorial approaches[103]. Clinical studies testing the efficacy of 6-diazo-5-oxo-L-norleucine (DON), which broadly inhibits glutamine-requiring metabolic reactions, failed due to gastrointestinal toxicities[104]. In summary, it will be critical to functionally and mechanistically delineate the numerous aspects of PDA glutamine metabolism to translate the preclinical findings into therapy.

Cysteine

Cysteine is an important amino acid for PDA progression[105]. Cystine, the oxidized dimer of cysteine, is a precursor for generation of glutathione, a major antioxidant mechanism against ROS. Cells uptake cystine through system xCT, and genetically ablating xCT led to PDA cell death via ferroptosis[106]. Ferroptosis is initiated by a failure of antioxidant defenses that rely on glutathione, ultimately resulting in excessive accumulation of lipid ROS[107].

Further investigation using genetically engineered mouse models provided promising evidence for targeting cysteine metabolism in PDA. Deletion of the xCT subunit, *Slc7a11*, induced ferroptosis in PDA and impaired tumor growth in mice[108]. Importantly, the phenotype was replicated using cyst(e)inase, an experimental drug that depletes cysteine and cystine in blood[108,109]. The clinical development of cyst(e)inase for treating cystinuria, a metabolic disorder, offers a pathway for testing this concept in human PDA. If successful, potential combination therapies that amplify the anti-tumor effect of cyst(e)inase should be investigated.

Macroautophagy

Macroautophagy (referred to as autophagy henceforth) maintains survival and cellular homeostasis during time of stress or starvation. This highly conserved, catabolic process involves sequestration of damaged organelles and macromolecules, targeting them to lysosomal degradation to provide building blocks for cancer cells.

Several studies have demonstrated the importance of autophagy for PDA tumorigenesis. PDA has an elevated level of basal autophagy, and genetic and pharmacological inhibition of autophagy decreased PDA cell proliferation and impaired tumor growth[110]. These results were recapitulated in autochthonous models and other genetically engineered mouse models that utilized Cre-Lox and Dox-inducible systems to allow temporal and spatial control of autophagy activity[111-113]. Notably, autophagy was critical for PDA tumor maintenance through both cell-

intrinsic and cell-extrinsic mechanisms. These studies also reveal that the immune system plays an important role in the anti-tumor response by autophagy inhibition.

Importantly, autophagy plays a non-metabolic role that may provide avenues to enhance immunotherapy, which has not had much clinical success in PDA. Both human and murine PDA tumors and the metastatic lesions in the liver have decreased level of major histocompatibility complex class I (MHC-I)[114]. MHC-I is found on the cell surface of all nucleated cells. MHC-I plays an important role in eliciting an immune attack against cancer cells because they display peptide fragments to cytotoxic T cells. In 2020, a group demonstrated that in human and murine PDA, immune evasion is induced by MHC-I being selectively targeted via autophagy-dependent degradation involving the autophagy cargo receptor NBR1[115]. Autophagy inhibition led to increased anti-tumor T cell activation and infiltration, and synergized with dual immune checkpoint therapy in mice[115]. These findings provide further rationale for targeting autophagy in PDA.

Macropinocytosis

Macropinocytosis is a nutrient scavenging system that is induced by oncogenic *RAS*[116]. Macropinocytosis is a non-selective endocytic program that can uptake extracellular proteins, such as serum albumins which are degraded in the lysosome, to provide amino acids to fuel cancer metabolism. Along the same line, a group demonstrated that under nutrient-limiting conditions, PDA can uptake collagen, which is found in high levels in the stroma, as a source of proline to support survival[117]. These studies directly demonstrate the contribution of macropinocytosis to support PDA survival and growth[118].

Although there is not an effective pharmacological agent to inhibit macropinocytosis, several studies have identified molecular regulators, which may help further define the role of macropinocytosis under different nutrient and tumor contexts. Constitutive macropinocytosis

requires sequential activation of PI3K signaling pathway and the downstream effectors Rac1 and Cdc42[119]. A full-genome short interfering RNA screen identified vacuolar ATPase as a target of oncogenic *Ras*, and is required for macropinocytosis[120]. An unbiased functional proteomic screen identified the heparan sulfate proteoglycan syndecan-1 as a critical mediator of macropinocytosis that is important for tumor maintenance[121].

Taken together, these studies implicate macropinocytosis as a potential therapeutic target. As autophagy and macropinocytosis both converge on the lysosome, an important question to address would be the possibility of compensatory mechanisms when either pathway is inhibited. The coordination between these two important scavenging pathways that fuel PDA metabolism would need further elucidation, especially under different stress and tumor microenvironment contexts.

### 1.7 The Hexosamine Biosynthetic Pathway

The hexosamine biosynthetic pathway (HBP) is an evolutionarily conserved pathway that is up-regulated in PDA by the oncogenic KRAS (**Fig. 1-3**)[84]. The final product of the HBP is

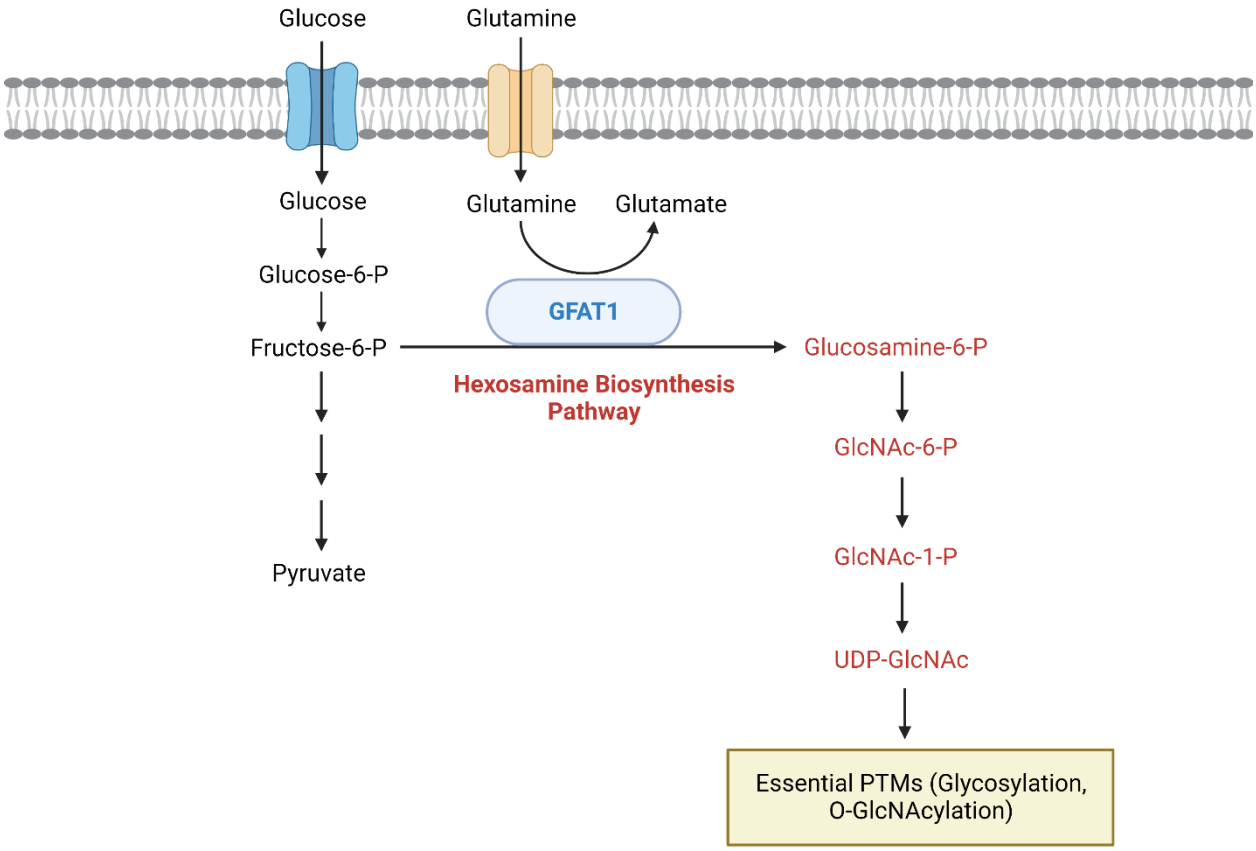


**Figure 1-3 The hexosamine biosynthetic pathway is up-regulated in pancreatic cancer.**

The hexosamine biosynthetic pathway is an evolutionarily conserved pathway that branches off of glycolysis. The first and rate-limiting enzyme is glutamine-fructose 6-phosphate amidotransferase 1 (GFAT1), which catalyzes the reaction that generates glucosamine-6-phosphate from fructose-6-phosphate and glutamine. The goal of the hexosamine biosynthetic pathway is the generation of uridine diphosphate *N*-acetylglucosamine (UDP-GlcNAc), a precursor for two essential post translational modifications (PTMs), glycosylation and O-GlcNAcylation. The hexosamine biosynthetic pathway is the only *de novo* pathway for UDP-GlcNAc generation.

uridine diphosphate N-acetylglucosamine (UDP-GlcNAc), which integrates glucose, glutamine, fatty acids, and nucleotide metabolism. Because the HBP incorporates major macromolecules to produce UDP-GlcNAc, the HBP is known as a sensor of energy availability. Furthermore, UDP-GlcNAc is a key precursor for glycosylation and O-GlcNAcylation, two essential post-translational modifications, which influence signaling, metabolism, gene regulation, and

epithelial to mesenchymal transition. Therefore, the HBP is at the center of numerous processes that are important in cancers, and defining the role of the HBP in PDA may reveal novel therapeutic strategies. Here, we discuss the HBP and the relevant pathways that lead to UDP-GlcNAc generation, the roles of O-GlcNAcylation and glycosylation in cancers, and the current efforts to target the HBP pharmacologically.

### Three Pathways to UDP-GlcNAc

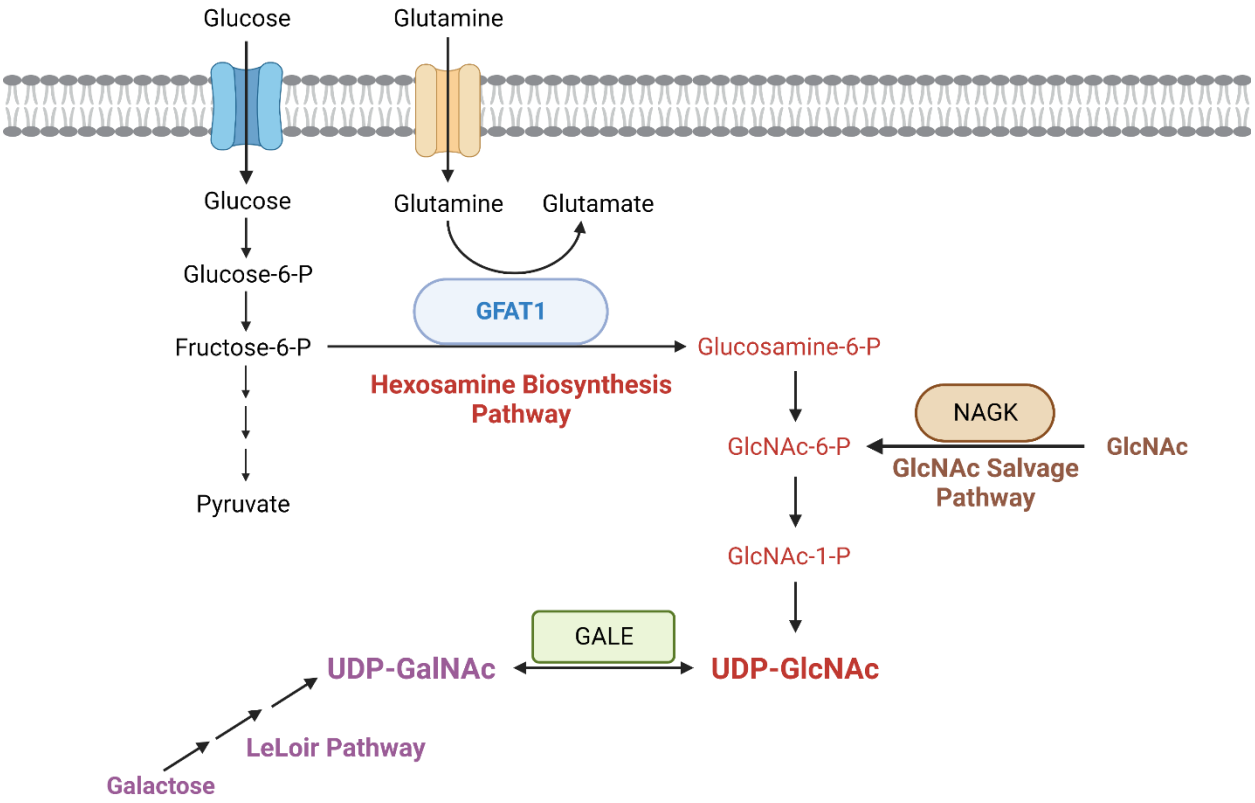


**Figure 1-4 The GlcNAc salvage pathway and the LeLoir pathway bypass the hexosamine biosynthesis pathway to generate UDP-GlcNAc.**

Two pathways feed into the hexosamine biosynthetic pathway, downstream of GFAT1 to generate UDP-GlcNAc. The first pathway is the GlcNAc salvage pathway, which is mediated by the enzyme NAGK. NAGK catalyzes the reaction that phosphorylate GlcNAc to generate GlcNAc-6-phsphate (GlcNAc-6-P), which is catalyzed to GlcNAc-1-phosphate (GlcNAc-1-P) before being converted to UDP-GlcNAc. The second pathway is the LeLoir pathway, which involves galactose metabolism. Galactose, through series of reactions, can be converted to UDP-GalNAc, which is epimerized by the enzyme GALE, to produce UDP-GlcNAc.

There are three characterized pathways to generate UDP-GlcNAc (**Fig. 1-4**). First, there is the *de novo* pathway in the HBP, which is mediated by the first and rate limiting enzyme glutamine-fructose 6-phosphate amidotransferase 1 (GFAT1). Second, there is the GlcNAc salvage pathway which bypasses GFAT1. The GlcNAc salvage pathway is mediated by the enzyme N-acetylglucosamine kinase (NAGK), catalyzing the phosphorylation of GlcNAc to GlcNAc-6-phosphate, which is subsequently converted to UDP-GlcNAc. The third and final pathway is the Leloir pathway, which bypasses both the HBP and GlcNAc salvage pathway. The Leloir pathway catalyzes reactions involving *N*-acetyl-galactosamine (GalNAc), an isomer of GlcNAc, to generate UDP-GalNAc. UDP-GalNAc is epimerized to UDP-GlcNAc by the third and final enzyme of the Leloir pathway. Elucidating the role of the HBP in PDA will require considering the potential compensatory effects via GlcNAc salvage pathway and Leloir's pathway.

**The HBP as a Cancer Therapy Target**

The role of HBP in sustaining growth and survival, and its upregulation in many cancers make it a promising anti-cancer target. Azaserine and 6-diazo-5-oxo-L-norleucine (DON), which is a glutamine analog, inhibited the HBP and demonstrated anti-tumor activity *in vitro* and *in vivo* in different cancer models[84,122-125]. However, these approaches have drawbacks because azaserine and DON inhibit a range of glutamine-utilizing enzymes beyond GFPT1, including enzymes involved in amino acids and nucleosides biosynthesis[126].

Several groups have tried to specifically target enzymes in the HBP with mixed results. A heterocyclic GFPT inhibitor from Roche had fairly low potency *in vitro*[127,128]. Another group targeting PGM3, the penultimate enzyme in the HBP, demonstrated anti-tumor effects in breast cancer cells and xenograft models, but much more work needs to be done to attain optimal potency, stability, and safety[129].

Elevated HBP activity and O-GlcNAcylation have been reported in essentially all cancer cells[130]. Developing a specific, potent HBP inhibitor would be a critical step in defining the role of the HBP and may offer new therapeutic strategies that can be combined with available treatments. It is important to note that GlcNAc salvage pathway and the Leloir pathway can lead to UDP-GlcNAc generation. In the context of PDA, the tumor microenvironment may provide the means to utilize these pathways to generate UDP-GlcNAc. Therefore, identifying potential GlcNAc and GalNAc sources in the tumor microenvironment can contribute to formulating improved therapies.

### 1.8 Hyaluronic Acid

Hyaluronic acid (HA) is a GlcNAc containing molecule that is found in abundance in PDA tumor microenvironment. It belongs to a group of non-protein, unsulfated glycosaminoglycans (GAGs). GAGs are long, linear, often highly sulfated, polysaccharides consisting of repeating disaccharide units. Expressed on the surfaces of all nucleated cells, GAGs are involved in embryogenesis, growth, proliferation, tissue hydration, and cell interactions via receptors[131].

Amongst all the GAGs, HA is especially relevant in PDA as it is abundant in PDA and avidly retains water, resulting in the supraphysiological pressure that impairs vascularity and impedes drug delivery[70,132]. Below, we briefly describe HA in normal physiological settings, its synthesis and degradation, the opposing effects of HA depending on its molecular weight, and the role of HA as a signaling molecule.

<u>HA in Normal Physiology</u>

HA is a polysaccharide with alternating units of D-glucuronic acid and GlcNAc. It is found in epithelial and nervous tissues, connective tissues, and blood vessel walls. HA concentration is the highest in the skin and synovial fluid[133]. In humans, HA is found in the ECM in the form of

sodium salt as sodium hyaluronate. Many studies have demonstrated HA involvement in wound healing, tissue structure, tissue hydration, and cell signaling[134].

HA Synthesis and Degradation

HA is synthesized by a class of integral membrane proteins called hyaluronan synthases (HAS). In vertebrates, there are three types: HAS1, HAS2, and HAS3, which have different catalytic activities and roles. HAS2 produces high molecular weight HA, and is particularly involved in the early embryonic development[135]. HAS3 is the most active enzyme, synthesizing low molecular weight HA for tissue growth and repair[136]. HAS1 is the least active enzyme and its role is relatively poorly understood[134]. It is worth noting that unlike other GAGs, which are mainly synthesized in the Golgi apparatus, HA is synthesized in the plasma membranes and then transported into the pericellular space.

HA is degraded by a family of enzymes called hyaluronidases (HYALs). In humans, there are five enzymes: HYAL1 through HYAL4, and PH-20[134]. The role of HYAL1 in housekeeping HA levels is well established, as HYAL1 is normally expressed in many cell types, within vesicles and lysosomes[137]. Furthermore, HYAL1 is also secreted into the tumor interstitial fluid and found in the conditioned media of cultured cancer cells[138]. Therefore, the expression and functional importance of hyaluronidases in cancer have most widely been characterized with respect to HYAL1. In primary PDA, strong HAS2 expression and weak HYAL1 expression were significantly associated with shorter survival post-surgery[139]. HYAL2 is GPI-anchored at the plasma membrane and is mostly known for its ability to promote uptake and endocytic internalization of HA[140,141]. HYAL3 and HYAL4 have either no reported or insignificant hyaluronidase activity and PH-20 expression and activity are testis-specific. In humans and mice, HA turnover occurs rapidly, with a half-life of a few hours to a few days at most[142].

Different Molecular Weight of HA: Opposing Properties and Cell Signaling

In non-pathological settings, HA is predominantly high molecular weight (HMW: >1000kDa[143]. There is a significantly elevated level of low molecular weight (LMW: 10-250kDa) and oligo-HA (o-HA: <10kDa) in tumors and tumor interstitial fluid[144]. Two major HA receptors have been identified: cluster differentiation 44 (CD44) and the HA-mediated mobility receptor (RHAMM)[145]. Different molecular weight HA can lead to different cell signals.

Many studies associate HMW-HA with anti-cancer properties via the CD44 receptor. HMW-HA can suppress cancer cell migration, decrease cell cycle progression and proliferation by inhibiting Rac-dependent signaling to cyclin D1[146]. HMW-HA can down-regulate cyclooxygenase-2 and matrix metalloproteinase production to decrease inflammation[147]. HMW-HA itself can increase ECM density to suppress cell mobility and tumor growth[142].

Unlike HMW-HA, oligo-HA and LMW-HA are associated with cancer-promoting properties. In papillary thyroid carcinoma, o-HA increased proliferation in mice via a toll-like receptor 4-dependent signaling pathway[148]. In breast tumors, o-HA contributes to increased angiogenesis[149]. LMW-HA interacts with CD44 to increase cancer cell proliferation, migration, and invasion via MAPK/ERK1/2 and RAS/PI3K/Akt signaling pathways[145].

HA has been widely studied for its biophysical properties as well as its molecular weight-dependent signaling roles in normal physiological and cancer settings. Interestingly, despite the fact that HA is a gigantic carbohydrate polymer that is found in abundance in the PDA tumor microenvironment, no group has tested its role as a potential nutrient for cancer cells. Here, we define the role of the HBP in PDA in the context of the tumor microenvironment as a source of novel nutrient(s) that can regulate PDA metabolism.

## References


1 Kleeff, J. *et al.* Pancreatic cancer. *Nature Reviews Disease Primers* **2**, 16022, doi:10.1038/nrdp.2016.22 (2016).

2 Siegel, R. L., Miller, K. D., Wagle, N. S. & Jemal, A. Cancer statistics, 2023. *CA: A Cancer Journal for Clinicians* **73**, 17-48, doi:https://doi.org/10.3322/caac.21763 (2023).

3 Rahib, L. *et al.* Projecting cancer incidence and deaths to 2030: the unexpected burden of thyroid, liver, and pancreas cancers in the United States. *Cancer Res* **74**, 2913-2921, doi:10.1158/0008-5472.Can-14-0155 (2014).

4 De Dosso, S. *et al.* Treatment landscape of metastatic pancreatic cancer. *Cancer Treat Rev* **96**, 102180, doi:10.1016/j.ctrv.2021.102180 (2021).

5 Bosetti, C. *et al.* Cigarette smoking and pancreatic cancer: an analysis from the International Pancreatic Cancer Case-Control Consortium (Panc4). *Ann Oncol* **23**, 1880-1888, doi:10.1093/annonc/mdr541 (2012).

6 Boffetta, P., Hecht, S., Gray, N., Gupta, P. & Straif, K. Smokeless tobacco and cancer. *Lancet Oncol* **9**, 667-675, doi:10.1016/s1470-2045(08)70173-6 (2008).

7 Behrens, G. *et al.* Physical activity and risk of pancreatic cancer: a systematic review and meta-analysis. *Eur J Epidemiol* **30**, 279-298, doi:10.1007/s10654-015-0014-9 (2015).

8 Bosetti, C. *et al.* Nutrient-based dietary patterns and pancreatic cancer risk. *Ann Epidemiol* **23**, 124-128, doi:10.1016/j.annepidem.2012.12.005 (2013).

9 Genkinger, J. M. *et al.* Central adiposity, obesity during early adulthood, and pancreatic cancer mortality in a pooled analysis of cohort studies. *Ann Oncol* **26**, 2257-2266, doi:10.1093/annonc/mdv355 (2015).

10 Larsson, S. C. & Wolk, A. Red and processed meat consumption and risk of pancreatic cancer: meta-analysis of prospective studies. *Br J Cancer* **106**, 603-607, doi:10.1038/bjc.2011.585 (2012).

11 Tramacere, I. *et al.* Alcohol drinking and pancreatic cancer risk: a meta-analysis of the dose-risk relation. *Int J Cancer* **126**, 1474-1486, doi:10.1002/ijc.24936 (2010).

12 Bosetti, C. *et al.* Diabetes, antidiabetic medications, and pancreatic cancer risk: an analysis from the International Pancreatic Cancer Case-Control Consortium. *Ann Oncol* **25**, 2065-2072, doi:10.1093/annonc/mdu276 (2014).

13 Chari, S. T. *et al.* Pancreatic cancer-associated diabetes mellitus: prevalence and temporal association with diagnosis of cancer. *Gastroenterology* **134**, 95-101, doi:10.1053/j.gastro.2007.10.040 (2008).

14 Turati, F. *et al.* Family history of cancer and the risk of cancer: a network of case-control studies. *Ann Oncol* **24**, 2651-2656, doi:10.1093/annonc/mdt280 (2013).

15 Llach, J., Carballal, S. & Moreira, L. Familial Pancreatic Cancer: Current Perspectives. *Cancer Manag Res* **12**, 743-758, doi:10.2147/cmar.S172421 (2020).

16 Yachida, S. *et al.* Distant metastasis occurs late during the genetic evolution of pancreatic cancer. *Nature* **467**, 1114-1117, doi:10.1038/nature09515 (2010).

17 Kim, J. E. *et al.* Clinical usefulness of carbohydrate antigen 19-9 as a screening test for pancreatic cancer in an asymptomatic population. *J Gastroenterol Hepatol* **19**, 182-186, doi:10.1111/j.1440-1746.2004.03219.x (2004).

18 Fahrmann, J. F. *et al.* A Plasma-Derived Protein-Metabolite Multiplexed Panel for Early-Stage Pancreatic Cancer. *J Natl Cancer Inst* **111**, 372-379, doi:10.1093/jnci/djy126 (2019).

19 Kato, S. & Honda, K. CA19-9 as a therapeutic target in pancreatitis. *Ann Transl Med* **7**, S318, doi:10.21037/atm.2019.09.161 (2019).

20 Ventrucci, M., Pozzato, P., Cipolla, A. & Uomo, G. Persistent elevation of serum CA 19-9 with no evidence of malignant disease. *Dig Liver Dis* **41**, 357-363, doi:10.1016/j.dld.2008.04.002 (2009).
21 Bauer, A. S. *et al.* Diagnosis of pancreatic ductal adenocarcinoma and chronic pancreatitis by measurement of microRNA abundance in blood and tissue. *PLoS One* **7**, e34151, doi:10.1371/journal.pone.0034151 (2012).
22 Hernandez, Y. G. & Lucas, A. L. MicroRNA in pancreatic ductal adenocarcinoma and its precursor lesions. *World J Gastrointest Oncol* **8**, 18-29, doi:10.4251/wjgo.v8.i1.18 (2016).
23 Komatsu, S. *et al.* Malignant potential in pancreatic neoplasm; new insights provided by circulating miR-223 in plasma. *Expert Opin Biol Ther* **15**, 773-785, doi:10.1517/14712598.2015.1029914 (2015).
24 Kahlert, C. *et al.* Identification of double-stranded genomic DNA spanning all chromosomes with mutated KRAS and p53 DNA in the serum exosomes of patients with pancreatic cancer. *J Biol Chem* **289**, 3869-3875, doi:10.1074/jbc.C113.532267 (2014).
25 Melo, S. A. *et al.* Glypican-1 identifies cancer exosomes and detects early pancreatic cancer. *Nature* **523**, 177-182, doi:10.1038/nature14581 (2015).
26 Kinugasa, H. *et al.* Detection of K-ras gene mutation by liquid biopsy in patients with pancreatic cancer. *Cancer* **121**, 2271-2280, doi:10.1002/cncr.29364 (2015).
27 Rhim, A. D. *et al.* Detection of circulating pancreas epithelial cells in patients with pancreatic cystic lesions. *Gastroenterology* **146**, 647-651, doi:10.1053/j.gastro.2013.12.007 (2014).
28 Tjensvoll, K. *et al.* Clinical relevance of circulating KRAS mutated DNA in plasma from patients with advanced pancreatic cancer. *Mol Oncol* **10**, 635-643, doi:10.1016/j.molonc.2015.11.012 (2016).
29 Conroy, T. *et al.* FOLFIRINOX or Gemcitabine as Adjuvant Therapy for Pancreatic Cancer. *N Engl J Med* **379**, 2395-2406, doi:10.1056/NEJMoa1809775 (2018).
30 Van Cutsem, E. *et al.* Randomized Phase III Trial of Pegvorhyaluronidase Alfa With Nab-Paclitaxel Plus Gemcitabine for Patients With Hyaluronan-High Metastatic Pancreatic Adenocarcinoma. *J Clin Oncol* **38**, 3185-3194, doi:10.1200/jco.20.00590 (2020).
31 Hecht, J. R. *et al.* Randomized Phase III Study of FOLFOX Alone or With Pegilodecakin as Second-Line Therapy in Patients With Metastatic Pancreatic Cancer That Progressed After Gemcitabine (SEQUOIA). *J Clin Oncol* **39**, 1108-1118, doi:10.1200/jco.20.02232 (2021).
32 Tempero, M. *et al.* Ibrutinib in combination with nab-paclitaxel and gemcitabine for first-line treatment of patients with metastatic pancreatic adenocarcinoma: phase III RESOLVE study. *Ann Oncol* **32**, 600-608, doi:10.1016/j.annonc.2021.01.070 (2021).
33 Waddell, N. *et al.* Whole genomes redefine the mutational landscape of pancreatic cancer. *Nature* **518**, 495-501, doi:10.1038/nature14169 (2015).
34 Witkiewicz, A. K. *et al.* Whole-exome sequencing of pancreatic cancer defines genetic diversity and therapeutic targets. *Nat Commun* **6**, 6744, doi:10.1038/ncomms7744 (2015).
35 Bamford, S. *et al.* The COSMIC (Catalogue of Somatic Mutations in Cancer) database and website. *Br J Cancer* **91**, 355-358, doi:10.1038/sj.bjc.6601894 (2004).
36 Cox, A. D., Fesik, S. W., Kimmelman, A. C., Luo, J. & Der, C. J. Drugging the undruggable RAS: Mission Possible? *Nature Reviews Drug Discovery* **13**, 828-851, doi:10.1038/nrd4389 (2014).
37 Janes, M. R. *et al.* Targeting KRAS Mutant Cancers with a Covalent G12C-Specific Inhibitor. *Cell* **172**, 578-589.e517, doi:10.1016/j.cell.2018.01.006 (2018).
38 Canon, J. *et al.* The clinical KRAS(G12C) inhibitor AMG 510 drives anti-tumour immunity. *Nature* **575**, 217-223, doi:10.1038/s41586-019-1694-1 (2019).

39 Skoulidis, F. *et al.* Sotorasib for Lung Cancers with KRAS p.G12C Mutation. *N Engl J Med* **384**, 2371-2381, doi:10.1056/NEJMoa2103695 (2021).
40 Wang, X. *et al.* Identification of MRTX1133, a Noncovalent, Potent, and Selective KRAS(G12D) Inhibitor. *J Med Chem* **65**, 3123-3133, doi:10.1021/acs.jmedchem.1c01688 (2022).
41 Gustafson, W. C. *et al.* Direct targeting of RAS in pancreatic ductal adenocarcinoma with RMC-6236, a first-in-class, RAS-selective, orally bioavailable, tri-complex RASMULTI(ON) inhibitor. *Journal of Clinical Oncology* **40**, 591-591, doi:10.1200/JCO.2022.40.4_suppl.591 (2022).
42 Hofmann, M. H. *et al.* BI-3406, a Potent and Selective SOS1-KRAS Interaction Inhibitor, Is Effective in KRAS-Driven Cancers through Combined MEK Inhibition. *Cancer Discov* **11**, 142-157, doi:10.1158/2159-8290.Cd-20-0142 (2021).
43 Xue, J. Y. *et al.* Rapid non-uniform adaptation to conformation-specific KRAS(G12C) inhibition. *Nature* **577**, 421-425, doi:10.1038/s41586-019-1884-x (2020).
44 Tanaka, N. *et al.* Clinical Acquired Resistance to KRAS(G12C) Inhibition through a Novel KRAS Switch-II Pocket Mutation and Polyclonal Alterations Converging on RAS-MAPK Reactivation. *Cancer Discov* **11**, 1913-1922, doi:10.1158/2159-8290.Cd-21-0365 (2021).
45 Ribas, A. & Wolchok, J. D. Cancer immunotherapy using checkpoint blockade. *Science* **359**, 1350-1355, doi:10.1126/science.aar4060 (2018).
46 Royal, R. E. *et al.* Phase 2 trial of single agent Ipilimumab (anti-CTLA-4) for locally advanced or metastatic pancreatic adenocarcinoma. *J Immunother* **33**, 828-833, doi:10.1097/CJI.0b013e3181eec14c (2010).
47 Brahmer, J. R. *et al.* Safety and activity of anti-PD-L1 antibody in patients with advanced cancer. *N Engl J Med* **366**, 2455-2465, doi:10.1056/NEJMoa1200694 (2012).
48 Schumacher, T. N. & Schreiber, R. D. Neoantigens in cancer immunotherapy. *Science* **348**, 69-74, doi:10.1126/science.aaa4971 (2015).
49 Hu, Z. I. *et al.* Evaluating Mismatch Repair Deficiency in Pancreatic Adenocarcinoma: Challenges and Recommendations. *Clin Cancer Res* **24**, 1326-1336, doi:10.1158/1078-0432.Ccr-17-3099 (2018).
50 Salem, M. E. *et al.* Landscape of Tumor Mutation Load, Mismatch Repair Deficiency, and PD-L1 Expression in a Large Patient Cohort of Gastrointestinal Cancers. *Mol Cancer Res* **16**, 805-812, doi:10.1158/1541-7786.Mcr-17-0735 (2018).
51 Schizas, D. *et al.* Immunotherapy for pancreatic cancer: A 2020 update. *Cancer Treat Rev* **86**, 102016, doi:10.1016/j.ctrv.2020.102016 (2020).
52 Chu, G. C., Kimmelman, A. C., Hezel, A. F. & DePinho, R. A. Stromal biology of pancreatic cancer. *J Cell Biochem* **101**, 887-907, doi:10.1002/jcb.21209 (2007).
53 Elyada, E. *et al.* Cross-Species Single-Cell Analysis of Pancreatic Ductal Adenocarcinoma Reveals Antigen-Presenting Cancer-Associated Fibroblasts. *Cancer Discov* **9**, 1102-1123, doi:10.1158/2159-8290.Cd-19-0094 (2019).
54 Steele, N. G. *et al.* Multimodal mapping of the tumor and peripheral blood immune landscape in human pancreatic cancer. *Nature Cancer* **1**, 1097-1112, doi:10.1038/s43018-020-00121-4 (2020).
55 Keenan, B. P. *et al.* A Listeria vaccine and depletion of T-regulatory cells activate immunity against early stage pancreatic intraepithelial neoplasms and prolong survival of mice. *Gastroenterology* **146**, 1784-1794.e1786, doi:10.1053/j.gastro.2014.02.055 (2014).
56 Zhang, Y. *et al.* Regulatory T-cell Depletion Alters the Tumor Microenvironment and Accelerates Pancreatic Carcinogenesis. *Cancer Discov* **10**, 422-439, doi:10.1158/2159-8290.Cd-19-0958 (2020).
57 Zhang, Y. *et al.* CD4+ T lymphocyte ablation prevents pancreatic carcinogenesis in mice. *Cancer Immunol Res* **2**, 423-435, doi:10.1158/2326-6066.Cir-14-0016-t (2014).

58 Beatty, G. L. *et al.* CD40 agonists alter tumor stroma and show efficacy against pancreatic carcinoma in mice and humans. *Science* **331**, 1612-1616, doi:10.1126/science.1198443 (2011).
59 Long, K. B., Collier, A. I. & Beatty, G. L. Macrophages: Key orchestrators of a tumor microenvironment defined by therapeutic resistance. *Mol Immunol* **110**, 3-12, doi:10.1016/j.molimm.2017.12.003 (2019).
60 Long, K. B. *et al.* IFNγ and CCL2 Cooperate to Redirect Tumor-Infiltrating Monocytes to Degrade Fibrosis and Enhance Chemotherapy Efficacy in Pancreatic Carcinoma. *Cancer Discov* **6**, 400-413, doi:10.1158/2159-8290.Cd-15-1032 (2016).
61 Hegde, S. *et al.* Dendritic Cell Paucity Leads to Dysfunctional Immune Surveillance in Pancreatic Cancer. *Cancer Cell* **37**, 289-307.e289, doi:10.1016/j.ccell.2020.02.008 (2020).
62 Ahrén, B. Autonomic regulation of islet hormone secretion – Implications for health and disease. *Diabetologia* **43**, 393-410, doi:10.1007/s001250051322 (2000).
63 Bapat, A. A., Hostetter, G., Von Hoff, D. D. & Han, H. Perineural invasion and associated pain in pancreatic cancer. *Nature Reviews Cancer* **11**, 695-707, doi:10.1038/nrc3131 (2011).
64 Belfiori, G. *et al.* Long-Term Survivors after Upfront Resection for Pancreatic Ductal Adenocarcinoma: An Actual 5-Year Analysis of Disease-Specific and Post-Recurrence Survival. *Annals of Surgical Oncology* **28**, 8249-8260, doi:10.1245/s10434-021-10401-7 (2021).
65 Stopczynski, R. E. *et al.* Neuroplastic changes occur early in the development of pancreatic ductal adenocarcinoma. *Cancer Res* **74**, 1718-1727, doi:10.1158/0008-5472.Can-13-2050 (2014).
66 Sinha, S. *et al.* PanIN Neuroendocrine Cells Promote Tumorigenesis via Neuronal Cross-talk. *Cancer Res* **77**, 1868-1879, doi:10.1158/0008-5472.Can-16-0899-t (2017).
67 Banh, R. S. *et al.* Neurons Release Serine to Support mRNA Translation in Pancreatic Cancer. *Cell* **183**, 1202-1218.e1225, doi:10.1016/j.cell.2020.10.016 (2020).
68 Dominguez, C. X. *et al.* Single-Cell RNA Sequencing Reveals Stromal Evolution into LRRC15(+) Myofibroblasts as a Determinant of Patient Response to Cancer Immunotherapy. *Cancer Discov* **10**, 232-253, doi:10.1158/2159-8290.Cd-19-0644 (2020).
69 Hosein, A. N. *et al.* Cellular heterogeneity during mouse pancreatic ductal adenocarcinoma progression at single-cell resolution. *JCI Insight* **5**, doi:10.1172/jci.insight.129212 (2019).
70 Provenzano, P. P. *et al.* Enzymatic targeting of the stroma ablates physical barriers to treatment of pancreatic ductal adenocarcinoma. *Cancer Cell* **21**, 418-429, doi:10.1016/j.ccr.2012.01.007 (2012).
71 Annese, T., Tamma, R., Ruggieri, S. & Ribatti, D. Angiogenesis in Pancreatic Cancer: Pre-Clinical and Clinical Studies. *Cancers (Basel)* **11**, doi:10.3390/cancers11030381 (2019).
72 Wu, X. Z., Chen, D. & Xie, G. R. Extracellular matrix remodeling in hepatocellular carcinoma: effects of soil on seed? *Med Hypotheses* **66**, 1115-1120, doi:10.1016/j.mehy.2005.12.043 (2006).
73 Parker, A. L. & Cox, T. R. The Role of the ECM in Lung Cancer Dormancy and Outgrowth. *Front Oncol* **10**, 1766, doi:10.3389/fonc.2020.01766 (2020).
74 Apte, M. V. *et al.* Desmoplastic reaction in pancreatic cancer: role of pancreatic stellate cells. *Pancreas* **29**, 179-187, doi:10.1097/00006676-200410000-00002 (2004).
75 Tian, C. *et al.* Proteomic analyses of ECM during pancreatic ductal adenocarcinoma progression reveal different contributions by tumor and stromal cells. *Proc Natl Acad Sci U S A* **116**, 19609-19618, doi:10.1073/pnas.1908626116 (2019).

76 Weniger, M., Honselmann, K. C. & Liss, A. S. The Extracellular Matrix and Pancreatic Cancer: A Complex Relationship. *Cancers* **10**, 316 (2018).
77 Elahi-Gedwillo, K. Y., Carlson, M., Zettervall, J. & Provenzano, P. P. Antifibrotic Therapy Disrupts Stromal Barriers and Modulates the Immune Landscape in Pancreatic Ductal Adenocarcinoma. *Cancer Res* **79**, 372-386, doi:10.1158/0008-5472.Can-18-1334 (2019).
78 Perez, V. M., Kearney, J. F. & Yeh, J. J. The PDAC Extracellular Matrix: A Review of the ECM Protein Composition, Tumor Cell Interaction, and Therapeutic Strategies. *Front Oncol* **11**, 751311, doi:10.3389/fonc.2021.751311 (2021).
79 Lee, J. J. *et al.* Stromal response to Hedgehog signaling restrains pancreatic cancer progression. *Proc Natl Acad Sci U S A* **111**, E3091-3100, doi:10.1073/pnas.1411679111 (2014).
80 Whittle, M. C. *et al.* RUNX3 Controls a Metastatic Switch in Pancreatic Ductal Adenocarcinoma. *Cell* **161**, 1345-1360, doi:10.1016/j.cell.2015.04.048 (2015).
81 Hanahan, D. & Weinberg, R. A. Hallmarks of cancer: the next generation. *Cell* **144**, 646-674, doi:10.1016/j.cell.2011.02.013 (2011).
82 Lunt, S. Y. & Vander Heiden, M. G. Aerobic glycolysis: meeting the metabolic requirements of cell proliferation. *Annu Rev Cell Dev Biol* **27**, 441-464, doi:10.1146/annurev-cellbio-092910-154237 (2011).
83 Vaupel, P. & Multhoff, G. Revisiting the Warburg effect: historical dogma versus current understanding. *J Physiol* **599**, 1745-1757, doi:10.1113/jp278810 (2021).
84 Ying, H. *et al.* Oncogenic Kras maintains pancreatic tumors through regulation of anabolic glucose metabolism. *Cell* **149**, 656-670, doi:10.1016/j.cell.2012.01.058 (2012).
85 Dey, P. *et al.* Oncogenic KRAS-Driven Metabolic Reprogramming in Pancreatic Cancer Cells Utilizes Cytokines from the Tumor Microenvironment. *Cancer Discov* **10**, 608-625, doi:10.1158/2159-8290.Cd-19-0297 (2020).
86 Cheung, E. C. *et al.* Dynamic ROS Control by TIGAR Regulates the Initiation and Progression of Pancreatic Cancer. *Cancer Cell* **37**, 168-182.e164, doi:10.1016/j.ccell.2019.12.012 (2020).
87 Sodir, N. M. *et al.* MYC Instructs and Maintains Pancreatic Adenocarcinoma Phenotype. *Cancer Discov* **10**, 588-607, doi:10.1158/2159-8290.Cd-19-0435 (2020).
88 Muthalagu, N. *et al.* Repression of the Type I Interferon Pathway Underlies MYC- and KRAS-Dependent Evasion of NK and B Cells in Pancreatic Ductal Adenocarcinoma. *Cancer Discov* **10**, 872-887, doi:10.1158/2159-8290.Cd-19-0620 (2020).
89 Hoxhaj, G. & Manning, B. D. The PI3K-AKT network at the interface of oncogenic signalling and cancer metabolism. *Nat Rev Cancer* **20**, 74-88, doi:10.1038/s41568-019-0216-7 (2020).
90 Hill, R. *et al.* PTEN loss accelerates KrasG12D-induced pancreatic cancer development. *Cancer Res* **70**, 7114-7124, doi:10.1158/0008-5472.Can-10-1649 (2010).
91 Ying, H. *et al.* PTEN is a major tumor suppressor in pancreatic ductal adenocarcinoma and regulates an NF-κB-cytokine network. *Cancer Discov* **1**, 158-169, doi:10.1158/2159-8290.Cd-11-0031 (2011).
92 Wu, C. Y. *et al.* PI3K regulation of RAC1 is required for KRAS-induced pancreatic tumorigenesis in mice. *Gastroenterology* **147**, 1405-1416.e1407, doi:10.1053/j.gastro.2014.08.032 (2014).
93 Halbrook, C. J. & Lyssiotis, C. A. Employing Metabolism to Improve the Diagnosis and Treatment of Pancreatic Cancer. *Cancer Cell* **31**, 5-19, doi:10.1016/j.ccell.2016.12.006 (2017).
94 Amendola, C. R. *et al.* KRAS4A directly regulates hexokinase 1. *Nature* **576**, 482-486, doi:10.1038/s41586-019-1832-9 (2019).
95 Altman, B. J., Stine, Z. E. & Dang, C. V. From Krebs to clinic: glutamine metabolism to cancer therapy. *Nat Rev Cancer* **16**, 619-634, doi:10.1038/nrc.2016.71 (2016).

96 Liou, G. Y. *et al.* Mutant KRas-Induced Mitochondrial Oxidative Stress in Acinar Cells Upregulates EGFR Signaling to Drive Formation of Pancreatic Precancerous Lesions. *Cell Rep* **14**, 2325-2336, doi:10.1016/j.celrep.2016.02.029 (2016).
97 Weinberg, F. *et al.* Mitochondrial metabolism and ROS generation are essential for Kras-mediated tumorigenicity. *Proc Natl Acad Sci U S A* **107**, 8788-8793, doi:10.1073/pnas.1003428107 (2010).
98 Son, J. *et al.* Glutamine supports pancreatic cancer growth through a KRAS-regulated metabolic pathway. *Nature* **496**, 101-105, doi:10.1038/nature12040 (2013).
99 Raho, S. *et al.* KRAS-regulated glutamine metabolism requires UCP2-mediated aspartate transport to support pancreatic cancer growth. *Nat Metab* **2**, 1373-1381, doi:10.1038/s42255-020-00315-1 (2020).
100 Bott, A. J. *et al.* Glutamine Anabolism Plays a Critical Role in Pancreatic Cancer by Coupling Carbon and Nitrogen Metabolism. *Cell Rep* **29**, 1287-1298.e1286, doi:10.1016/j.celrep.2019.09.056 (2019).
101 Yoo, H. C. *et al.* A Variant of SLC1A5 Is a Mitochondrial Glutamine Transporter for Metabolic Reprogramming in Cancer Cells. *Cell Metab* **31**, 267-283.e212, doi:10.1016/j.cmet.2019.11.020 (2020).
102 Recouvreux, M. V. *et al.* Glutamine depletion regulates Slug to promote EMT and metastasis in pancreatic cancer. *J Exp Med* **217**, doi:10.1084/jem.20200388 (2020).
103 Biancur, D. E. *et al.* Compensatory metabolic networks in pancreatic cancers upon perturbation of glutamine metabolism. *Nat Commun* **8**, 15965, doi:10.1038/ncomms15965 (2017).
104 Lemberg, K. M., Vornov, J. J., Rais, R. & Slusher, B. S. We're Not "DON" Yet: Optimal Dosing and Prodrug Delivery of 6-Diazo-5-oxo-L-norleucine. *Mol Cancer Ther* **17**, 1824-1832, doi:10.1158/1535-7163.Mct-17-1148 (2018).
105 Harris, I. S. & DeNicola, G. M. The Complex Interplay between Antioxidants and ROS in Cancer. *Trends Cell Biol* **30**, 440-451, doi:10.1016/j.tcb.2020.03.002 (2020).
106 Daher, B. *et al.* Genetic Ablation of the Cystine Transporter xCT in PDAC Cells Inhibits mTORC1, Growth, Survival, and Tumor Formation via Nutrient and Oxidative Stresses. *Cancer Res* **79**, 3877-3890, doi:10.1158/0008-5472.Can-18-3855 (2019).
107 Stockwell, B. R., Jiang, X. & Gu, W. Emerging Mechanisms and Disease Relevance of Ferroptosis. *Trends Cell Biol* **30**, 478-490, doi:10.1016/j.tcb.2020.02.009 (2020).
108 Badgley, M. A. *et al.* Cysteine depletion induces pancreatic tumor ferroptosis in mice. *Science* **368**, 85-89, doi:10.1126/science.aaw9872 (2020).
109 Cramer, S. L. *et al.* Systemic depletion of L-cyst(e)ine with cyst(e)inase increases reactive oxygen species and suppresses tumor growth. *Nat Med* **23**, 120-127, doi:10.1038/nm.4232 (2017).
110 Yang, S. *et al.* Pancreatic cancers require autophagy for tumor growth. *Genes Dev* **25**, 717-729, doi:10.1101/gad.2016111 (2011).
111 Yang, A. *et al.* Autophagy is critical for pancreatic tumor growth and progression in tumors with p53 alterations. *Cancer Discov* **4**, 905-913, doi:10.1158/2159-8290.Cd-14-0362 (2014).
112 Rosenfeldt, M. T. *et al.* p53 status determines the role of autophagy in pancreatic tumour development. *Nature* **504**, 296-300, doi:10.1038/nature12865 (2013).
113 Yang, A. *et al.* Autophagy Sustains Pancreatic Cancer Growth through Both Cell-Autonomous and Nonautonomous Mechanisms. *Cancer Discov* **8**, 276-287, doi:10.1158/2159-8290.Cd-17-0952 (2018).
114 Pommier, A. *et al.* Unresolved endoplasmic reticulum stress engenders immune-resistant, latent pancreatic cancer metastases. *Science* **360**, doi:10.1126/science.aao4908 (2018).

115 Yamamoto, K. *et al.* Autophagy promotes immune evasion of pancreatic cancer by degrading MHC-I. *Nature* **581**, 100-105, doi:10.1038/s41586-020-2229-5 (2020).
116 Commisso, C. *et al.* Macropinocytosis of protein is an amino acid supply route in Ras-transformed cells. *Nature* **497**, 633-637, doi:10.1038/nature12138 (2013).
117 Olivares, O. *et al.* Collagen-derived proline promotes pancreatic ductal adenocarcinoma cell survival under nutrient limited conditions. *Nature Communications* **8**, 16031, doi:10.1038/ncomms16031 (2017).
118 Kamphorst, J. J. *et al.* Human pancreatic cancer tumors are nutrient poor and tumor cells actively scavenge extracellular protein. *Cancer Res* **75**, 544-553, doi:10.1158/0008-5472.Can-14-2211 (2015).
119 Amyere, M. *et al.* Constitutive macropinocytosis in oncogene-transformed fibroblasts depends on sequential permanent activation of phosphoinositide 3-kinase and phospholipase C. *Mol Biol Cell* **11**, 3453-3467, doi:10.1091/mbc.11.10.3453 (2000).
120 Ramirez, C., Hauser, A. D., Vucic, E. A. & Bar-Sagi, D. Plasma membrane V-ATPase controls oncogenic RAS-induced macropinocytosis. *Nature* **576**, 477-481, doi:10.1038/s41586-019-1831-x (2019).
121 Yao, W. *et al.* Syndecan 1 is a critical mediator of macropinocytosis in pancreatic cancer. *Nature* **568**, 410-414, doi:10.1038/s41586-019-1062-1 (2019).
122 Asthana, A., Ramakrishnan, P., Vicioso, Y., Zhang, K. & Parameswaran, R. Hexosamine Biosynthetic Pathway Inhibition Leads to AML Cell Differentiation and Cell Death. *Mol Cancer Ther* **17**, 2226-2237, doi:10.1158/1535-7163.Mct-18-0426 (2018).
123 Pham, L. V. *et al.* Targeting the hexosamine biosynthetic pathway and O-linked N-acetylglucosamine cycling for therapeutic and imaging capabilities in diffuse large B-cell lymphoma. *Oncotarget* **7**, 80599-80611, doi:10.18632/oncotarget.12413 (2016).
124 Vasconcelos-Dos-Santos, A. *et al.* Hyperglycemia exacerbates colon cancer malignancy through hexosamine biosynthetic pathway. *Oncogenesis* **6**, e306, doi:10.1038/oncsis.2017.2 (2017).
125 Wellen, K. E. *et al.* The hexosamine biosynthetic pathway couples growth factor-induced glutamine uptake to glucose metabolism. *Genes Dev* **24**, 2784-2799, doi:10.1101/gad.1985910 (2010).
126 Pinkus, L. M. Glutamine binding sites. *Methods Enzymol* **46**, 414-427, doi:10.1016/s0076-6879(77)46049-x (1977).
127 Qian, Y. *et al.* Discovery of 1-arylcarbonyl-6,7-dimethoxyisoquinoline derivatives as glutamine fructose-6-phosphate amidotransferase (GFAT) inhibitors. *Bioorg Med Chem Lett* **21**, 6264-6269, doi:10.1016/j.bmcl.2011.09.009 (2011).
128 Walter, L. A. *et al.* Inhibiting the Hexosamine Biosynthetic Pathway Lowers O-GlcNAcylation Levels and Sensitizes Cancer to Environmental Stress. *Biochemistry* **59**, 3169-3179, doi:10.1021/acs.biochem.9b00560 (2020).
129 Ricciardiello, F. *et al.* Inhibition of the Hexosamine Biosynthetic Pathway by targeting PGM3 causes breast cancer growth arrest and apoptosis. *Cell Death Dis* **9**, 377, doi:10.1038/s41419-018-0405-4 (2018).
130 Akella, N. M., Ciraku, L. & Reginato, M. J. Fueling the fire: emerging role of the hexosamine biosynthetic pathway in cancer. *BMC Biology* **17**, 52, doi:10.1186/s12915-019-0671-3 (2019).
131 Khan, S. A., Mason, R. W., Kobayashi, H., Yamaguchi, S. & Tomatsu, S. Advances in glycosaminoglycan detection. *Mol Genet Metab* **130**, 101-109, doi:10.1016/j.ymgme.2020.03.004 (2020).
132 Jacobetz, M. A. *et al.* Hyaluronan impairs vascular function and drug delivery in a mouse model of pancreatic cancer. *Gut* **62**, 112-120, doi:10.1136/gutjnl-2012-302529 (2013).

133 Volpi, N., Schiller, J., Stern, R. & Soltés, L. Role, metabolism, chemical modifications and applications of hyaluronan. *Curr Med Chem* **16**, 1718-1745, doi:10.2174/092986709788186138 (2009).
134 Michalczyk, M., Humeniuk, E., Adamczuk, G. & Korga-Plewko, A. Hyaluronic Acid as a Modern Approach in Anticancer Therapy-Review. *Int J Mol Sci* **24**, doi:10.3390/ijms24010103 (2022).
135 Camenisch, T. D. *et al.* Disruption of hyaluronan synthase-2 abrogates normal cardiac morphogenesis and hyaluronan-mediated transformation of epithelium to mesenchyme. *J Clin Invest* **106**, 349-360, doi:10.1172/jci10272 (2000).
136 Frenkel, J. S. The role of hyaluronan in wound healing. *Int Wound J* **11**, 159-163, doi:10.1111/j.1742-481X.2012.01057.x (2014).
137 Puissant, E. *et al.* Subcellular trafficking and activity of Hyal-1 and its processed forms in murine macrophages. *Traffic* **15**, 500-515, doi:10.1111/tra.12162 (2014).
138 Lokeshwar, V. B., Cerwinka, W. H., Isoyama, T. & Lokeshwar, B. L. HYAL1 hyaluronidase in prostate cancer: a tumor promoter and suppressor. *Cancer Res* **65**, 7782-7789, doi:10.1158/0008-5472.Can-05-1022 (2005).
139 Cheng, X. B., Sato, N., Kohi, S. & Yamaguchi, K. Prognostic impact of hyaluronan and its regulators in pancreatic ductal adenocarcinoma. *PLoS One* **8**, e80765, doi:10.1371/journal.pone.0080765 (2013).
140 Andre, B. *et al.* Hyal2 is a glycosylphosphatidylinositol-anchored, lipid raft-associated hyaluronidase. *Biochem Biophys Res Commun* **411**, 175-179, doi:10.1016/j.bbrc.2011.06.125 (2011).
141 Harada, H. & Takahashi, M. CD44-dependent intracellular and extracellular catabolism of hyaluronic acid by hyaluronidase-1 and -2. *J Biol Chem* **282**, 5597-5607, doi:10.1074/jbc.M608358200 (2007).
142 McAtee, C. O., Barycki, J. J. & Simpson, M. A. Emerging roles for hyaluronidase in cancer metastasis and therapy. *Adv Cancer Res* **123**, 1-34, doi:10.1016/b978-0-12-800092-2.00001-0 (2014).
143 Monslow, J., Govindaraju, P. & Puré, E. Hyaluronan - a functional and structural sweet spot in the tissue microenvironment. *Front Immunol* **6**, 231, doi:10.3389/fimmu.2015.00231 (2015).
144 Schmaus, A. *et al.* Accumulation of small hyaluronan oligosaccharides in tumour interstitial fluid correlates with lymphatic invasion and lymph node metastasis. *Br J Cancer* **111**, 559-567, doi:10.1038/bjc.2014.332 (2014).
145 Misra, S., Hascall, V. C., Markwald, R. R. & Ghatak, S. Interactions between Hyaluronan and Its Receptors (CD44, RHAMM) Regulate the Activities of Inflammation and Cancer. *Front Immunol* **6**, 201, doi:10.3389/fimmu.2015.00201 (2015).
146 Kothapalli, D. *et al.* Hyaluronan and CD44 antagonize mitogen-dependent cyclin D1 expression in mesenchymal cells. *J Cell Biol* **176**, 535-544, doi:10.1083/jcb.200611058 (2007).
147 Chang, C. C. *et al.* Hyaluronan regulates PPARγ and inflammatory responses in IL-1β-stimulated human chondrosarcoma cells, a model for osteoarthritis. *Carbohydr Polym* **90**, 1168-1175, doi:10.1016/j.carbpol.2012.06.071 (2012).
148 Dang, S. *et al.* Stimulation of TLR4 by LMW-HA induces metastasis in human papillary thyroid carcinoma through CXCR7. *Clin Dev Immunol* **2013**, 712561, doi:10.1155/2013/712561 (2013).
149 Koyama, H. *et al.* Hyperproduction of hyaluronan in neu-induced mammary tumor accelerates angiogenesis through stromal cell recruitment: possible involvement of versican/PG-M. *Am J Pathol* **170**, 1086-1099, doi:10.2353/ajpath.2007.060793 (2007).

# Chapter 2

## Hyaluronic Acid Fuels Pancreatic Cancer Cell Growth

This chapter consists of a published primary article: **Kim PK***, Halbrook CJ*, Kerk SA*, Radyk M, Wisner S, Kremer DM, Sajjakulnukit P, Andren A, Hou SW, Trivedi A, Thurston G, Anand A, Yan L, Salamanca-Cardona L, Welling SD, Zhang L, Pratt MR, Keshari KR, Ying H, Lyssiotis CA. Hyaluronic acid fuels pancreatic cancer cell growth. ***Elife***. 2021 Dec 24;10:e62645. doi: 10.7554/eLife.62645. PMID: 34951587; PMCID: PMC8730721.
*these authors contributed equally

## 2.1 Introduction

As discussed in Chapter 1, PDA is one of the deadliest human cancers with no clinically effective treatment options[1]. PDA is characterized by an intense fibroinflammatory stroma, poor vascularity, deregulated nutrient levels, and rich deposition of extracellular matrix components. To survive and proliferate in this nutrient dysregulated tumor microenvironment, the oncogenic driver in PDA, KRAS*, facilitates the rewiring of PDA metabolism[2-5].

One example of this, which has been demonstrated in previous work[6] and introduced in Chapter 1, is the effect of KRAS* on the activity of the hexosamine biosynthesis pathway (HBP). Signaling downstream of KRAS* results in upregulated expression of *Gfpt1*, which encodes glutamine-fructose 6-phosphate amidotransferase 1 (GFAT1). The HBP is an evolutionarily conserved pathway that integrates glucose, glutamine, fatty acid, and nucleotide metabolism to generate the final product uridine diphosphate N-acetylglucosamine (UDP-GlcNAc). UDP-GlcNAc is a crucial donor molecule for glycosylation and O-GlcNAcylation, two essential post-translational modifications required for cellular structure, signaling, and survival[7]. The HBP is the only pathway able to generate UDP-GlcNAc *de novo*. Because the HBP integrates nutrients

from several major macromolecular classes to produce UDP-GlcNAc, it predictably functions as a nutrient sensing mechanism for available energy within a cell[8]. Indeed, numerous studies across cancer subtypes have demonstrated how HBP activity is enhanced to support tumor survival and growth[9-12] and even immune evasion through alteration of extracellular glycosylation content[13].

A compendium of studies during the last decade have revealed that PDA cells fuel their aberrant metabolic programs through nutrient scavenging[6,14-18]. Mechanisms include sustained activation of intracellular recycling pathways (e.g. autophagy), the upregulation of nutrient transporter expression (e.g. carbohydrate, lipid, and amino acid transporters), and the activation of extracellular nutrient scavenging pathways (e.g. macropinocytosis). Further, PDA cells also participate in metabolic crosstalk and nutrient acquisition with non-cancerous cells in the tumor microenvironment (TME), such as cancer-associated fibroblasts (CAFs) and tumor-associated macrophages (TAMs)[19-23]. A notable example is the observation that PDA cells can directly obtain nutrients from the CAF-derived extracellular matrix (ECM), such as collagen[18]. Taken together, elucidating the interaction of PDA cells with different cell populations and ECM components will be instrumental for delineating deregulated PDA metabolism and improving therapeutic strategies.

A major structural component of the TME is hyaluronic acid (HA), a hydrophilic glycosaminoglycan. HA is ubiquitously present in human tissue, especially in skin, connective tissue, and joints, and it is richly abundant in pancreatic tumors[24]. HA is thought to be primarily deposited by CAFs and, to some extent, by PDA cells[25,26]. HA avidly retains water, which is responsible for both its lubricating properties and, in PDA tumors, the supraphysiological pressure that impairs vascularity and limits drug penetrance[27,28]. An aspect of HA biology that has not previously been studied is its potential role as a nutrient. This is surprising given that HA

is a carbohydrate polymer whose monomeric unit is a disaccharide of glucuronic acid and N-acetyl-glucosamine (GlcNAc).

Herein, we set forth to determine the utility of targeting the HBP in PDA. We found that GFAT1 was required for cell survival in vitro. In marked contrast, GFAT1 knockout tumors readily grew in vivo. Based on this observation, we hypothesized that GlcNAc-containing components of the TME could bypass the HBP in vivo by way of the GlcNAc salvage pathway. We demonstrate that HA can be metabolized by PDA cells to support survival and proliferation by refilling the HBP. In sum, our study identifies HA as a novel nutrient source in PDA and contributes to a growing body of data illuminating the important role of the TME in cancer metabolism.

## 2.2 Results

### *2.2.1 Pancreatic cancer cells require de novo HBP fidelity in vitro but not in vivo*

Previously, we found that mutant Kras transcriptionally activates *Gfpt1* expression downstream of MAPK signaling in a murine model of PDA to facilitate HBP activity[6]. GFAT1 catalyzes the reaction that generates glucosamine 6-phosphate and glutamate from fructose 6-phosphate and glutamine **(Fig. 2-1A)**. In another previous study we demonstrated that PDA cells are dependent on glutamine anaplerosis for proliferation[29]. Thus, we hypothesized that inhibiting GFAT1 in PDA would have the simultaneous benefit of blocking two major metabolic pathways that support PDA proliferation, thereby providing a considerable therapeutic window.

Our previous results targeting GFAT1 in murine cells with shRNA yielded insufficient knockdown to draw a conclusion as to its necessity in PDA[6]. Thus, here we used CRISPR/Cas9 to knockout GFAT1 from three established human PDA cell lines: HPAC, TU8988T, and MiaPaCa2. During selection, the pooled polyclonal populations were grown in GlcNAc, which

bypasses GFAT1 via the GlcNAc salvage pathway **(Fig. 2-1A)**. This supplement was included to minimize metabolic rewiring within the selected populations.

The GFAT1 knockout lines had differential response to GlcNAc withdrawal. Among the three GFAT1 knockout cell lines, only the HPAC line exhibited a marked reduction in cell number, consistent with loss of viability, in the 4 days following GlcNAc withdrawal (**Fig. 2-2A**). The impact on proliferation was similarly reflected in decrease of the UDP-GlcNAc pool, which was analyzed using liquid chromatography-coupled tandem mass spectrometry (LC-MS/MS) (**Fig. 2-2B**). Consistent with the proliferative phenotypes across lines, the HPAC line also had a significantly smaller UDP-GlcNAc pool than that of either MiaPaCa2 or 8988T cells (**Fig. 2-2C**). Cellular O-GlcNAcylation of the proteome was also measured by immunoblot three days after GlcNAc withdrawal. Again, consistent with the LC-MS/MS analysis, O-GlcNAc expression was significantly reduced in HPAC but was maintained in TU8988T (**Fig. 2-2D**).

The data from TU8988T and MiaPaca2 were similar to those from our earlier studies[6], and thus we posited that knockout of GFAT1 was incomplete. As such, we subsequently generated clonal cell lines from the pooled populations. This analysis revealed that the degree of GFAT1 knockout varied by cell line and by clone, and this correlated with differential growth and sensitivity to GlcNAc withdrawal *in vitro* (**Fig. 2-2E,F**). Clones for each cell line without detectable GFAT1 expression **(Fig. 2-1B)** were further validated by sequencing and were subsequently used to examine the role of the HBP without interference from GFAT1 proficient cells.

Using our genomically-sequenced and bona fide GFAT1 knockout clonal lines, we found that GFAT1 knockout led to an abolishment of colony formation **(Fig. 2-1C)** and potently impaired proliferation **(Fig. 2-1D, Fig. 2-2G**) in all three PDA cell lines in vitro. We then moved these cells into *in vivo* tumor models. Surprisingly, when either the pooled or the clonal knockout lines were implanted into the flanks of immunocompromised mice, they readily formed tumors

that were comparable to their wild type counterparts in terms of weight and volume (**Fig. 2-1E,F** and **Fig. 2-2H**). Similar results were obtained for GFAT1 knockout clonal lines implanted orthotopically into the pancreas (**Fig. 2-1G**). Of note, while clearly capable of forming tumors, the GFAT1 knockout clonal lines grown in the pancreas were smaller than the wild type tumors at endpoint. The marked discrepancy in phenotype between *in vitro* and *in vivo* settings led us to hypothesize that GFAT1 knockout clones were scavenging nutrients from the TME to refill the HBP, which enabled their survival and tumor growth.

### *2.2.2 Conditioned media rescues proliferation of GFAT1 knockout PDA cells*

To test our scavenging hypothesis, we generated conditioned media (CM) from CAFs, the most abundant stromal cell type in the pancreatic TME[30,31]. When GFAT1 knockout clones were incubated in patient-derived CAF CM, we observed a significant, albeit modest, rescue in colony formation (**Fig. 2-3A,B**). Unexpectedly, we observed a more robust, dose-dependent rescue of colony formation in GFAT1 knockout cells with CM from wild type TU8988T cells (**Fig. 2-3C-F** and **Fig. 2-4A**). Similarly, CM from wild type HPAC and MiaPaCa2 cells was able to partially rescue proliferation of a subset of GFAT1 knockout clones (**Fig. 2-3G** and **Fig. 2-4B,C**).

To begin to identify the rescue factors in the CM, we subjected the CM to boiling or repeated cycles of freezing and thawing (F/T). In each of these conditions, both the CAF and the PDA CM retained the ability to support colony formation in GFAT1 knockout cells (**Fig. 2-3A-D**). These results suggested the relevant factor(s) did not require tertiary structure. Additionally, we observed that the rescue activity of the CM was dose dependent (**Fig. 2-3E-G** and **Fig. 2-4A-C**).

As GlcNAc was used to establish our GFAT1 knockout lines, we first quantitated the GlcNAc concentration in the CM by mass spectrometry. GlcNAc dose response curves demonstrated that millimolar quantities of GlcNAc (>0.625mM) were required to rescue colony

formation of GFAT1 knockout PDA cells (**Fig. 2-3H** and **Fig. 2-4D**). By contrast, LC-MS/MS quantification of GlcNAc in the CM revealed that it was in the low micromolar range (**Fig. 2-3I**), several orders of magnitude below the millimolar doses of exogenous GlcNAc required to maintain proliferation (**Fig. 2-3H** and **Fig. 2-4D**). These results illustrated that free GlcNAc was not the relevant molecule in the CM mediating rescue. This led us to consider alternate possibilities, including GlcNAc-containing components of the TME.

### *2.2.3 Hyaluronic acid rescues GFAT1 knockout PDA cells*

GlcNAc is a widely utilized molecule as a structural component of the extracellular matrix, a modification of various lipid species, and a post-translational modification on proteins[32,33]. Thus, we hypothesized that GlcNAc was released into CM as a component part of a lipid, protein, or glycosaminoglycan polymer, and that this mediated rescue of *GFAT1* knockout. To test this, we first applied necrotic cellular debris from the murine hematopoietic FL5.12 cell line[34] to GFAT1 knockout cells grown at clonal density. The necrotic cellular debris contains the full complement of biomolecules, including GlcNAc-containing proteins and lipids. Necrotic cell debris was unable to rescue GFAT1 knockout across our cell line panel (**Fig. 2-6A-F**). Next, we tested if glycosaminoglycan carbohydrate polymers could mediate rescue of GFAT1 knockout, in a matter akin to CM. High dose heparin was not able to rescue colony formation in GFAT1 knockout cells (**Fig. 2-6A-F**). In contrast, 78 kDa HA provided a modest but significant rescue (**Fig. 2-5A,B**).

HA is a carbohydrate polymer and an extracellular matrix component that is abundant in the PDA tumor microenvironment[24]. The monomeric form of HA is a repeating disaccharide consisting of glucuronic acid and GlcNAc. HA polymer length, often described by its molecular weight (MW), has important impacts on its biological activity. In non-pathological settings, newly synthesized HA is predominantly high molecular weight (HMW; >1000kDa)[35]. However, in tumors and tumor interstitial fluid, there is a significantly elevated level of low molecular weight

(LMW; 10-250kDa) and oligo-HA (o-HA; <10kDa)[36,37]. Consistent with the rescue of colony formation in GFAT1 knockout cells, LMW HA (78 kDa) was also able to rescue total proteome O-GlcNAc levels, as assessed by western blot (**Fig. 2-5C-E**).

Cancer cells have been reported to uptake HA via macropinocytosis[38]. Thus, a possible explanation for the modest rescue could be low macropinocytosis activity. However, in PDA, mutant Kras drives macropinocytosis[14], and quantitation of macropinocytotic activity with a fluorescent dextran-based assay revealed that our three PDA cell lines exhibited considerable macropinocytosis (**Fig. 2-6G**). Similarly, following HA uptake using a fluorescently-conjugated HA (HA-FITC) revealed GFAT1 proficient and GFAT1 knockout cells readily take up HA (**Fig. 2-5F, Fig. 2-6H**).

This led us to hypothesize that the rate limiting step is not HA entry into cells, but rather, the cleavage of HA into smaller fragments. Consistent with this hypothesis, utilizing hyaluronidase to break down LMW HA enhanced the rescue of colony formation (**Fig. 2-5G**). Of note, hyaluronidase was heat-inactivated after it was used to cleave HA (i.e. before its application to GFAT1 knockout cells; **Fig. 2-6I**), as hyaluronidase has been reported to directly impact cellular metabolism[39]. Next, we tracked the rescue of proliferation using HA of varying size: LMW HA (60kDa) and o-HA (5kDa). This analysis revealed that HA-mediated rescue, as measured through proliferation quantification, was considerably higher for o-HA than for LMW HA, and comparable to PDA CM (**Fig. 2-5H,I and Fig. 2-7A-D**).

To relate these studies back to our CM rescue studies, we employed an enzyme-linked immunosorbent assay (ELISA) to quantitate HA in the PDA and CAF CM (**Fig. 2-7E**). CAF CM contained considerably more HA than PDA CM, consistent with the known role for fibroblasts in the production of HA (**Fig. 2-7F**). However, we found that the lower limit of detection for the ELISA was ~50kDA HA. Indeed, we demonstrated this by digesting 10mM HA, CAF CM, or PDA CM with HAase. Post-digestion, we are unable to detect appreciable levels of HA (**Fig. 2-**

**7F,G**). These results illustrate the CAF CM produces more high molecular weight HA, which we posit explains its limited rescue of GFAT1 knockout in vitro.

HA is produced by the family of HA synthases (HAS), which can be inhibited in vitro with the tool compound 4-methylumbelliferone (4-MU)[40]. To determine if HA is the relevant metabolite in wildtype PDA CM facilitating rescue of GFAT1 knockout, we first treated wildtype PDA cells with a range of 4-MU doses. Cell proliferation was followed to assess off-target toxicity and HA in CM was quantitated using the HA ELISA. Of note, while PDA cells produce much less detectable HA than CAFs, they do produce a sufficient amount so as to analyze 4-MU activity (**Fig. 2-7F**). Indeed, we demonstrated that 4-MU dose dependently blocked HA release into CM (**Fig. 2-8A**) while also exhibiting proliferative defects at the highest concentration tested (**Fig. 2-8B-D**). Application of CM from 4-MU-treated wildtype PDA cells in GFAT1 rescue assays revealed that the reduction in HA content paralleled the decrease in CM rescue activity in GFAT1 knockout cells (**Fig. 2-8E**). These collective in vitro studies illustrate that HA can rescue the proliferation of GFAT1 knockout cells and strongly suggest that HA is the relevant factor mediating the rescue activity of PDA CM. However, while we believe these collective results are convincing, detection and quantitation of o-HA in PDA CM will be required to draw a definitive conclusion.

To relate this work back to our tumor studies (**Fig. 2-1E-G**), we probed for HA content in tumor slices by immunohistochemical detection of HA binding protein (HABP) [41]. We stained normal pancreas as the negative control (note: positive staining of vasculature) and a murine pancreatic tumor as a positive control (**Fig. 2-8F**). We then stained 10 tumor slices from GFAT1 proficient and deficient tumors from the subcutaneous and the orthotopic models. Blinded scoring using a 0-3 scale (**Fig. 2-8G**) revealed more HA in the subcutaneous than orthotopic setting (**Fig. 2-8H**). Tumor genotype did not influence HABP levels in the subcutaneous model, whereas there was a marked reduction in HABP staining in the orthotopic GFAT1 knockout

tumors (**Fig. 2-8H**). First, these data demonstrate that HA is available to PDA tumors in these models. Further, they suggest that the difference in growth of GFAT1 knockout tumors in the orthotopic model compared to subcutaneous, as observed in Fig.1-1E-G, may result from less HA availability.

### *2.2.4 Hyaluronic acid rescues GFAT1 null PDA via the GlcNAc salvage pathway*

The GlcNAc salvage pathway bypasses GFAT1 by catalyzing the phosphorylation of GlcNAc to GlcNAc-6-phsophate, in a reaction mediated by N-acetyl-glucosamine kinase (NAGK). This GlcNAc-6-phosphate is subsequently converted into UDP-GlcNAc (**Fig. 2-1A**). Therefore, we hypothesized that the carbohydrate polymer HA, which is 50% GlcNAc, fuels the HBP via the GlcNAc salvage pathway through NAGK. To test this, we employed the same CRISPR/Cas9 strategy to target NAGK (**Fig. 2-9A**). Knockout of NAGK in parental TU8988T and MiaPaCa2 cell lines had no impact on colony formation, while reducing the colony forming capacity of HPAC cells (**Fig. 2-9B,C**). These results correlated with the elevated expression of NAGK in wild type HPAC cells (**Fig. 2-9D**). Of note, NAGK knockout did not result in up-regulation of GFAT1 (**Fig. 2-9A**), which could have suggested a compensatory metabolic rewiring.

Next, we targeted NAGK in our GFAT1 knockout clones. GFAT1/NAGK double knockout cells were generated in media containing N-acetyl-galactosamine (GalNAc), an isomer of GlcNAc. Supplementation with GalNAc enables bypass of both the *de novo* HBP and the GlcNAc salvage pathway, by way of the Leloir pathway[42], to support UDP-GalNAc and ultimately UDP-GlcNAc biogenesis (**Fig. 2-9E**). In this way, we were again able to select viable lines while avoiding the selection of those with unpredictable metabolic adaptations.

The GalNAc dose response for GFAT1 knockout clones was comparable to that of GlcNAc (**Fig. 2-3H**), demonstrating that they are indeed viable in GalNAc (**Fig. 2-9F, Fig. 2-**

**10H**). Although NAGK expression was efficiently knocked down in our pooled populations (**Fig. 2-9G**), we again selected for clones in the TU8988T cell line in order to minimize the effect of NAGK-proficient clones persisting in the bulk population. From among these, we selected four GFAT1/NAGK clones and tracked their proliferation upon rescue with varying sizes of HA, GalNAc, or PDA CM. These were compared relative to wild type TU8988T cells and the GFAT1 knockout line. In stark contrast to the GFAT1 knockout line, LMW HA, o-HA and PDA CM was unable to rescue GFAT1/NAGK double knockout lines (**Fig. 2-9H-K, Fig. 2-10A-F**). Similar results were obtained in the MiaPaCa2 cell line (**Fig. 2-10G-J**).

Finally, we used LC/MS-MS to assess HBP metabolite levels and western blotting to follow proteome O-GlcNAcylation in the GFAT1 and GFAT1/NAGK double knockout cells. HA or PDA CM rescue of GFAT1 knockout cells restores UDP-GlcNAc pools and proteome O-GlcNAcylation, and this was blocked by knocking out NAGK (**Fig. 2-9L,M and Fig. 2-10K-N**). These results illustrate that HA rescue requires NAGK and the GlcNAc salvage pathway, consistent with the idea that HA-derived GlcNAc fuels UDP-GlcNAc biosynthesis upon GFAT1 knockout. Altogether, our data implicate HA as a novel nutrient for PDA, where HA regulates PDA metabolism by refueling the HBP via the GlcNAc salvage pathway. This supports PDA survival and proliferation (**Fig. 2-9N**).

## 2.3 Discussion

The HBP is activated in a KRAS*-dependent manner in PDA via transcriptional regulation of *Gfpt1*[6], and it is similarly elevated in numerous cancers to provide a diverse set of functions, including the regulation of proliferation, survival, angiogenesis, and metastasis[10]. As such, we and others have proposed that the HBP may provide a selective vulnerability for cancer therapy, with GFAT1 as an attractive therapeutic target[6,11,43,44]. Of note, GFAT2 is a homolog of GFAT1, and it too has been implicated as a drug target with context and tissue-

specific functions[45,46]. We did not pursue GFAT2 in this study because it was neither regulated by KRAS* nor basally expressed in the models employed herein.

Several pan glutamine-deamidase inhibitors (e.g. azaserine and 6-diazo-5-oxo-L-norleucine), which potently suppress GFAT activity, have demonstrated anti-tumor activity *in vitro* and *in vivo* in PDA and other cancers[47,48]*.* However, because these drugs are not specific to the HBP, it has not been clear what impact GFAT-specific inhibition had on these phenotypes. As such, we took a genetic approach to knock out GFAT1 to elucidate the role of the HBP in PDA. In the PDA models tested, we found that GFAT1 knockout was not compatible with PDA cell proliferation *in vitro,* unless the media were supplemented with GlcNAc or GalNAc (**Fig. 2-1C,D** and **Fig. 2-9F**). However, these same cells readily formed tumors *in vivo* in subcutaneous and orthotopic models (**Fig. 2-1E-G**).

The stark discrepancy in phenotypes led us to hypothesize that the TME was providing the means to bypass GFAT1. Indeed, we found that denatured conditioned media from CAFs and wild type PDA cells were able to rescue viability in GFAT1 knockout PDA cells, implicating a molecule(s) without tertiary structure (**Fig. 2-3**). By examining several GlcNAc-containing candidates, we discovered a previously unknown role of HA as a nutrient source for PDA (**Fig. 2-5,8**). Of note, despite identifying that wild type PDA cells can produce HA, it is not our intention to indicate that HA in PDA tumors was deposited by the cancer cells. For example, HA is abundantly deposited in GFAT1 knockout subcutaneous PDA tumors (**Fig. 2-8H**). Rather, we found that wild type PDA CM could rescue the proliferation of GFAT1 knockout PDA cells in vitro, and we utilized this as a tool to study the process. The constellation of cell types in the pancreatic TME that produce/deposit/process HA is an area of active investigation. Either way, in sum we report that HA can refill the HBP via the GlcNAc salvage pathway to support PDA survival and proliferation.

HA is traditionally regarded as a structural component in physiology[49]. In addition to this role, a wealth of studies have ascribed other functions to HA. For example, HA can activate cell-cell contact-mediated signal transduction through CD44 and/or receptor for HA-mediated motility (RHAMM)[50]. The signaling activity/function of HA depends on its MW[49,51]. Similarly, a recent study illustrated that breakdown of the HA matrix with hyaluronidase enabled the interaction between growth factors and growth factor receptors[39]. This promoted glucose metabolism, cellular proliferation, and migration. The role of HA in GFAT1 knockout PDA cells described herein is likely independent of its structural and signaling functions, given that we observe considerably greater rescue with o-HA (**Fig. 2-5H,I**), a form of HA that is not traditionally considered for these purposes. Together with the increased rescue by o-HA, several additional experiments also suggested that intracellular catabolism of high molecular weight HA impedes its use as a fuel. Namely, while high molecular weight HA-FITC is readily captured by PDA cells (**Fig. 2-5F**), HAase catabolism of HA potentiates rescue of GFAT1 (**Fig. 2-5G**).

Our study introduces a novel role to HA as a fuel for PDA tumor growth (**Fig. 2-5H,I**), further highlighting the significance and biological complexity of this predominant glycosaminoglycan. Additionally, our study suggests that NAGK, through which HA-mediated GlcNAc presumably refuels the HBP in vivo, may be an attractive therapeutic target for PDA. Indeed, a recent study demonstrated that NAGK knockout in PDA impairs tumor growth in vivo, while only exhibiting a modest impact on cellular proliferation in vitro[52]. These results are consistent with our observations that the GlcNAc salvage pathway is used to fill UDP-GlcNAc pools with HA-derived GlcNAc (**Fig. 2-9N**). Our study also contributes to a growing body of data illuminating unexpected nutrient sources in the TME that support cancer metabolism[14,15,17-22,53], and this raises the possibility that other glycosaminoglycans may be similarly scavenged.

Due to its extremely hydrophilic nature, HA retains water and acts as a cushioning agent in tissue homeostasis and biomechanical integrity[49]. In PDA, HA is a predominant component of the TME, and its water-retaining property is one of the main drivers of the supraphysiological intratumoral pressure[54]. This pressure can exceed 10-fold that observed in the normal pancreas, and, as a result, tumor vasculature collapses [41,55,56]. The limited access to circulation impairs nutrient and oxygen delivery, and it has been proposed that this is a critical impediment to tumoral drug delivery[57]. Indeed, in animal models, breakdown of the HA matrix with a therapeutic hyaluronidase (PEGPH20) reduces intratumoral pressure, restores circulation, which facilitates drug delivery, and thereby improves response to chemotherapy[41,56]. Based on these promising observations, PEGPH20 was tested in clinical trials alongside standard of care chemotherapy. Despite the successes in the preclinical models, PEGPH20 did not extend PDA patient survival[58].

The discrepancy between the clinical response to PEGPH20 and the preclinical data remains an active area of investigation and may concern the myriad additional roles of HA. For example, the HA matrix may be necessary to restrain tumor dissemination, as was shown for CAF depletion studies in PDA[59-62]. Thus, the benefits afforded by enhanced drug penetration facilitated by PEGPH20 may be negated by this side effect. Along these lines, HA degradation may also enhance tumor metabolism and growth. This could occur through growth factor signaling-dependent[39] as well as signaling-independent pathways, like the GlcNAc salvage pathway described herein. In contrast, reduction in the HA content of tumors also facilitates T cell invasion[48], which may complement immunotherapy approaches, a concept that would be hindered by immunosuppressive chemotherapies. Given the conflicting roles of HA in tumor restraint and tumor growth, considerable work remains to be done to determine the most effective way to exploit this feature of pancreatic cancer.

## 2.4 Materials and Methods

*Cell Culture*

MiaPaCa2 (ATCC Cat# CRM-CRL-1420, RRID:CVCL_0428) and HPAC (ATCC Cat# CRL-2119, RRID:CVCL_3517) were obtained from ATCC. TU8988T (DSMZ Cat# ACC-162, RRID:CVCL_1847) was obtained from DSMZ. Patient-derived CAFs[63] were a generous gift from Rosa Hwang, and FL5.12 cells were a generous gift from Dr. Aimee Edinger. All cells were routinely checked for mycoplasma contamination with MycoAlert PLUS (Lonza) and validated for authenticity annually by STR profiling. Cells were maintained in standard high glucose DMEM without pyruvate (Gibco) supplemented with 10% fetal bovine serum (FBS; Corning). GFAT1 null PDA were cultured in standard media supplemented with 10mM GlcNAc (Sigma). GFAT1 null NAGK knockout PDA were cultured in standard media supplemented with 10mM GalNAc (Sigma). Low nutrient media was made with DMEM without glucose, glutamine and pyruvate (Gibco). Glucose, glutamine, and FBS were added to the final concentration of 1.25mM, 0.2mM and 1%, respectively. FL5.12 cells were maintained in RPMI 1640 (Gibco) supplemented with 10% FBS, 10mM HEPES (Sigma), 55μM β-mercaptoethanol (Sigma), antibiotics, 2mM glutamine, and 500 pg/mL recombinant murine IL-3 (Peprotech 213-13).

*Generation of CRISPR/Cas9 knockout clones*

GFAT1 and NAGK knockout PDA cell lines were generated using CRISPR/Cas9 method described previously (22). Overlapping oligonucleotides (Feng Zhang lab human GeCKOv2 CRISPR knockout pooled library; Addgene #1000000048) were annealed to generate sgRNA targeting GFAT1 or NAGK. sgRNA was cloned directly into the overhangs of PX459 V2.0 vector (Feng Zhang lab; Addgene plasmid #62988) that was digested with BbsI. The resulting CRISPR/Cas9 plasmid was transformed into chemically competent Stbl3 cells, miniprepped for plasmid DNA, and sequence-verified. sgRNA oligonucleotide pairs for GFAT1[11] and NAGK are as follows: GFAT1 (sg1 Fwd 5′-CACCgCTTCAGAGACTGGAGTACAG-3′; sg1 Rev 5′-

AAACCTGTACTCCAGTCTCTGAAGc-3′) and NAGK (sg1 Fwd 5'-CACCgTAGGGGAGGCACACGATCCG; sg1 Rev 5'-AAACCGGATCGTGTGCCTCCCCTAc-3'; sg2 Fwd 5'-CACCgGCCTAGGGCCTATCTCTGAG-3'; sg2 Rev 5'-AAACCTCAGAGATAGGCCCTAGGCc-3'). Human PDA were transiently transfected using Lipofectamine 3000 according to the manufacturer's instructions. Cells were selected with puromycin in the presence of GlcNAc (GFAT1 knockout bulk population) or GalNAc (GFAT1 NAGK double knockout bulk population). To select clones, polyclonal pools were seeded into 96-well plates at a density of 1 cell per well. Individual clones were expanded and verified via western blot and Sanger sequencing. TU8988T clone B9 has a 10 base pair (bp) and a 1bp deletion in GFAT1; TU8988T clone D10 has 2 different 1bp deletions in GFAT1; MiaPaCa2 clone M12 has 2 different 1bp deletions in GFAT1; HPAC clone H1 has a 187bp deletion in GFAT1; HPAC clone H7 has a 187bp deletion in GFAT1.

*Conditioned media*

Conditioned media was generated by culturing cells in 15 $cm^2$ plates (25mL growth media/plate) for 72 hours at 37°C, 5% $CO_2$, so that they reached ~90% confluence. The media were then filtered through a 0.45µm polyethersulfone membrane (VWR). Boiled conditioned media was warmed to 100°C for 15 minutes. Freeze-thaw conditioned media were initially stored at -80°C and were thawed in a 37°C water bath on the day of the experiment. As indicated, fresh growth media were added to the conditioned media at the ratios indicated to avoid nutrient/metabolite exhaustion.

*Colony formation and proliferation assays*

For colony formation assays, cells were plated in a 6-well plate in biological triplicate at 500 cells/well in 2 mL of media and grown for 9-12 days. For proliferation assays, 5000 cells/well were plated. At end point, assays were fixed with 100% methanol for 10 minutes and stained with 0.5% crystal violet solution for 15 minutes. Relative colony formation was quantitated

manually in a blinded fashion. Proliferation was quantified by removing the dye with 10% acetic acid and measuring OD595.

*CyQUANT viability assay*

Cells were seeded in 96-well black wall, clear bottom plates at 1000 cells/well in 50µL of media and incubated at 37°C, 5% $CO_2$ for indicated time points. At each time point, media was aspirated and plates were stored at -80°C. Proliferation was determined by CyQUANT (Invitrogen) according to the manufacturer's instructions. SpectraMax M3 Microplate reader (Molecular Devices) was used to measure fluorescence.

*IncuCyte S3: Real-time, live-cell proliferation assay*

1000 cells were seeded per well in a 96-well plate and incubated at 37°C, 5% $CO_2$ for cells to equilibrate. The next day, media were aspirated, washed once with PBS, and replaced with different media as indicated. Proliferation was measured on IncuCyte S3 using phase object confluence as a readout.

*HA-FITC Uptake Experiments*

TU8988T cells (WT, B9-GFAT1KO, D10-GFAT1KO), and BxPC3 cells were seeded in 6-well plates with DMEM + 10% FBS + GlcNAc. The next day, cells were rinsed with PBS and the media was switched to DMEM + 10% FBS. The following day, cells were seeded on a chamber slide and grown in DMEM + 10% FBS. MiaPaCa2 cells (WT, M12-GFAT1KO) were treated similarly and were seeded in 6-well plates with DMEM + 10% FBS + GlcNAc. The next day, cells were rinsed with PBS and seeded on a chamber slide in DMEM + 10% FBS.

After one day in chamber slides, the media was removed, cells were rinsed with PBS, and cells were incubated with HA-FITC media for one hour at 37°C (or 1 min at 37°C as a negative control). After incubation, cells were rinsed and fixed with 10% formalin for 15 minutes at room temp. Wells were rinsed three times with PBS + 0.3% BSA and cells were blocked for one hour

at room temperature with PBS + 1% BSA. Cells were incubated overnight at 4°C with Mouse anti-panCK (Cytokeratin, DAKO M3515, [1:100]) in PBS + 1% BSA. The following day, cells were rinsed three times with PBS + 0.3% BSA and incubated 1 hour at room temperature with an anti-mouse Alexa fluor secondary antibody (Invitrogen) in PBS + 1% BSA. Following incubation, cells were rinsed and mounted with ProLong Gold Antifade Mountant with DAPI (Invitrogen).

Olympus BX53F microscope, Olympus DP80 digital camera, and CellSens Standard software were used for imaging and 6 representative images were taken per cell line and condition. Uptake index was calculated using the Analyze Particles feature in ImageJ after automatic thresholding. The cell outlines and regions of interest were determined using panCK expression and HA-FITC particles were measured. HA-FITC particle area was plotted as a percent of total cell area.

### *HA ELISA*

An HA ELISA kit (cat no. DY3614, R&D Systems) was used to determine the concentration of HA in all the different conditioned media samples as per manufacturer's instructions.

### *Metabolite sample preparation*

Intracellular metabolite fractions were prepared from cells grown in 6-well plates. The media was aspirated, and cells were incubated with cold (−80°C) 80% methanol (1mL/well) on dry ice for 10 minutes. Then, the wells were scraped with a cell scraper and transferred to 1.5mL tubes on dry ice. To measure GlcNAc concentration in different conditioned media, 0.8mL of ice-cold 100% methanol was added to 0.2mL of conditioned media, and the mixture was incubated on dry ice for 10 minutes.

After incubation of cell or media fractions on dry ice, the tubes were centrifuged at 15,000rpm for 10 minutes at 4°C to pellet the insoluble material, and the supernatant was collected in a

fresh 1.5mL tube. Metabolite levels of intercellular fractions were normalized to the protein content of a parallel sample, and all samples were lyophilized on a SpeedVac, and re-suspended in a 50:50 mixture of methanol and water in HPLC vials for LC-MS/MS analysis.

*Liquid chromatography-coupled mass spectrometry*

To detect UDP-GlcNAc, the Shimadzu NEXERA integrated UHPLC system with a LC30AD pump, SIL30AC autosampler, CTO30A column oven, CBM20A controller was coupled with the AB Sciex TripleTOF 5600 MS system with DuoSpray ion source. All calibrations and operations were under control of Analyst TF 1.7.1. Calibrations of TOF-MS and TOF-MS/MS were achieved through reference APCI source of SCEIX calibration solution. A high throughput LC method of 8 min with flowrate of 0.4 ml/min with a Supelco Ascentis Express HILIC (75 mm X 3.0 mm, 2.7 µm). Solvent A was made of 20 mM ammonium acetate of 95% water and 5% acetonitrile at pH 9.0. Solvent B was 95% acetonitrile and 5% water. LC gradient 0.0-0.5 min 90% B, 3 min 50% B, 4.10 min 1% B, 5.5 min 1% B, 5.6 min 90% B, 6.5 min 90% B, 8 min stopping. Key parameters on the MS were the CE and CE spread of -35ev, 15ev. Data were compared to a reference standard. Data processing was performed by Sciex PeakView, MasterView, LibraryView and MQ software tools and ChemSpider database.

To measure GlcNAc concentration in the various conditioned media, we utilized an Agilent Technologies Triple Quad 6470 LC/MS system consisting of 1290 Infinity II LC Flexible Pump (Quaternary Pump), 1290 Infinity II Multisampler, 1290 Infinity II Multicolumn Thermostat with 6 port valve and 6470 triple quad mass spectrometer. Agilent Masshunter Workstation Software LC/MS Data Acquisition for 6400 Series Triple Quadrupole MS with Version B.08.02 is used for compound optimization and sample data acquisition.

A GlcNAc standard was used to establish parameters, against which conditioned media were analyzed. For LC, an Agilent ZORBAX RRHD Extend-C18, 2.1 × 150 mm, 1.8 um and ZORBAX

Extend Fast Guards for UHPLC were used in the separation. LC gradient profile is: at 0.25 ml/min, 0-2.5 min, 100% A; 7.5 min, 80% A and 20% C; 13 min 55% A and 45% C; 20 min, 1% A and 99% C; 24 min, 1% A and 99% C; 24.05 min, 1% A and 99% D; 27 min, 1% A and 99% D; at 0.8 ml/min, 27.5-31.35 min, 1% A and 99% D; at 0.6 ml/min, 31.50 min, 1% A and 99% D; at 0.4 ml/min, 32.25-39.9 min, 100% A; at 0.25 ml/min, 40 min, 100% A. Column temp is kept at 35 ºC, samples are at 4 ºC, injection volume is 2 µl. Solvent A is 97% water and 3% methanol 15 mM acetic acid and 10 mM tributylamine at pH of 5. Solvent C is 15 mM acetic acid and 10 mM tributylamine in methanol. Washing Solvent D is acetonitrile. LC system seal washing solvent 90% water and 10% isopropanol, needle wash solvent 75% methanol, 25% water.

6470 Triple Quad MS is calibrated with ESI-L Low concentration Tuning mix. Source parameters: Gas temp 150 ºC, Gas flow 10 l/min, Nebulizer 45 psi, Sheath gas temp 325 ºC, Sheath gas flow 12 l/min, Capillary -2000 V, Delta EMV -200 V. Dynamic MRM scan type is used with 0.07 min peak width, acquisition time is 24 min. Delta retention time of plus and minus 1 min, fragmentor of 40 eV and cell accelerator of 5 eV are incorporated in the method.

*Xenograft studies*

Animal experiments were conducted in accordance with the Office of Laboratory Animal Welfare and approved by the Institutional Animal Care and Use Committees of the University of Michigan. NOD-SCID gamma (NSG) mice (Jackson Laboratory), 6-10 weeks old of both sexes, were maintained in the facilities of the Unit for Laboratory Animal Medicine (ULAM) under specific pathogen-free conditions. Protocol#: PRO00008877.

Wild type TU8988T and two verified GFAT1 null clones (B9 and D10) were trypsinized and suspended at 1:1 ratio of DMEM (Gibco, 11965-092) cell suspension to Matrigel (Corning, 354234). 150-200µL were used per injection. Orthotopic tumors were established by injecting $0.5 \times 10^6$ cells in 50µL of 1:1 DMEM to Matrigel mixture. The experiment lasted five weeks. For

subcutaneous xenograft studies with the pooled populations or validated clones, tumors were established with 5 x $10^6$ cells in 200µL of 1:1 DMEM to Matrigel mixture.

Tumor size was measured with digital calipers two times per week. Tumor volume (V) was calculated as V = 1/2(length x width$^2$). At endpoint, final tumor volume and mass were measured prior to processing. Tissue was snap-frozen in liquid nitrogen then stored at −80°C.

*Western blot analysis*

After SDS-PAGE, proteins were transferred to PVDF membrane, blocked with 5% milk, and incubated with primary antibody overnight at 4°C. The membranes were washed with TBST, incubated with the appropriate horseradish peroxidase-conjugated secondary antibody for 1hr and visualized on Bio-Rad imager with enhanced chemiluminescence detection system or exposed on radiographic film.

*Immunohistochemistry on subcutaneous and orthotopic tumors*

Subcutaneous and orthotopic tumors were fixed in Z-fix overnight, paraffin embedded, and sectioned onto slides. Sections were deparaffinized in xylene, rehydrated, and blocked with 2.5% BSA prior to incubation with biotinylated HABP antibody (Calbiochem #385911, [1:200]) overnight at 4°C. Vector Laboratories Vectastain Elite ABC-HRP Kit (PK-6100) and Vector Laboratories DAB Substrate Kit (SK-4100) were used for peroxidase detection of HABP signal.

*Histological Scoring*

HABP-stained tumors, normal pancreas tissue (negative control), and transformed pancreas tissue from KC mice (positive control) were processed and stained for HABP as described above. Ten representative 20x images from each group were scored blinded based on HABP staining. Staining was scored on the following scale: 0, no staining; 1, minimal staining; 2, moderate to strong staining in at least 20% of cells; 3, strong staining in at least 50% of cells.

*Antibodies*

The following antibodies were used in this study: VINCULIN (Cell Signaling 13901), ACTIN (Santa Cruz sc-47778), GAPDH (Cell Signaling 5174), GFAT1 (Abcam 125069), NAGK (Atlas Antibodies HPA035207), O-GlcNAc (Abcam 2735), panCK (Cytokeratin, DAKO M3515), biotinylated HABP (Calbiochem 385911), secondary anti-mouse-HRP (Cell Signaling 7076), and secondary anti-rabbit-HRP (Cell Signaling 7074).

*Detection and quantification of macropinocytosis*

The macropinocytosis index was measured as previously described[64]. In brief, cells were seeded on the coverslips in 24-well plate for 24 hours and serum-starved for 18 h. Cells were incubated with 1mg/ml high molecular weight TMR–dextran (Fina Biosolutions) in serum-free medium for 30 min at 37 °C. Cells were then washed 5 times with cold DPBS and fixed in 4% polyformaldehyde for 15 min. The coverslips were mounted onto slides using DAKO Mounting Medium (DAKO) in which nuclei were stained with DAPI. At least six images were captured for each sample using an Olympus FV1000 confocal microscope and analyzed using the particle analysis feature in ImageJ (NIH). The micropinocytosis index for each field was calculated as follow: Macropinocytosis Index = (total particle area/total cell area) × 100%.

*Hyaluronic acid, hyaluronidase, and heparin*

Heparin was obtained from Sigma (H3393). Oligo HA (5kDa) was obtained from Lifecore Biomedical. Two different LMW HA were used in this study: 78 kDa HA (Pure Health solutions) and 60kDa HA (Lifecore Biomedical). To make 10mM oligo- or LMW HA media, HA was added slowly into high glucose DMEM without pyruvate, stirred for two hours at room temperature, and filtered through 0.20μm polyethersulfone membrane. FBS was added to a final concentration of 10%.

Hyaluronidase (Sigma H3506) treatment was performed as follows: 10mM LMW HA media and control media (DMEM + 10% FBS) were incubated with hyaluronidase, according to manufacturer's instructions, overnight in a 37°C water bath. The next day, media were boiled for 15 minutes to denature hyaluronidase. The resulting media were mixed 1:1 with fresh growth media to avoid effects of nutrient/metabolite exhaustion.

### *Preparation of necrotic FL5.12 cells*

Necrotic FL5.12 cells were prepared as described previously[34]. Cells were washed three times with PBS, cultured in the FL5.12 media without IL-3 (100 million cells/mL) for 72 hours. The necrotic cells were spun down at 13,000 rpm for 10 minutes at 4°C, and the pellets were stored at -80°C until use.

### *Statistical analysis*

Statistics were performed using GraphPad Prism 8. Groups of two were analyzed with two-tailed students t test. Groups of more than two were analyzed with one-way ANOVA Tukey post-hoc test. All error bars represent mean with standard deviation. A *P* value of less than 0.05 was considered statistically significant. All group numbers and explanation of significant values are presented within the figure legends.

## 2.5 Figures

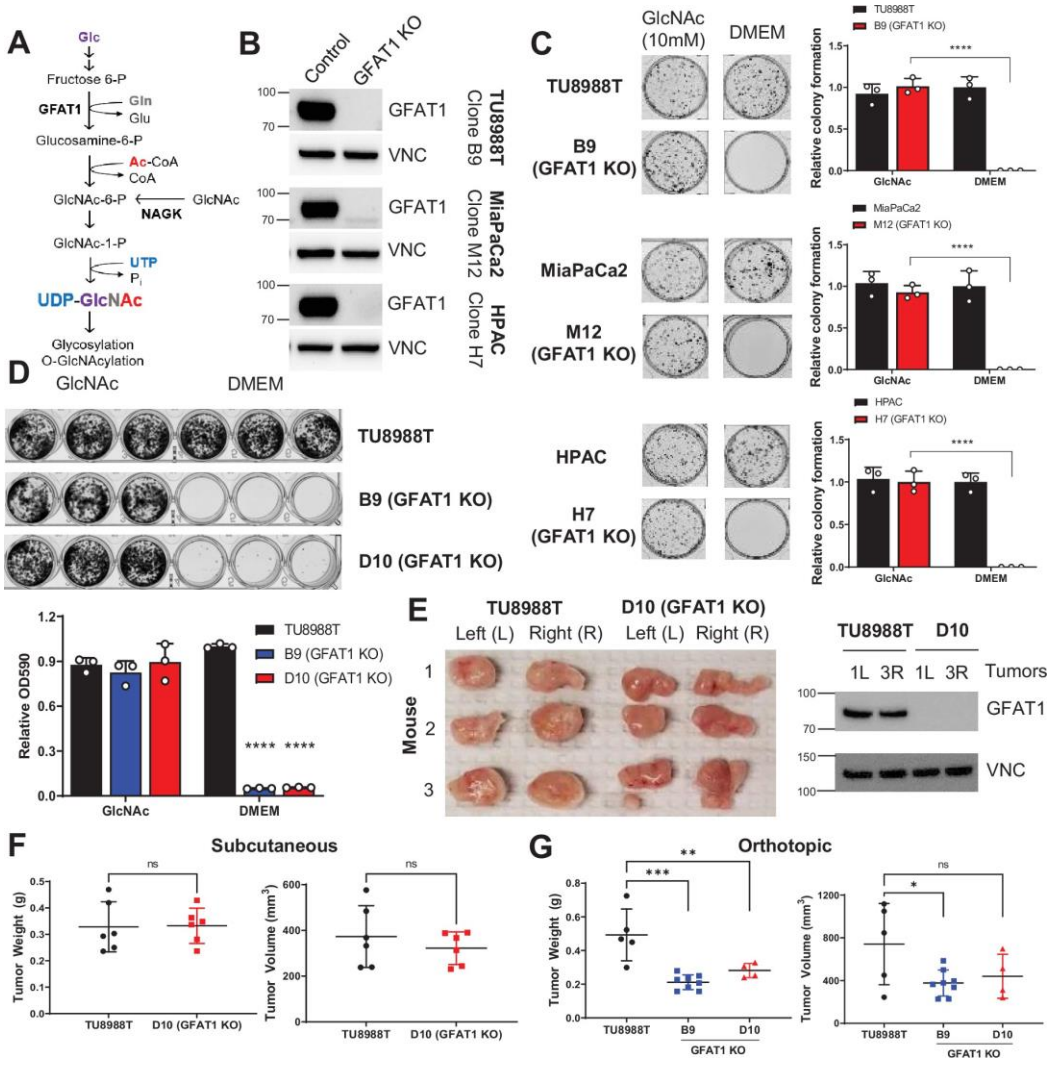


**Figure 2-1 PDA requires de novo hexosamine biosynthetic pathway fidelity in vitro but not in vivo.**

(**A**) Schematic overview of the hexosamine biosynthetic pathway (HBP) and the nutrient inputs. Ac-CoA, acetyl-coenzyme A; GFAT1, glutamine fructose 6-phosphate amidotransferase 1; Glc, glucose; GlcNAc, N-acetyl-glucosamine; Gln, glutamine; Glu, glutamate; NAGK, N-acetyl-glucosamine kinase; $P_i$, inorganic phosphorus; UTP, uridine-triphosphate. (**B**) Western blot of GFAT1 and loading control VINCULIN (VNC) from validated CRISPR/Cas9 knockout TU8988T, MiaPaca2, and HPAC clones and their control (non-targeted sgRNA). (**C**) Representative wells from a colony-forming assay in parental and clonally-derived GFAT1 knockout cell lines grown in base media (DMEM) or base media supplemented with 10mM GlcNAc. Data quantitated at right, n=3. (**D**) Proliferation assay in parental and two GFAT1 knockout clonal TU8988T cell lines. Representative wells are presented above data quantitated by crystal violet extraction and measured by optical density (OD) at 590nm, n=3. (**E**) Tumors from parental TU8988T (n=6) and GFAT1 knockout clone D10 (n=6) grown subcutaneously in immunocompromised mice. Accompanying western blot for GFAT1 and VNC loading control from representative tumor lysates. (**F**) Tumor volume and tumor weight from samples in **E**. (**G**) Tumor volume and tumor weight from parental TU8988T (n=5) and GFAT1 knockout clones B9 (n=8) and D10 (n=4) implanted and grown orthotopically in the pancreas of immunocompromised mice. Error bars represent mean ± SD. n.s., non-significant; *$P$ < 0.05; ** $P$ <0.01; *** $P$ <0.001; **** $P$ <0.0001.

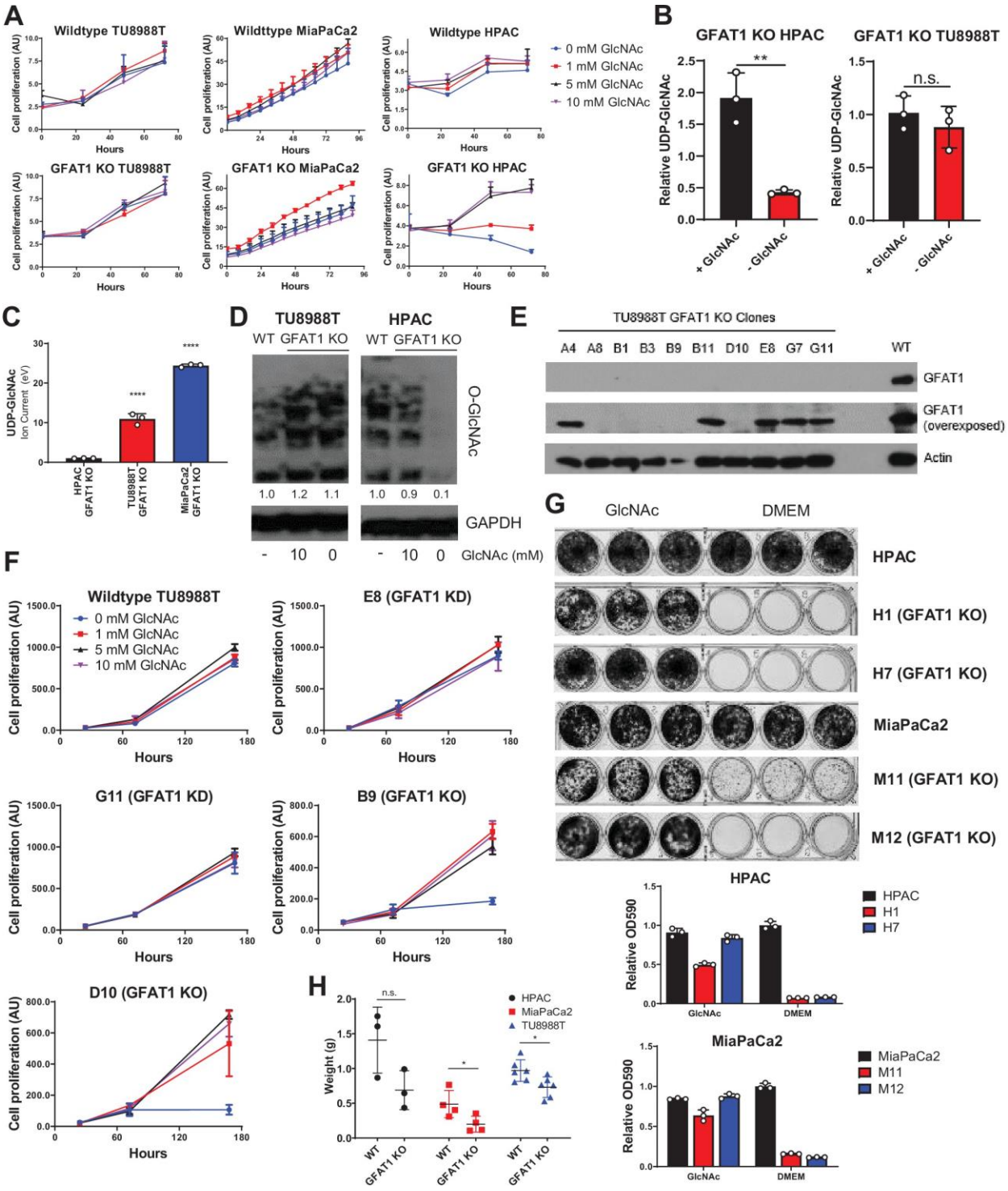


**Figure 2-2 Additional characterization of GFAT1 knockout PDA populations and clonal lines.**

(**A**) Proliferation kinetics of parental PDA cell lines and corresponding pooled populations of GFAT1 knockout cells supplemented with varying concentrations of GlcNAc (n=3). Cell quantity was assessed by Cyquant (DNA intercalating dye) and plotted in absorbance units (AU). (**B,C**) UDP-GlcNAc levels measured by liquid chromatography-coupled tandem mass spectrometry (LC-MS/MS) in (**B**) TU8988T and HPAC GFAT1 knockout lines in the presence or absence of 10 mM GlcNAc for 3 days, presented as

relative abundance (n=3), and (**C**) TU8988T, HPAC, and MiaPaCa2 GFAT1 knockout cells grown without GlcNAc for 3 days (n=3), presented as relative ion abundance. (**D**) Western blot of proteome O-GlcNAc and loading control GAPDH in parental and GFAT1 knockout TU8988T and HPAC. GFAT1 knockout lines were grown in the presence or absence of 10mM GlcNAc for 3 days. (**E**) Western blot for GFAT1, at short and long exposure, and ACTIN loading control in a panel of clonal cell lines selected from the pooled population of GFAT1 knockout TU8988T cells. (**F**) Proliferation kinetics of parental TU8988T (GFAT1 WT) and clonal cell lines E8, G11, B9, and D10 selected from the pooled GFAT1 knockout population supplemented with varying concentrations of GlcNAc (n=3). Clones correspond to those in the western blot in **E**. Cell quantity was assessed by cell titer glo and plotted in relative fluorescent units (RFU). (**G**) Representative wells from proliferation assay in parental and two GFAT1 knockout clonal HPAC and MiaPaCa2 cell lines. At bottom, data are quantitated by crystal violet extraction and measurement of optical density (OD) at 590nm, n=3. (**H**) Tumors from parental (n=3) and GFAT1 knockout (n=3) HPAC; parental (n=4) and GFAT1 knockout (n=4) MiaPaCa2; and parental (n=6) and GFAT1 knockout (n=6) TU8988T cell lines grown subcutaneously in immunocompromised mice. Error bars represent mean ± SD. n.s., non-significant; *$P < 0.05$; ** $P < 0.01$; **** $P < 0.0001$.

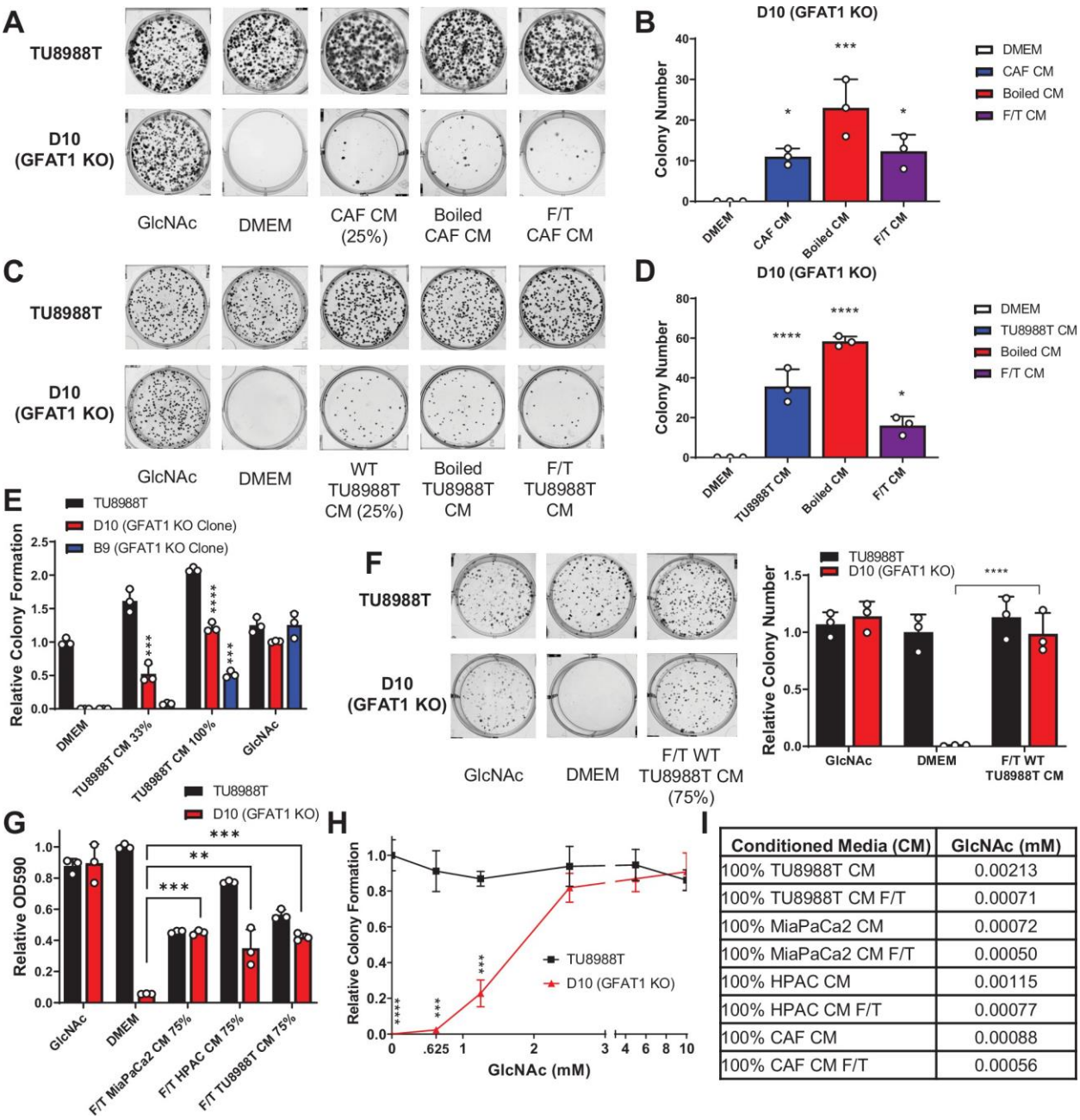


| Conditioned Media (CM) | GlcNAc (mM) |
|---|---|
| 100% TU8988T CM | 0.00213 |
| 100% TU8988T CM F/T | 0.00071 |
| 100% MiaPaCa2 CM | 0.00072 |
| 100% MiaPaCa2 CM F/T | 0.00050 |
| 100% HPAC CM | 0.00115 |
| 100% HPAC CM F/T | 0.00077 |
| 100% CAF CM | 0.00088 |
| 100% CAF CM F/T | 0.00056 |

**Figure 2-3 Conditioned media from CAFs and wild type PDA cells support proliferation of GFAT1 knockout cells.**

(**A**) Representative wells from a colony-forming assay in parental TU8988T and GFAT1 knockout clonal line D10 in 10mM GlcNAc, base media (DMEM), or base media supplemented 1:3 (25%) with cancer associated fibroblast (CAF) conditioned media (CM), boiled CAF CM, or CAF CM subject to freeze-thaw (F/T). (**B**) Quantitation of colonies from data in **A** (n=3). (**C**) Representative wells from a colony-forming assay in parental TU8988T and GFAT1 knockout clonal line D10 in 10mM GlcNAc, DMEM, or base media supplemented 1:3 (25%) with CM from wild type TU8988T cells, boiled TU8988T CM, or TU8988T CM subject to F/T. (**D**) Quantitation of colonies from data in **C** (n=3). (**E**) Quantitation of colony forming assay data of parental and GFAT1 knockout clonal TU8988T lines in base media, positive control GlcNAc, wild type TU8988T CM diluted 1:2 (33%) or used directly (100%) (n=3). (**F**) Representative wells and quantitation of colony forming assay data of parental and GFAT1 knockout clonal TU8988T lines in

base media, positive control GlcNAc, and wild type TU8988T CM subject to F/T and diluted 3:1 (75%) (n=3). (**G**) Quantitation of colony forming assay data of parental and GFAT1 knockout clonal TU8988T lines in base media, positive control GlcNAc, or wild type TU8988T, HPAC, or MiaPaCa2 CM subject to F/T and diluted 3:1 (75%) (n=3). (**H**) GlcNAc dose response curve presented as relative colony number for parental and GFAT1 knockout TU8988T cells (n=3). (**I**) Mean of absolute quantitation of GlcNAc in various CM by LC-MS/MS (n=3). Error bars represent mean ± SD. *P < 0.05; ** P <0.01; *** P <0.001; **** P <0.0001.

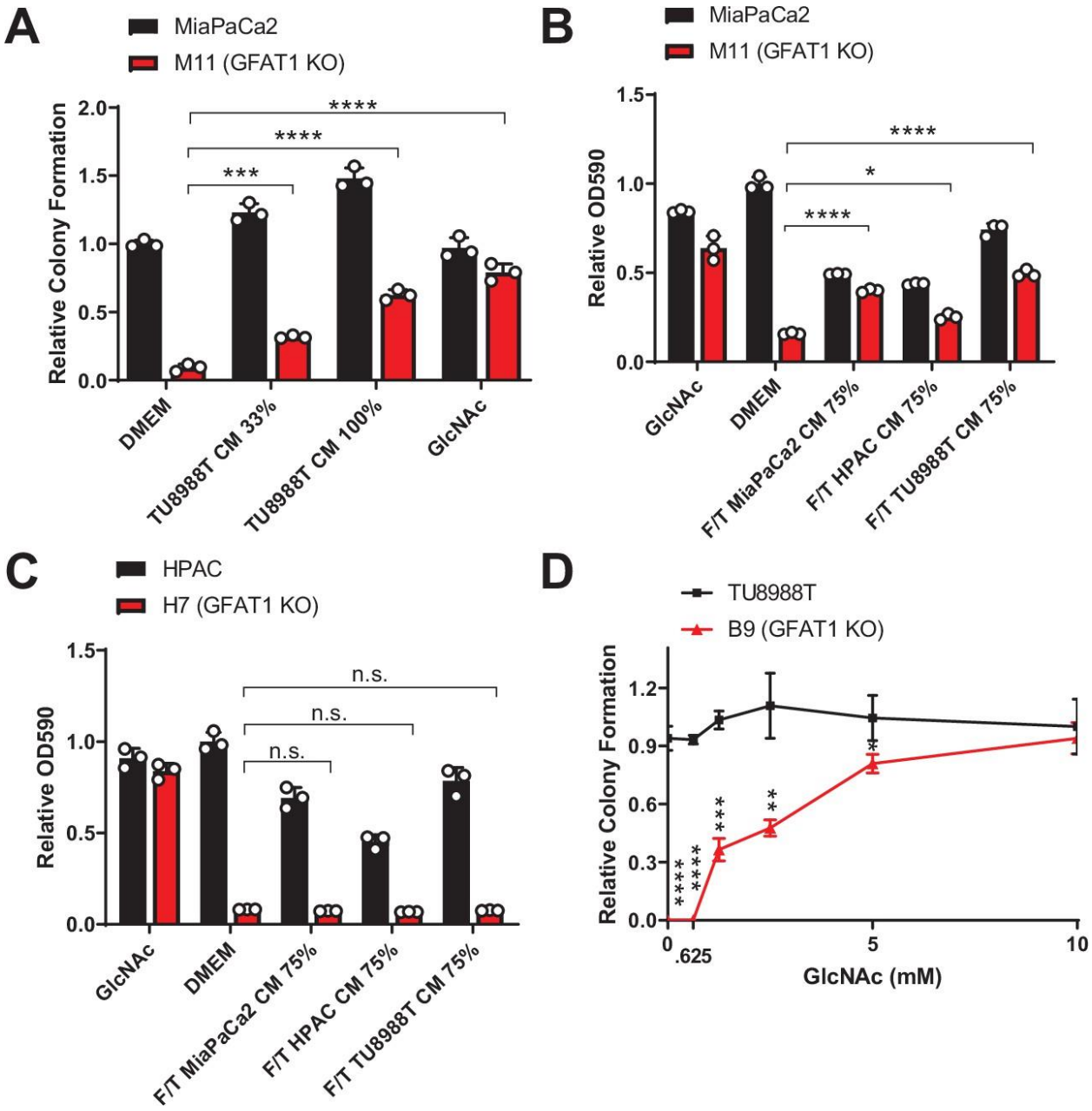


**Figure 2-4 Rescue activity of conditioned media and GlcNAc in GFAT1 knockout cells.**

(**A**) Quantitation of colony forming assay data of parental MiaPaCa2 and GFAT1 knockout clonal line M11 in base media (DMEM), positive control GlcNAc, wild type TU8988T CM diluted 1:2 (33%) or used directly (100%) (n=3). (**B,C**) Quantitation of proliferation assay data of (**B**) parental MiaPaCa2 and GFAT1 knockout clonal line M11 and (**C**) parental HPAC and GFAT1 knockout clonal line H7 in base media (DMEM), positive control GlcNAc, or wild type TU8988T, HPAC, or MiaPaCa2 CM diluted 3:1 (75%) that was subjected to freeze-thaw (F/T) (n=3). Data represent crystal violet extracted from cells at endpoint and measured by optical density (OD) at 590nm. (**D**) GlcNAc dose response curve presented as relative colony number for parental TU8988T cells and GFAT1 knockout clonal line B9 (n=3). Error bars represent mean ± SD. n.s., non-significant; *$P$ < 0.05; ** $P$ <0.01; *** $P$ <0.001; **** $P$ <0.0001.

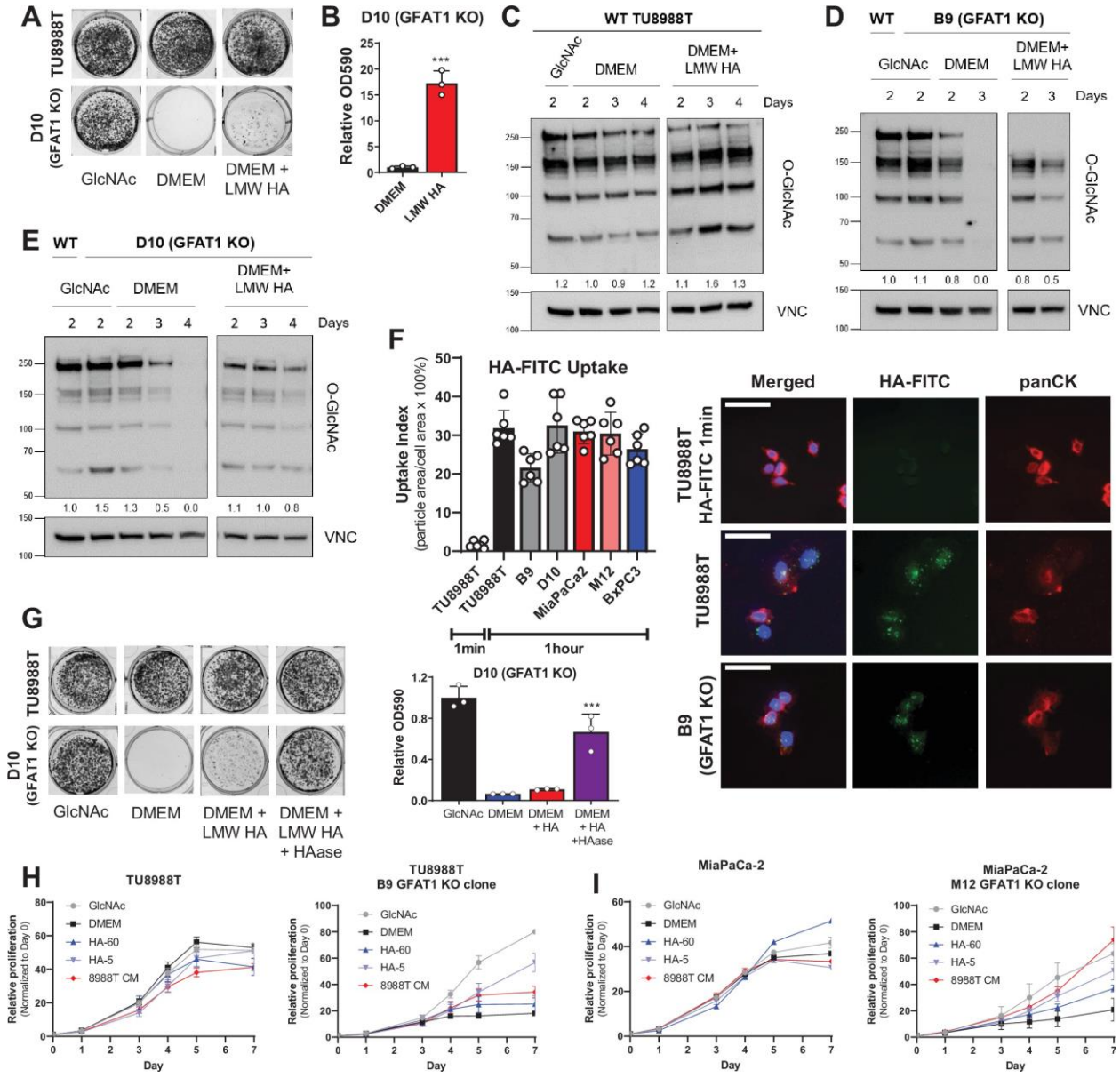


**Figure 2-5 Hyaluronic acid rescues GFAT1 knockout PDA cells.**

(**A**) Representative wells from a colony-forming assay in parental and clonally-derived GFAT1 knockout TU8988T cell lines grown in base media (DMEM), positive control GlcNAc (10mM), or low molecular weight (LMW) hyaluronic acid (78kDa HA, 10mM). (**B**) Quantitation of data from **A** (n=3). (**C**) Western blot of proteome O-GlcNAc and loading control VINCULIN (VNC) in parental TU8988T cells grown in base media (DMEM) plus GlcNAc or LMW HA for the indicated time points. Band density was quantitated, normalized to control, and presented below the blot. (**D,E**) Western blot of proteome O-GlcNAc and loading control VNC in GFAT1 knockout clonal lines (**D**) B9 and (**E**) D10 in base media (DMEM) plus GlcNAc or LMW HA for the indicated time points. Wild type [65] TU8988T included as control. Band density was quantitated, normalized to control, and presented below the blot. (**F**) Quantitation of HA-FITC uptake in wild type (TU8988T, MiaPaCa2, BxPC3) and GFAT1 knockout clones (B9, D10, M12) presented as percent total particle area over total cell area at 1 minute or 1 hour; n=6 frames per condition. Cell area was calculated by staining for pan-cytokeratin (panCK). At right, representative images. Scale bar, 50 µm. (**G**) Representative wells of a proliferation assay in parental TU8988T and GFAT1 knockout clonal line D10 grown in base media (DMEM), positive control GlcNAc (10mM), or base media supplemented

1:1 with boiled LMW HA (10mM) with and without pre-digestion with hyaluronidase (HAase). At endpoint, cells are stained with crystal violet, and the stain was then extracted and quantitated by OD at 590nm (n=3). (**H,I**) Proliferation time course, as measured on the Incucyte, of (**H**) TU8988T and (**I**) MiaPaCa parental and GFAT1 knockout cells in base media (DMEM), positive control (GlcNAc), 60 kDa HA (LMW HA), 5 kDa HA (o-HA), or wild type TU8988T CM (n=3). Error bars represent mean ± SD. *** *P* <0.001.

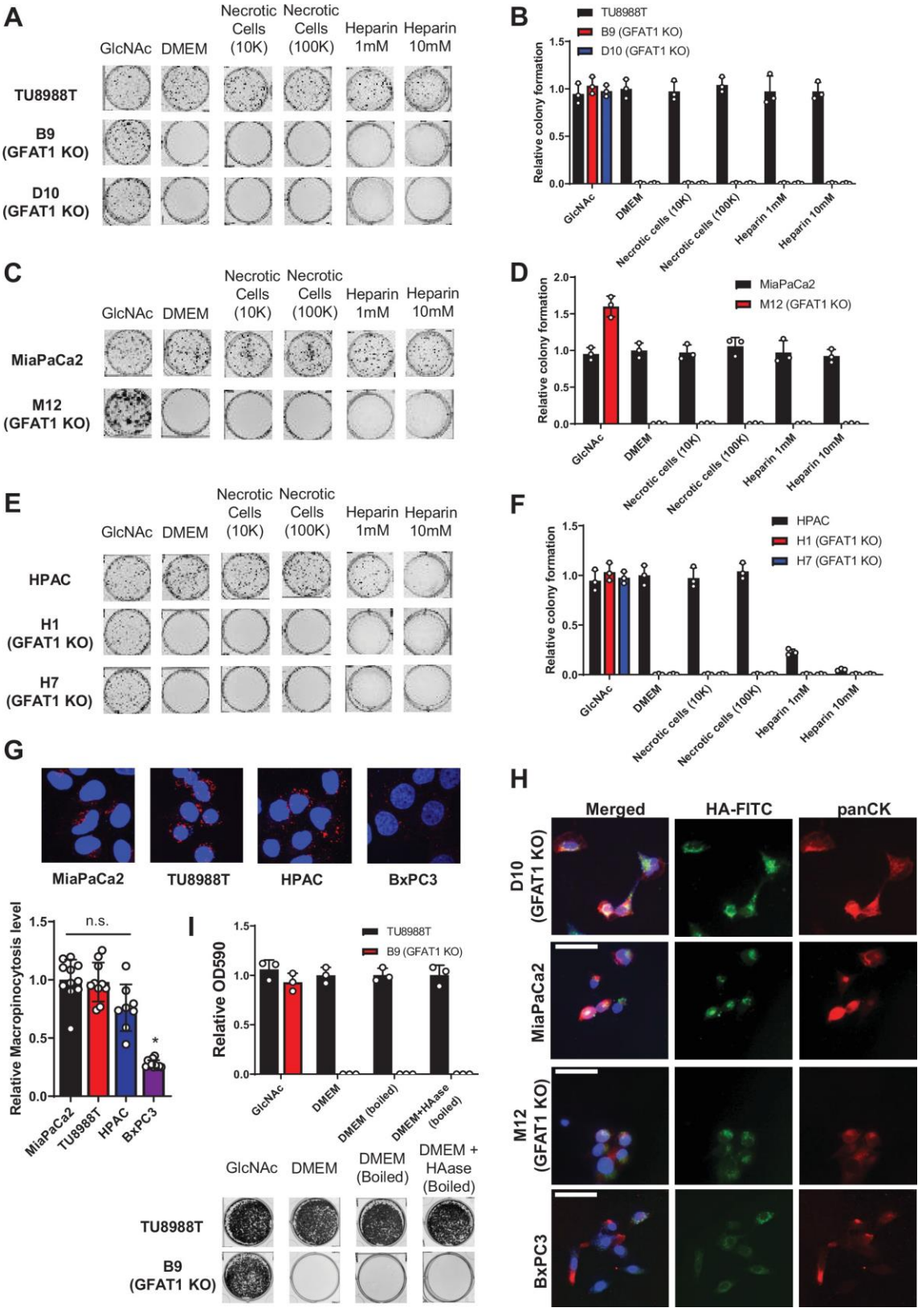


**Figure 2-1 Characterization of macropinocytosis and glycosaminoglycan rescue activity in PDA and GFAT1 knockout cells.**

(**A-F**) Representative colony formation assays and their quantitation following treatment with two concentrations of heparin or necrotic cell debris that contain complete cellular contents, relative to base media (DMEM) and positive control GlcNAc in (**A,B**) parental and GFAT1 knockout TU8988T, (**C,D**) parental and GFAT1 knockout MiaPaCa2, and (**E,F**) parental and GFAT1 knockout HPAC. (**G**) Immunostaining images of intracellular fluorescently-tagged dextran (red) engulfed by macropinocytosis in PDA cell lines. Nuclear DAPI staining in blue. Quantitation of macropinocytotic index presented at bottom for n=6 wells per biological replicate (n=3). (**H**) Representative images for the data presented in Figure 3F. HA-FITC is presented in green with pan-cytokeratin (panCK) in red. Nuclear staining with DAPI in blue. Scale bar, 50 μm. (**I**) Quantitated data are presented above representative wells from a proliferation assay in parental TU8988T and GFAT1 knockout clone B9 in 10mM GlcNAc, base media (DMEM), base media supplemented 1:1 with boiled DMEM, or base media supplemented 1:1 with boiled HAase-treated DMEM. Quantitated data represent crystal violet extracted from cells at endpoint and measured by optical density (OD) at 590nm (n=3). Error bars represent mean ± SD. n.s., non-significant; *$P < 0.05$.

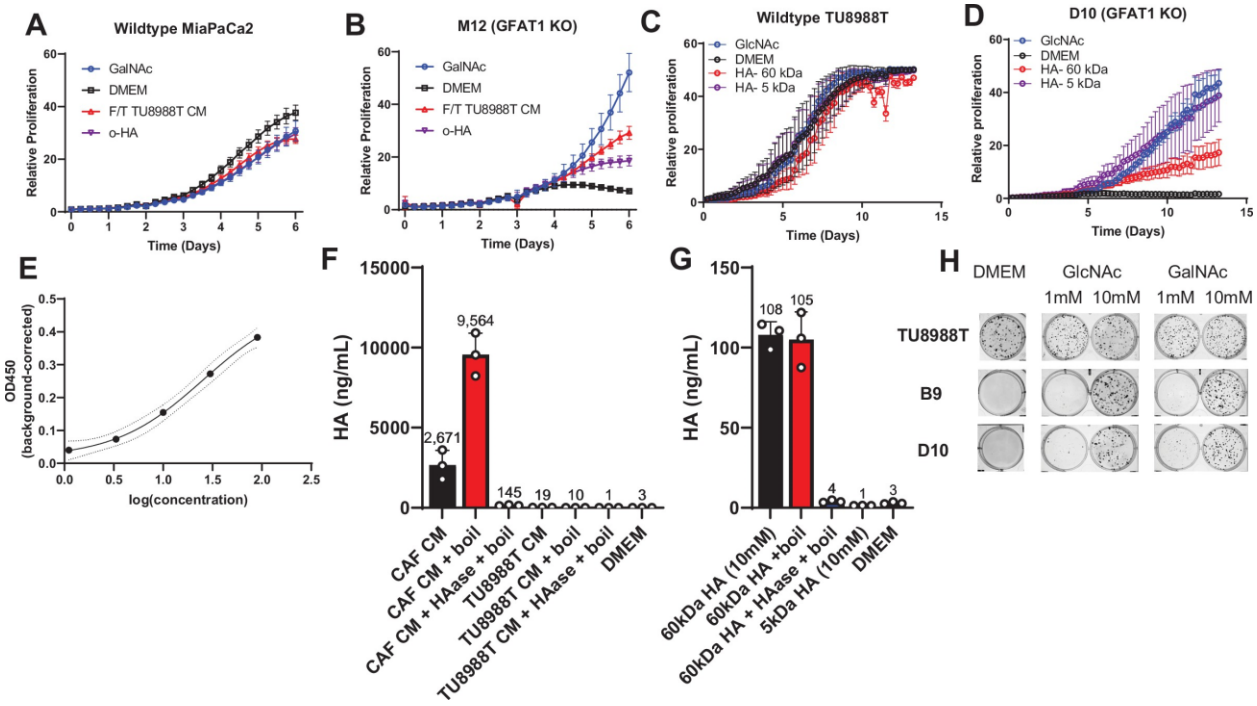


**Figure 2-7 Analysis of hyaluronic acid formulation on GFAT1 rescue and composition in conditioned media.**

(**A,B**) Proliferation time course of (**A**) parental MiaPaCa2 and (**B**) GFAT1 knockout cells in base media (DMEM), positive control (GlcNAc), 5 kDa HA (o-HA), or wild type TU8988T conditioned media (CM) subject to freeze thaw (F/T) (n=3). (**C,D**) Proliferation time course of (**C**) parental TU8988T and (**D**) GFAT1 knockout cells in base media (DMEM), positive control (GlcNAc), 60 kDa HA (LMW HA), or 5 kDa HA (o-HA).(**E**) Dynamic range of HA detection by ELISA, employed to quantitate HA. (**F**) HA content in cancer associated fibroblast (CAF) and wildtype TU8988T CM, that treated with HAase, and that treated with boiled HAase, relative to DMEM alone negative control. (**G**) Detection of 10mM 60kDa and 5kDa HA standard and 60kDa standard treated with HAase, as well as that treated with boiled HAase, relative to DMEM alone negative control. (**H**) Representative wells from colony formation assays in parental and GFAT1 knockout clonal TU8988T cell lines in base media (DMEM), positive control GlcNAc, and N-acetyl-galactosamine (GalNAc). Quantitated data are presented in **Fig. 2-5F**. Error bars represent mean ± SD.

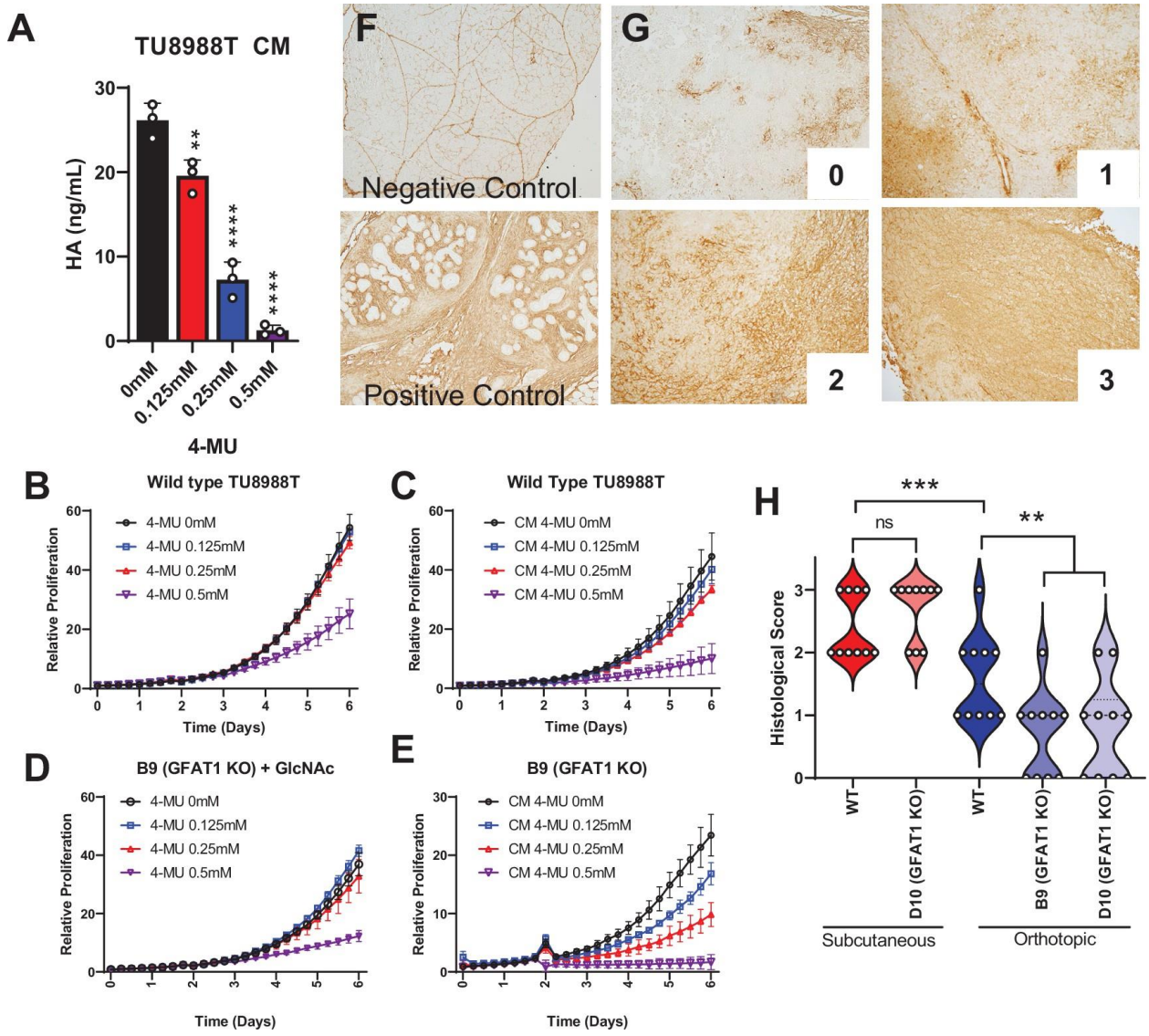


**Figure 2-8 Hyaluronic acid in conditioned media rescues GFAT1 knockout.**

**(A)** Quantification of HA in CM from wildtype TU8988T cells treated with varying doses of 4-MU (n=3). **(B-E)** Proliferation time course of (B,C) wild type TU8988T and (D,E) GFAT1 knockout TU8988T grown (B,D) directly in varying concentrations of 4-MU or (C,E) in CM from wild type TU8988T cells exposed to 4-MU during media conditioning. GFAT1 knockout cells in (D) were propagated in GlcNAc to maintain viability (n=3 for all cell lines and conditions). **(F)** HABP staining of normal murine pancreas (negative control) and a murine pancreatic tumor (positive control). **(G)** Representative images for HABP staining classification used in H. **(H)** 10 representative slides from wildtype [65] and GFAT1 knockout subcutaneous and orthotopic tumors (Figure 1F,G) were stained and blindly scored using the classification metric in G (n=10). Error bars represent mean ± SD. *P < 0.05; ** P <0.01; *** P <0.001; **** P <0.0001.

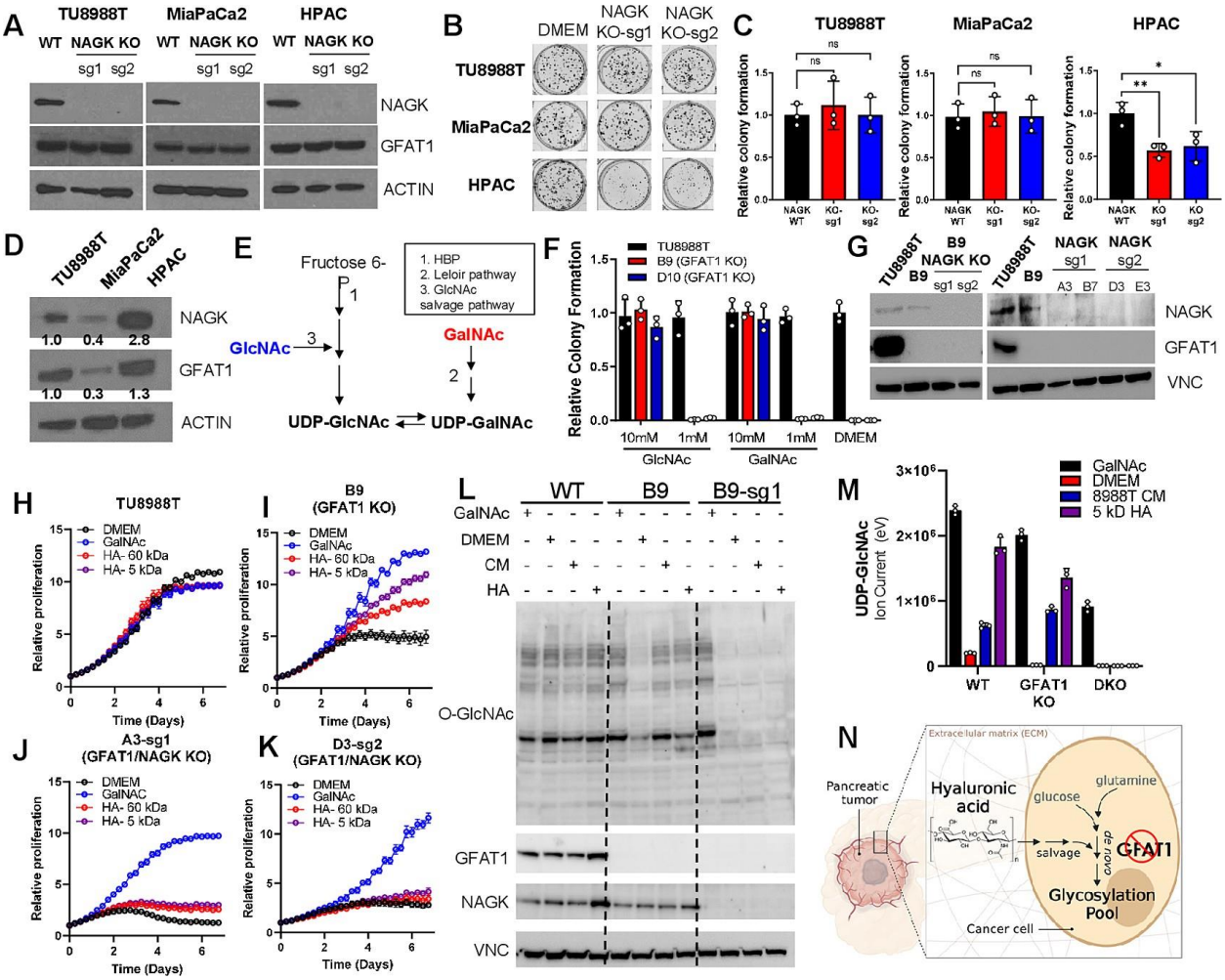


**Figure 2-9 Hyaluronic acid-derived GlcNAc rescues GFAT1 loss via the GlcNAc salvage pathway.**

(**A**) Western blot of NAGK, GFAT1, and ACTIN loading control from TU8988T, MiaPaCa2, and HPAC parental (wild type, WT) and NAGK knockout (KO) populations. NAGK was knocked out using two independent sgRNAs (sg1, sg2). (**B**) Representative wells from a colony forming assay for parental and NAGK knockout lines. (**C**) Quantitation of colony forming assay data in **B** (n=3). (**D**) Western blot for NAGK, GFAT1, and loading control ACTIN in parental PDA cell lines. Band density was quantitated, normalized to control, and presented below the blot. (**E**) Schematic overview of the Leloir pathway of galactose catabolism integrated with the HBP and GlcNAc salvage pathway. (**F**) Quantitated data from colony formation assays in parental and GFAT1 knockout clonal TU8988T cell lines in base media (DMEM), positive control GlcNAc, and N-acetyl-galactosamine (GalNAc) (n=3) (**G**) Western blot for GFAT1, NAGK, and loading control VINCULIN (VNC) in parental TU8988T and HPAC, GFAT1 knockout clones, and GFAT/NAGK double targeted lines. (**H-K**) Proliferation time course of (**H,I**) parental TU8988T and GFAT1 knockout line B9 in base media, GalNAc positive control, 60 kDa HA, or 5 kDa HA; (**J,K**) GFAT1/NAGK double targeted clones in base media, GalNAc positive control, 60 kDa HA, or 5 kDa HA (n=3). (**L**) Western blot for proteome O-GlcNAcylation (O-GlcNAc), GFAT1, NAGK, and VCN in parental [65], GFAT1 knockout (B9) and GFAT1/NAGK double knockout (B9-sg1) TU8988T cells treated with 10mM GalNAc, DMEM, CM or o-HA. (**M**) LC-MS/MS analysis of UDP-GlcNAc from the samples in **L** (n=3). (**N**) Schematic overview of the HA metabolism through the GlcNAc salvage pathway to fuel glycosylation in GFAT1 knockout PDA. Error bars represent mean ± SD. n.s., non-significant; *$P < 0.05$; ** $P < 0.01$.

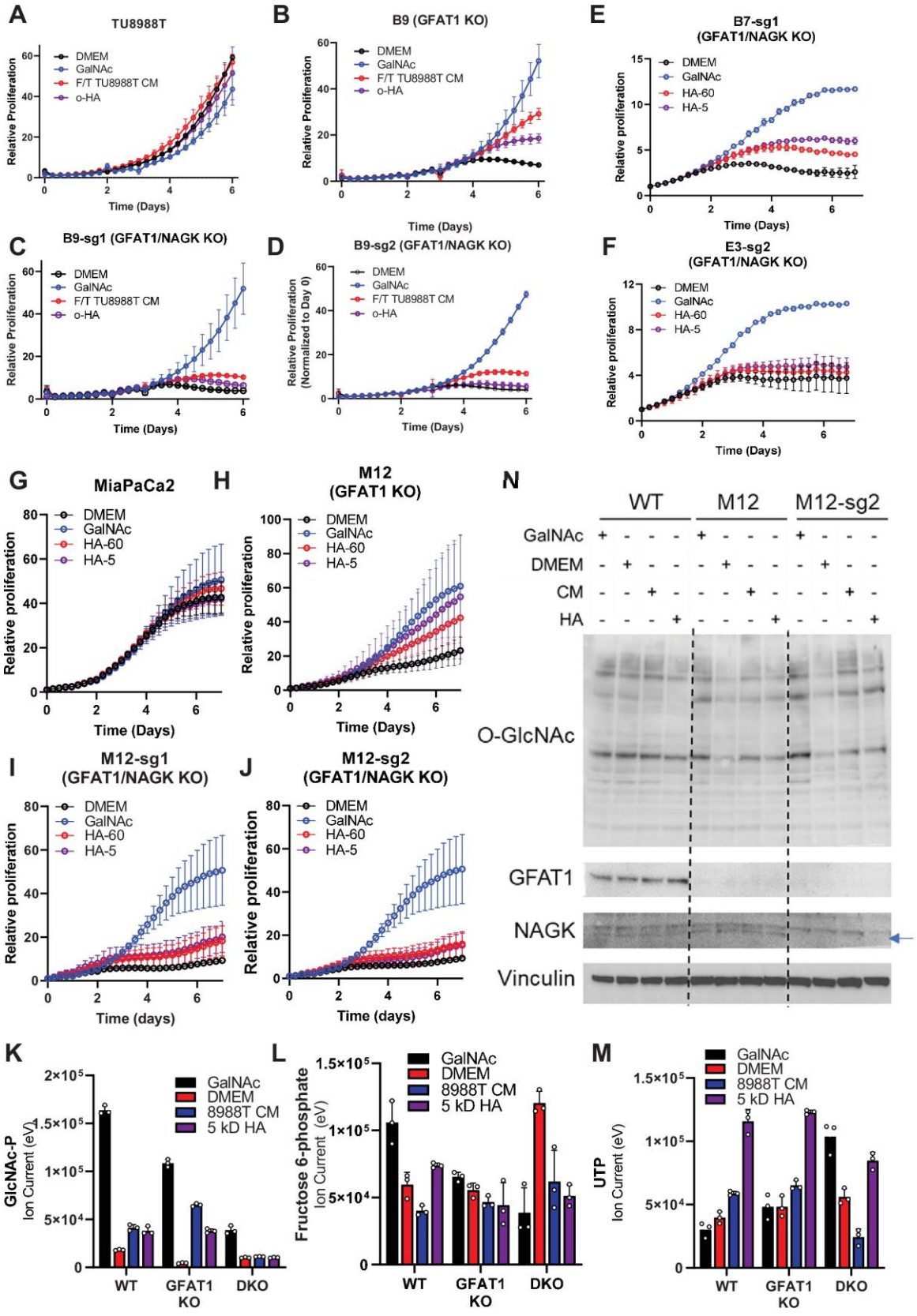


**Figure 2-10 Additional characterization of HA rescue in GFAT1/NAGK double knockout cell lines.**

(**A-D**) Proliferation time course of (**A**) parental TU8988T, (**B**) GFAT1 knockout cells, and (**C,D**) two GFAT1/NAGK double knockout cell lines in base media (DMEM), positive control (GlcNAc), 5 kDa HA (o-HA), or wild type TU8988T conditioned media (CM) subject to freeze thaw (F/T) (n=3). (**E,F**) Proliferation time course of two additional GFAT1/NAGK double knockout cells lines from main text **Figure 5H-K** in base media (DMEM), positive control (GalNAc), 5 kDa HA (o-HA), or 60kDa HA (n=3). [66] Proliferation time course of (**G**) wildtype MiaPaCa2, (**H**) GFAT1 knockout line M12, and (**I,J**) GFAT1/NAGK double knockout cells in base media, GalNAc positive control, 60 kDa HA, or 5 kDa o-HA (n=3). (**K-M**) LC-MS/MS analysis of (**K**) GlcNAc-phosphate (GlcNAc-P), (**L**) fructose 6-phosphate, and (**M**) uridine triphosphate from the samples in **Fig. 2-5L** (n=3). (**N**) Western blot for proteome O-GlcNAcylation (O-GlcNAc), GFAT1, NAGK, and VCN in parental [65], GFAT1 knockout (M12) and GFAT1/NAGK double knockout MiaPaCa2 cells treated with 10mM GalNAc, DMEM, CM or o-HA. The NAGK band appears below a non-specific band, as indicated by the blue arrow. Error bars represent mean ± SD.

# Chapter 3

## Inhibition of the Hexosamine Biosynthesis Pathway May Sensitize Pancreatic Cancer to Anti-PD-(L)1 Therapy

This project originates from the underlying theme of defining the role of the hexosamine biosynthesis pathway in pancreatic cancer. This project focuses more on leveraging that information to potentially improve a type of immunotherapy that targets the anti-PD1/PD-L1 axis. While the project is still ongoing, the background, results, and the discussion listed below will serve as future resources for the Lyssiotis lab.

### 3.1 INTRODUCTION

Immune checkpoint blockade targeting the axis of programmed death protein 1 (PD1) and programmed death-ligand 1 (PD-L1) is famous for the Nobel prize in 2018 and is a specific mechanism cancer cells utilize for immune evasion. PD1 is commonly found on the surface of T cells and is a critical regulator of downregulating immune response and maintaining self-tolerance. PD-L1 is overexpressed on the surface of cancer cells, and upon binding to PD1, leads to inhibition of T cell proliferation, cytokine production, and cytolytic activity[67].

Reactivation of T cell immunity by targeting the PD1/PD-L1 axis has revolutionized cancer treatment in the clinic. FDA has approved antibodies targeting PD1 (pembrolizumab and nivolumab) or PD-L1 (durvalumab, avelumab, and atezolizumab) as second or even first-line

treatment against melanoma, non-small-cell lung cancer, renal cell carcinoma, head and neck squamous cell carcinoma, and Hodgkin lymphma[68-70].

Despite the early success of anti-PD1/PD-L1 therapy in various cancer types, the majority of pancreatic cancer patients are resistant to this monotherapy. A multicenter, phase I trial of an anti-PD-L1 antibody showed that no objective response was observed in the fourteen pancreatic cancer patients[71]. Similarly, another phase I trial testing anti-PD-L1 therapy included one pancreatic cancer patient who did not respond[72]. Several factors contribute to this lack of clinical success including the immunosuppressive tumor microenvironment and the immune-desert phenotype of most patients.

To overcome this challenge, numerous pre-clinical and clinical studies evaluated combining anti-PD(L)1 therapy with various systemic and locoregional therapies[73]. Such strategies involve combination therapy with chemotherapy, radiotherapy, molecularly targeted therapy, and immunotherapy. A significant challenge of combination therapies is whether adverse effects exceed clinical limits. One study that combined pembrolizumab with gemcitabine and nab-paclitaxel resulted in 70.6% of patients experiencing grade 3 or 4 treatment emergent adverse events[74]. Another study that employed a similar therapeutic strategy, but with nivolumab instead of pembrolizumab, observed that 36% of patients discontinued treatment due to treatment emergent adverse events[75]. Adverse event occurrences varied amongst studies and were closely associated with drug dosage[73]. The necessary optimization to address this problem will require comprehensive evaluations before, during and after treatments, which represent huge cost and logistical challenges.

A different strategy from combination therapy involves sensitizing pancreatic cancer to anti-PD(L)1 therapy. A 2020 study demonstrated that targeting the intrinsic hexosamine biosynthetic pathway (HBP) with the glutamine analog 6-diazo-5-oxo-L-norleucine (DON) sensitized pancreatic cancer to anti-PD1 antibody in mice[48]. Furthermore, the group observed

significant remodeling of the extracellular matrix due to a decrease in hyaluronic acid and collagen, as well as increased infiltration of cytotoxic T cells. Whether all these effects were specific to inhibition of the HBP is unclear since DON is a glutamine analog and therefore has pleiotropic effects. Genetic ablation of glutamine-fructose 6-phosphate amidotransferase 1 (GFAT1), the first and rate-limiting enzyme of HBP, in several syngeneic cell lines can test whether specific HBP inhibition can sensitize pancreatic cancer to anti-PD1 therapy *in vivo*.

There are recent studies that suggest that inhibiting HBP may sensitize pancreatic cancer to anti-PD-L1 therapy. HBP is the only *de novo* pathway to produce uridine diphosphate N-acetylglucosamine (UDP-GlcNAc), a crucial precursor for glycosylation, an essential post translational modification. Glycosylation affects the structure of the protein as well as its interaction with other molecules. Thus, glycosylation regulates protein biosynthesis, localization, and function[76]. PD-L1, which is overexpressed in pancreatic cancer cells, is heavily glycosylated. Glycosylation is critical for stabilizing PD-L1, which suppresses T cell activity[66]. A type of glycosylation called N-linked glycosylation of PD-L1 accounts for approximately 50% of its molecular weight[77]. Therefore, the glycosylation could impede binding of PD-L1 with anti-PD-L1 antibody by rendering the polypeptide antigens inaccessible. Indeed, a study demonstrated that using enzyme digestion to de-glycosylate patient samples significantly increased binding affinity, resulting in a more accurate immunohistochemical PD-L1 readout and prediction of clinical outcome[78].

Taken together, we hypothesize that specifically inhibiting the HBP can sensitize pancreatic cancer to anti-PD(L)1 therapy. We generated and validated several GFAT1 knockout CRISPR clones in two syngeneic murine cell lines, MT3 and M7940. GFAT1 was required for survival *in vitro*. Subcutaneous injection of various CRISPR clones into syngeneic mouse models showed that GFAT1 ablation had antitumor effects. However, a few mice still formed

tumors. Future experiments and the respective analysis of both expected and potential, unexpected results will be addressed in the discussion section.

## 3.2 RESULTS

### 3.2.1 Pancreatic cancer cells require de novo HBP fidelity in vitro

Previously, we demonstrated that in a murine model of pancreatic cancer, mutant Kras transcriptionally activates *Gfpt1*, which encodes for glutamine-fructose 6-phosphate amidotransferase 1 (GFAT1), the rate-limiting enzyme for HBP[6]. In another study, we showed that pancreatic cancer proliferation relies on glutamine anaplerosis[29]. Since GFAT1 is a glutamine-utilizing, rate-limiting enzyme of a highly conserved metabolic pathway, we investigated the role of GFAT1 in human pancreatic cancer cells, and found that GFAT1 was required *in vitro* but not *in vivo*[79].

Here, we employed the same CRISPR/Cas9 strategy with GlcNAc supplementation to generate GFAT1 KO cells in two murine pancreatic cancer cell lines, KPC M7940b and MT3-2D (referred hereafter as M7940 and MT3, respectively). GlcNAc, which can bypass GFAT1 via the GlcNAc salvage pathway, was supplemented during selection of pooled polyclonal population to minimize metabolic rewiring.

We generated three bona fide MT3 GFAT1 KO clones and two M7940 GFAT1 KO clones via immunoblotting and Sanger sequencing (**Fig 3-1A**). Generation of these clones was important for two reasons. First, we were interested to test whether hyaluronic acid, a GlcNAc-containing glycosaminoglycan that is found in abundance in the tumor microenvironment, could fuel murine pancreatic cancer cell growth as it did human pancreatic cancer cells[79]. Second, and more importantly, testing whether GFAT1 ablation synergizes with anti-PD(L)1 therapy required murine pancreatic cancer cell lines that will not be rejected by mice upon implantation.

We found that GFAT1 was required for survival *in vitro* for both cell lines (**Fig. 3-1B**). The complete abolishment of colony formation in GFAT1 KO cell lines was identical to that of human GFAT1 KO cell lines[79].

**A**

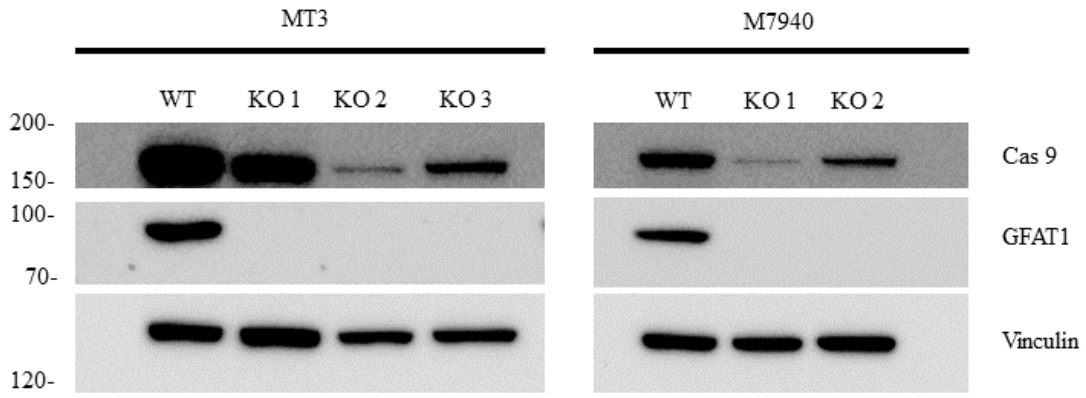


**B**

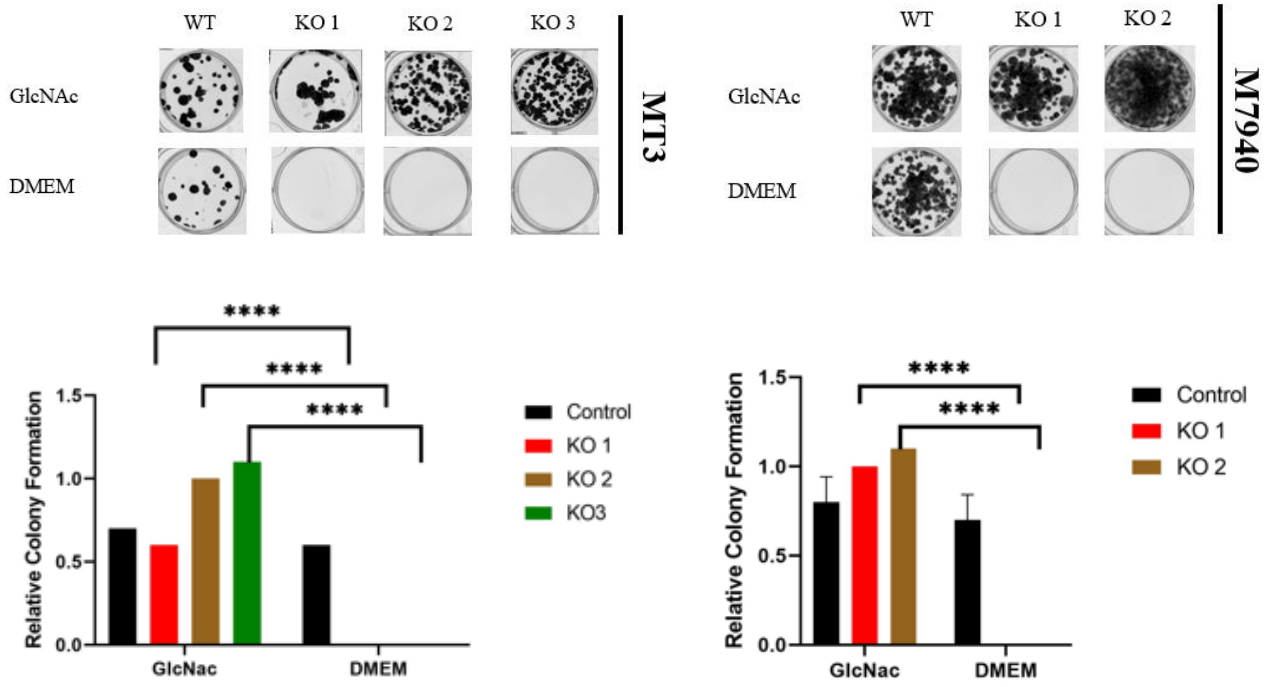


**Figure 3-1 Pancreatic ductal adenocarcinoma requires de novo hexosamine biosynthetic pathway fidelity in vitro.**

**(A)** Western blot of GFAT1, Cas9, and the loading control Vinculin from validated CRISPR/Cas9 knockout MT3 and M7940 clones and their control.

**(B)** Representative wells from a colony formation assay in parentally and clonally derived GFAT1 knockout cell lines grown in base media (DMEM) or base media supplemented with 10mM GlcNAc (GlcNAc). Quantified data on the bottom (n=5 for MT3; n=4 for M7940.

### 3.2.2 Pancreatic cancer cells appear to require de novo HBP fidelity in vivo

We moved the GFAT1 knockout clones into the flanks of immunocompetent mice to test whether the all-or-nothing phenotype *in vitro* was recapitulated *in vivo*. All three MT3 GFAT1 knockout clones failed to form tumors (**Fig. 3-2A**). One out of two M7940 GFAT1 knockout clones formed tumors, but were significantly smaller in terms of weight and volume relative to the wildtype counterparts (**Fig. 3-2B**). The other M7940 clone failed to form any palpable tumors.

**A**

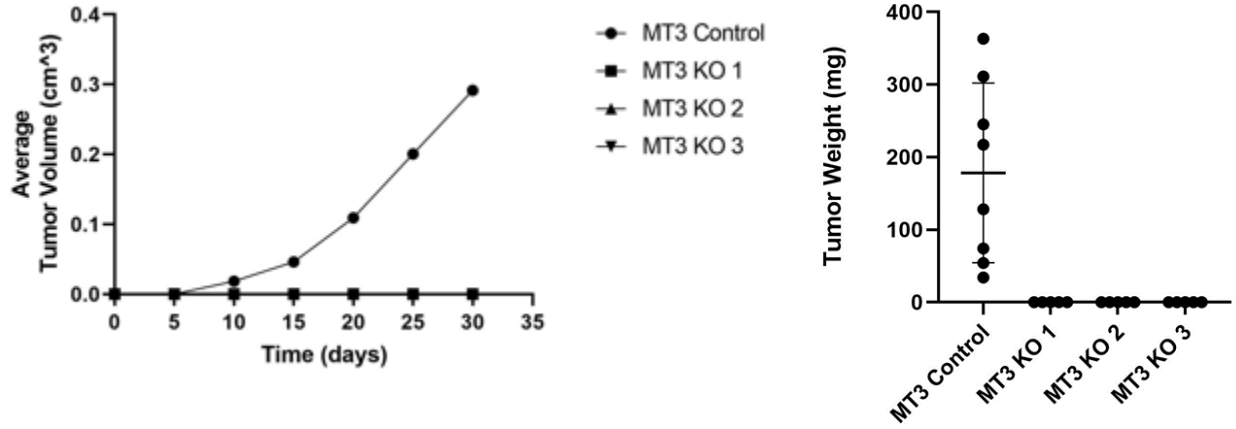


**B**

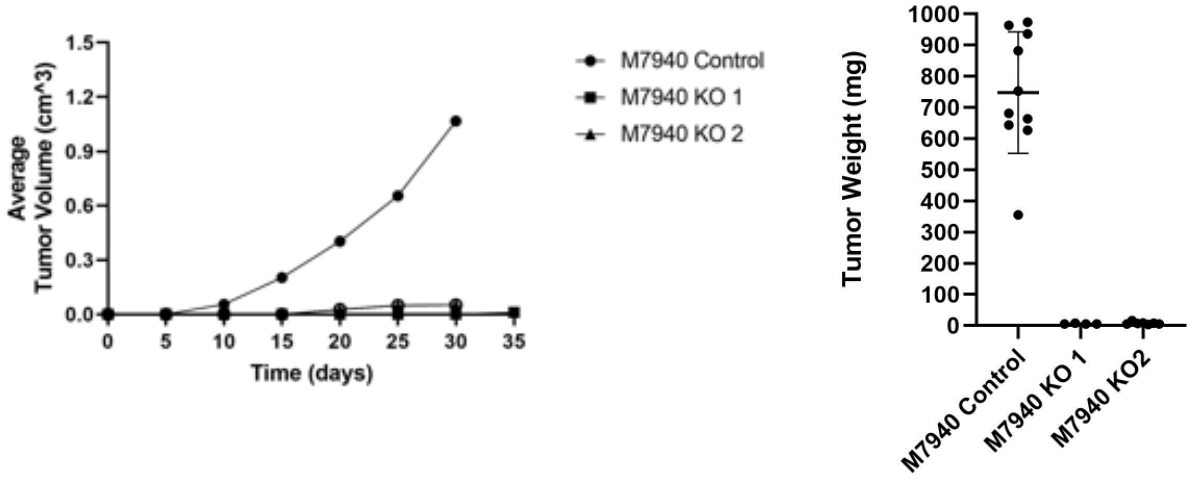

**Figure 3-2 Pancreatic cancer cells appear to require de novo hexosamine biosynthetic pathway fidelity in vivo.**

**(A)** Average tumor volume and weight for parental MT3 (n=8) and GFAT1 KO (n=0 for MT3 KO1-3) grown subcutaneously in immunocompetent mice.
**(B)** Average tumor volume and weight for parental M7940 (n=10) and GFAT1 KO (n=0 for M7940 KO1; n=4 for M7940 KO2) grown subcutaneously in immunocompetent mice.

## 3.3 DISCUSSION

In PDA, the HBP is transcriptionally regulated in a Kras-dependent manner[6]. Furthermore, HBP is elevated in various cancers and regulates proliferation, survival, metastasis, and angiogenesis[10]. This points to GFAT1, the rate-limiting enzyme of the HBP, as a potential therapeutic target. Previous attempts to suppress GFAT1 activity with pan glutamine-deamidase inhibitors demonstrated anti-tumor activity in vitro and in vivo[47,48]. It was particularly striking that DON, a pan glutamine-deamidase inhibitor, sensitized pancreatic cancer to anti-PD1 therapy, given that checkpoint blockade immunotherapy has been largely unsuccessful in pancreatic cancer[48]. Because DON is not specific to the HBP, we took a genetic approach to knock out GFAT1 to test whether HBP inhibition alone was sufficient to sensitize PDA to checkpoint blockade immunotherapy.

We found that knocking out GFAT1 in two murine cancer cell lines led to a complete ablation of colony formation unless supplemented with GlcNAc (**Fig 3-1B**). This was consistent with what we observed previously in human PDA cell lines[79]. However, upon subcutaneous injection, only one out of the five murine GFAT1 null clones, M7940 KO2, formed tumors, while the other four failed to establish any palpable tumors (**Fig 3-2**). It should also be noted that M7940 KO2 did not form tumors in all mice. This was in stark contrast to the human GFAT1 null clones, which readily formed tumors in a subcutaneous model. The most significant difference between the two experiments is the presence of an intact immune system. Elucidating this difference not only deviates from the original hypothesis, but it also would be biologically and statistically insignificant with such few tumors originating from a single GFAT1 null clone.

Instead, we suggest the following experiments to directly test the original hypothesis of whether specific GFAT1 inhibition can sensitize pancreatic cancer cells to anti-PD1 therapy. First, we would test whether conditioned media from the cancer cells, cancer associated fibroblasts (CAFs), or direct supplementation of hyaluronic acid can rescue survival in vitro via colony formation assay. We predict that there will be rescue to a varying degree, similar to what we previously observed with human GFAT1 null clones. The rescue would point to the importance of the extracellular matrix, the majority of which is hyaluronic acid in PDA, and factors and metabolites released by cancer cells and CAFs.

Second, we would perform orthotopic, co-transplantation of the control or GFAT1 null cells with CAFs into immunocompetent mice. The co-transplantation with CAFs would depend on whether rescue was achieved in vitro with CAF conditioned media and/or via a transwell co-culture system. If we observe a lack of tumor establishment in the majority of our clones as we did in the subcutaneous model, then we would have to switch to a dox-inducible system to knock down GFAT1 *in vitro* and *in vivo*. We would have to wait for tumors to establish and then treat with doxycycline to test the effect of GFAT1 inhibition on ECM remodeling, $CD8^+$ T cells infiltration, and sensitization to anti-PD1 therapy. This would also indicate that GFAT1 plays an important role in tumor establishment in immunocompetent models, which could be the foundation for a different project.

On the other hand, if we were to observe tumor formation in GFAT1 null clones, we would test via immunohistochemistry for GFAT1, cleaved caspase 3, Ki67, and HABP to ensure GFAT1 was knocked out at end point, and to check for cell death, proliferation, and hyaluronic acid level, respectively. It would be interesting to test whether the size of the tumors correlates with hyaluronic acid level, as this would be another evidence that implicates hyaluronic acid as a fuel for cancer cells in vivo[79]. More importantly, HABP level and Sirius red staining to observe collagen in these tumors would directly test whether GFAT1 inhibition in cancer cells was

sufficient to regulate extracellular matrix remodeling, which was observed upon DON treatment[48].

The next step would be to compare the immune landscape of the control with GFAT1 null tumors. This could be achieved via flow cytometry or immunohistochemistry. Specifically, we will check for myeloid cells, $CD68^+$ macrophages, and $CD8^+$ T cells. Myeloid cell depletion has been shown to induce tumor cell death and enhance infiltration of $CD8^+$ T cells into tumors[80]. DON treatment led to increased infiltration of $CD68^+$ macrophages, which can secrete tumoricidal cytokines such as TNFα and IL-12[48]. Finally, $CD8^+$ T cells are the direct mediators of tumor cell killing via PD1/PD-L1 pathway. If GFAT1 inhibition is sufficient to sensitize cancer cells to anti-PD1 therapy, we predict we would observe decreased immunosuppressive myeloid cells, increased $CD68^+$ macrophages, and most importantly, increased CD8+ T cells.

The experiments listed above are what we propose to be the most direct, quickest way to test our hypothesis. Assuming that the experiments above yield results that support our hypothesis, the final, most important experiment is to test in vivo whether inhibition of tumor-intrinsic HBP can sensitize cancer cells to anti-PD1 therapy in our orthotopic, co-transplantation model. The experiment would comprise of an isotype control and anti-PD1 arms in parental cells or GFAT1 null clones. We would measure the final volume, weight, and survival and perform tumor studies listed above to check for extracellular matrix remodeling and changes in immune landscape. If our hypothesis is true, then we would observe a moderate anti-tumor effect in GFAT1 null clones + isotype control arm, and a significant anti-tumor effect in GFAT1 null clones + anti-PD1 arm compared to parental cells + isotype control arm.

We will now address the second part of our original hypothesis, namely that GFAT1 inhibition can sensitize pancreatic cancer cells to anti-PD-L1 therapy. PD-L1 is overexpressed in cancer cells and binds to PD1 to evade immunosurveillance. PD-L1 is heavily N-glycosylated, a type of post translational modification that is regulated by the HBP. The glycan moiety plays a

critical role in binding to PD1 and is also responsible for disrupting the antibody recognition of PD-L1. As such, removal of N-glycosylation via enzymatic digestions enhanced anti-PD-L1 antibody binding affinity, resulting in a more accurate PD-L1 quantification and clinical outcome prediction[78]. Therefore, we hypothesize that specifically targeting GFAT1 will lead to a de-glycosylated state of PD-L1, sensitizing PDA cells to anti-PD-L1 therapy.

The first step would be to check for PD-L1 expression in parental cells and GFAT1 null clones via immunoblotting, and validate glycosylated and de-glycosylated forms of PD-L1. Glycosylated proteins often yield heterogenous pattern on western blots. For example, in breast cancer cells, the predominant form of PD-L1 was found around 45kDa as a giant band (glycosylated), but a faint band (de-glycosylated) was found around 33kDa[66]. We predict a similar pattern in our parental cancer cells. Using shRNA against PD-L1 to test which band expressions are decreased and then reconstituting PD-L1 to rescue expression would reveal which bands correspond to PD-L1. To validate that the top band is indeed the glycosylated form and the bottom band is the de-glycosylated form, we would treat parental cells with peptide-*N*-glycosidase (PNGaseF) to remove the entire N-glycan structure. This would result in the bottom band being the predominant form instead of the top band. These experiments would validate the anti-PD-L1 antibody, and identify which bands correspond to glycosylated and de-glycosylated PD-L1. We predict that in parental cell lines, the predominant band would be the top band (glycosylated), and in GFAT1 null clones, it would be the bottom band (de-glycosylated).

To determine whether the N-glycan moieties hinder anti-PD-L1 antibody detection at the cell surface, we would perform immunofluorescence confocal microscopy analysis to detect PD-L1 in parental cells and GFAT1 null clones. The negative and positive controls would be parental cells without and with PNGaseF treatment, respectively. If the N-glycan moieties do interfere with anti-PD-L1 antibody binding, then the non-treated parental cells, which predominantly have the glycosylated form, would have the weakest PD-L1 signal. This signal

would increase upon PNGaseF treatment, which removes PD-L1 of its N-glycan moieties. We predict that our GFAT1 null clones would have PD-L1 signal that is comparable to that of PNGaseF-treated parental cells. Confirmation of these results would indicate that inhibiting the HBP sensitizes anti-PD-L1 binding in vitro.

The final step would be to test in vivo whether GFAT1 inhibition sensitizes pancreatic cancer cells to anti-PD-L1 therapy. The experimental design and the follow-up tumor analysis would be similar to the anti-PD1 study mentioned above, except now the antibody would be against PD-L1. The biological significance of potential extracellular matrix remodeling and infiltration of $CD8^+$ T cells would apply here as well. If our hypothesis is correct, we would expect the GFAT1 null clones + anti-PD-L1 arm to have significantly lower tumor weight, volume, and higher survival than GFAT1 null clones + isotype control arm.

In conclusion, the experiments and the expected results stated above represent the most direct, time-efficient strategy to test whether inhibition of tumor-intrinsic HBP could sensitize PDA cells to anti-PD(L)1 therapy.

## 3.4 MATERIALS AND METHODS

*Cell Culture*

Murine PDA cell lines KPC 7940b and MT3-2D were provided by Drs. G. Beatty and D. Tuveson, respectively, under a material transfer agreement. The cell lines were STR-validated and were routinely tested for mycoplasma with MycoAlert (Lonza, LT07-318). Cells were maintained in high glucose DMEM without pyruvate (Gibco, 11965092) supplemented with 10% fetal bovine serum (Corning, 35-010-CV) at 37°C and 5% $CO_2$. GFAT1 null PDA were cultured in standard media supplemented with 10mM GlcNAc (Sigma, A8625).

*Generation of CRISPR/Cas9 Knockout Clones*

The expression vector pspCas9(BB)-2A-Puro (PX459; Addgene Plasmid 48139) was used to generate the GFAT1 CRISPR-Cas9 constructs. Murine GFAT1 sgRNA sequences were inserted into the plasmid cut with the restriction enzyme BbsI, as previously described[81]. The sequences were obtained from the Genome-Scale Crispr Knock-Out (GeCKO) library. The resulting CRISPR/Cas9 plasmid was transformed into chemically competent stbl3 cells, mini-prepped for plasmid DNA, and sequence-verified. Murine PDA cells were transiently transfected using Lipofectamine 3000 according to manufacturer's instructions, and were selected with puromycin in the presence of GlcNAc (GFAT1 KO bulk population). Polyclonal pools were seeded into 96-well plates at a density of one cell per well to select for individual clones. The clones were expanded and verified via Western blot and Sanger sequencing.

*Colony formation assay*

500 cells per well were plated in a six-well plate in biological triplicates. After 9-12 days, the colonies were fixed with 100% methanol for ten minutes, and stained with 0.5% crystal violet solution for fifteen minutes. The dye was removed with 10% acetic acid, and OD595 was measured to calculate relative cell viability.

*Western blot analysis*

Cell lysates were collected with radioimmunoprecipiataion assay buffer (Sigma-Aldrich, R0278) supplemented with phosphatase and protease inhibitors. Lysis and lysates collection were performed on ice. After a 10-minute incubation on ice, lysates were centrifuged at 4°C for 10 minutes at 18,000*g* to extract the sample supernatant. Protein concentrations were measured with Pierce BCA Protein Assay Kit (ThermoFisher, 23227) according to the manufacturer's instructions.

After SDS-PAGE, proteins were transferred to methanol-activated PVDF membrane, incubated with a blocking buffer (Bio-Rad, 1706404) in TBS-T solution (Bio-Rad, 1706435) with 0.1% Tween-20 (Sigma-Aldrich, 9005-64-5) at room temperature for 1 hour, and incubated with primary antibody overnight at 4°C. The following day, membranes were washed with TBS-T solution 3 times for 5 minutes each, and incubated with the appropriate HRP-conjugated secondary antibody for 1 hour at room temperature. Membranes were incubated with chemiluminescence reagent (Clarity Max Western ECL substrate, 705062) according to the manufacturer's instructions. Blot images were obtained with a Bio-Rad ChemiDoc Imaging System (Image Lab Touch Software version 2.4.0.003).

*Antibodies*

The following antibodies were used in this study: VINCULIN (Cell Signaling, 13901), GFAT1 (Abcam, 125609), anti-CRISPR/Cas9 (Abcam, 191468), secondary anti-mouse-HRP (Cell Signaling, 7076), and secondary anti-rabbit-HRP (Cell Signaling, 7074).

*Mouse tumor studies*

Animal studies were conducted in accordance with the Office of Laboratory Animal Welfare and approved by the Institutional Animal Care and Use Committee of the University of Michigan. Male and female 6- to 10-week-old C57BL/6J mice were obtained from The Jackson Laboratory and maintained in the facilities of the Unit for Laboratory Animal Medicine under specific pathogen-free conditions (Protocol #: PRO00008877).

Prior to the subcutaneous injection, control MT3 and M7940 cells and five verified GFAT1 null clones were collected from culture plates according to standard cell culture procedures. Cells were counted, washed once with PBS, and resuspended in 1:1 solution of serum-free DMEM (Gibco, 11965-092) and Matrigel (Corning, 354234). The injection was

performed at ~1 x $10^6$ cells in 200µL final volume. Tumor size was measured with a digital caliper 2-3 times per week. Tumor volume was calculated as V = 1/2 (length x $width^2$). At endpoint, final tumor volume and mass were measured prior to processing.

*Statistical Analysis*

Statistics were performed using GraphPad Prism 8 (GraphPad Software Inc.). Data from experimental groups were compared using the two-tailed *t*-test or analysis of variance (ANOVA). All error bars represent mean with standard deviation. Statistical significance was accepted if $P < 0.05$.

## References


1 Siegel, R. L., Miller, K. D. & Jemal, A. Cancer statistics, 2020. *CA: A Cancer Journal for Clinicians* **70**, 7-30, doi:10.3322/caac.21590 (2020).

2 Halbrook, C. J. & Lyssiotis, C. A. Employing Metabolism to Improve the Diagnosis and Treatment of Pancreatic Cancer. *Cancer Cell* **31**, 5-19, doi:10.1016/j.ccell.2016.12.006 (2017).

3 Perera, R. M. & Bardeesy, N. Pancreatic Cancer Metabolism: Breaking It Down to Build It Back Up. *Cancer Discov* **5**, 1247-1261, doi:10.1158/2159-8290.CD-15-0671 (2015).

4 Ying, H. *et al.* Genetics and biology of pancreatic ductal adenocarcinoma. *Genes Dev* **30**, 355-385, doi:10.1101/gad.275776.115 (2016).

5 Kerk, S. A., Papagiannakopoulos, T., Shah, Y. M. & Lyssiotis, C. A. Metabolic networks in mutant KRAS-driven tumours: tissue specificities and the microenvironment. *Nat Rev Cancer* **21**, 510-525, doi:10.1038/s41568-021-00375-9 (2021).

6 Ying, H. *et al.* Oncogenic Kras maintains pancreatic tumors through regulation of anabolic glucose metabolism. *Cell* **149**, 656-670, doi:10.1016/j.cell.2012.01.058 (2012).

7 Akella, N. M., Ciraku, L. & Reginato, M. J. Fueling the fire: emerging role of the hexosamine biosynthetic pathway in cancer. *BMC Biol* **17**, 52-52, doi:10.1186/s12915-019-0671-3 (2019).

8 Wellen, K. E. *et al.* The hexosamine biosynthetic pathway couples growth factor-induced glutamine uptake to glucose metabolism. *Genes Dev* **24**, 2784-2799, doi:10.1101/gad.1985910 (2010).

9 Paszek, M. J. *et al.* The cancer glycocalyx mechanically primes integrin-mediated growth and survival. *Nature* **511**, 319-325, doi:10.1038/nature13535 (2014).

10 Akella, N. M., Ciraku, L. & Reginato, M. J. Fueling the fire: emerging role of the hexosamine biosynthetic pathway in cancer. *BMC Biol* **17**, 52, doi:10.1186/s12915-019-0671-3 (2019).

11 Walter, L. A. *et al.* Inhibiting the Hexosamine Biosynthetic Pathway Lowers O-GlcNAcylation Levels and Sensitizes Cancer to Environmental Stress. *Biochemistry*, doi:10.1021/acs.biochem.9b00560 (2019).

12 Yang, C. *et al.* High expression of GFAT1 predicts poor prognosis in patients with pancreatic cancer. *Sci Rep* **6**, 39044, doi:10.1038/srep39044 (2016).

13 Lee, H. H. *et al.* Removal of N-Linked Glycosylation Enhances PD-L1 Detection and Predicts Anti-PD-1/PD-L1 Therapeutic Efficacy. *Cancer Cell* **36**, 168-178 e164, doi:10.1016/j.ccell.2019.06.008 (2019).

14 Commisso, C. *et al.* Macropinocytosis of protein is an amino acid supply route in Ras-transformed cells. *Nature* **497**, 633-637, doi:10.1038/nature12138 (2013).

15 Kamphorst, J. J. *et al.* Human pancreatic cancer tumors are nutrient poor and tumor cells actively scavenge extracellular protein. *Cancer Res* **75**, 544-553, doi:10.1158/0008-5472.Can-14-2211 (2015).

16 Yang, S. *et al.* Pancreatic cancers require autophagy for tumor growth. *Genes Dev* **25**, 717-729, doi:10.1101/gad.2016111 (2011).

17 Davidson, S. M. *et al.* Direct evidence for cancer-cell-autonomous extracellular protein catabolism in pancreatic tumors. *Nat Med* **23**, 235-241, doi:10.1038/nm.4256 (2017).

18 Olivares, O. *et al.* Collagen-derived proline promotes pancreatic ductal adenocarcinoma cell survival under nutrient limited conditions. *Nat Commun* **8**, 16031, doi:10.1038/ncomms16031 (2017).

19 Sousa, C. M. *et al.* Pancreatic stellate cells support tumour metabolism through autophagic alanine secretion. *Nature* **536**, 479-483, doi:10.1038/nature19084 (2016).

20 Dalin, S. *et al.* Deoxycytidine Release from Pancreatic Stellate Cells Promotes Gemcitabine Resistance. *Cancer Res* **79**, 5723-5733, doi:10.1158/0008-5472.Can-19-0960 (2019).
21 Halbrook, C. J. *et al.* Macrophage-Released Pyrimidines Inhibit Gemcitabine Therapy in Pancreatic Cancer. *Cell Metab* **29**, 1390-1399 e1396, doi:10.1016/j.cmet.2019.02.001 (2019).
22 Zhu, Z. *et al.* Tumour-reprogrammed stromal BCAT1 fuels branched-chain ketoacid dependency in stromal-rich PDAC tumours. *Nat Metab*, doi:10.1038/s42255-020-0226-5 (2020).
23 Lyssiotis, C. A. & Kimmelman, A. C. Metabolic Interactions in the Tumor Microenvironment. *Trends Cell Biol* **27**, 863-875, doi:10.1016/j.tcb.2017.06.003 (2017).
24 Theocharis, A. D., Tsara, M. E., Papageorgacopoulou, N., Karavias, D. D. & Theocharis, D. A. Pancreatic carcinoma is characterized by elevated content of hyaluronan and chondroitin sulfate with altered disaccharide composition. *Biochim Biophys Acta* **1502**, 201-206, doi:10.1016/s0925-4439(00)00051-x (2000).
25 Goossens, P. *et al.* Membrane Cholesterol Efflux Drives Tumor-Associated Macrophage Reprogramming and Tumor Progression. *Cell Metab* **29**, 1376-1389.e1374, doi:10.1016/j.cmet.2019.02.016 (2019).
26 Mahlbacher, V., Sewing, A., Elsässer, H. P. & Kern, H. F. Hyaluronan is a secretory product of human pancreatic adenocarcinoma cells. *Eur J Cell Biol* **58**, 28-34 (1992).
27 Jacobetz, M. A. *et al.* Hyaluronan impairs vascular function and drug delivery in a mouse model of pancreatic cancer. *Gut* **62**, 112, doi:10.1136/gutjnl-2012-302529 (2013).
28 Provenzano, P. P. *et al.* Enzymatic targeting of the stroma ablates physical barriers to treatment of pancreatic ductal adenocarcinoma. *Cancer cell* **21**, 418-429, doi:10.1016/j.ccr.2012.01.007 (2012).
29 Son, J. *et al.* Glutamine supports pancreatic cancer growth through a KRAS-regulated metabolic pathway. *Nature* **496**, 101-105, doi:10.1038/nature12040 (2013).
30 Zhang, Y., Crawford, H. C. & Pasca di Magliano, M. Epithelial-Stromal Interactions in Pancreatic Cancer. *Annual review of physiology* **81**, 211-233, doi:10.1146/annurev-physiol-020518-114515 (2019).
31 Neesse, A. *et al.* Stromal biology and therapy in pancreatic cancer: ready for clinical translation? *Gut* **68**, 159-171, doi:10.1136/gutjnl-2018-316451 (2019).
32 Moussian, B. The role of GlcNAc in formation and function of extracellular matrices. *Comp Biochem Physiol B Biochem Mol Biol* **149**, 215-226, doi:10.1016/j.cbpb.2007.10.009 (2008).
33 Bond, M. R. & Hanover, J. A. A little sugar goes a long way: the cell biology of O-GlcNAc. *J Cell Biol* **208**, 869-880, doi:10.1083/jcb.201501101 (2015).
34 Kim, S. M. *et al.* PTEN Deficiency and AMPK Activation Promote Nutrient Scavenging and Anabolism in Prostate Cancer Cells. *Cancer Discov* **8**, 866-883, doi:10.1158/2159-8290.CD-17-1215 (2018).
35 Monslow, J., Govindaraju, P. & Puré, E. Hyaluronan - a functional and structural sweet spot in the tissue microenvironment. *Front Immunol* **6**, 231, doi:10.3389/fimmu.2015.00231 (2015).
36 Schmaus, A. *et al.* Accumulation of small hyaluronan oligosaccharides in tumour interstitial fluid correlates with lymphatic invasion and lymph node metastasis. *Br J Cancer* **111**, 559-567, doi:10.1038/bjc.2014.332 (2014).
37 Lv, H. *et al.* Elevate level of glycosaminoglycans and altered sulfation pattern of chondroitin sulfate are associated with differentiation status and histological type of human primary hepatic carcinoma. *Oncology* **72**, 347-356, doi:10.1159/000113145 (2007).

38 Greyner, H. J., Wiraszka, T., Zhang, L. S., Petroll, W. M. & Mummert, M. E. Inducible macropinocytosis of hyaluronan in B16-F10 melanoma cells. *Matrix Biol* **29**, 503-510, doi:10.1016/j.matbio.2010.06.004 (2010).
39 Sullivan, W. J. *et al.* Extracellular Matrix Remodeling Regulates Glucose Metabolism through TXNIP Destabilization. *Cell* **175**, 117-132 e121, doi:10.1016/j.cell.2018.08.017 (2018).
40 Nagy, N. *et al.* 4-methylumbelliferone treatment and hyaluronan inhibition as a therapeutic strategy in inflammation, autoimmunity, and cancer. *Front Immunol* **6**, 123, doi:10.3389/fimmu.2015.00123 (2015).
41 Provenzano, P. P. *et al.* Enzymatic targeting of the stroma ablates physical barriers to treatment of pancreatic ductal adenocarcinoma. *Cancer Cell* **21**, 418-429, doi:10.1016/j.ccr.2012.01.007 (2012).
42 Termini, J. M. *et al.* HEK293T cell lines defective for O-linked glycosylation. *PLoS One* **12**, e0179949, doi:10.1371/journal.pone.0179949 (2017).
43 Guillaumond, F. *et al.* Strengthened glycolysis under hypoxia supports tumor symbiosis and hexosamine biosynthesis in pancreatic adenocarcinoma. *Proc Natl Acad Sci U S A* **110**, 3919-3924, doi:10.1073/pnas.1219555110 (2013).
44 Lucena, M. C. *et al.* Epithelial Mesenchymal Transition Induces Aberrant Glycosylation through Hexosamine Biosynthetic Pathway Activation. *J Biol Chem* **291**, 12917-12929, doi:10.1074/jbc.M116.729236 (2016).
45 Kim, J. *et al.* The hexosamine biosynthesis pathway is a targetable liability in KRAS/LKB1 mutant lung cancer. *Nat Metab* **2**, 1401-1412, doi:10.1038/s42255-020-00316-0 (2020).
46 Zhang, W. *et al.* GFPT2-Expressing Cancer-Associated Fibroblasts Mediate Metabolic Reprogramming in Human Lung Adenocarcinoma. *Cancer Res* **78**, 3445-3457, doi:10.1158/0008-5472.CAN-17-2928 (2018).
47 Leone, R. D. *et al.* Glutamine blockade induces divergent metabolic programs to overcome tumor immune evasion. *Science* **366**, 1013-1021, doi:10.1126/science.aav2588 (2019).
48 Sharma, N. S. *et al.* Targeting tumor-intrinsic hexosamine biosynthesis sensitizes pancreatic cancer to anti-PD1 therapy. *J Clin Invest* **130**, 451-465, doi:10.1172/jci127515 (2020).
49 Toole, B. P. Hyaluronan: from extracellular glue to pericellular cue. *Nat Rev Cancer* **4**, 528-539, doi:10.1038/nrc1391 (2004).
50 Misra, S., Hascall, V. C., Markwald, R. R. & Ghatak, S. Interactions between Hyaluronan and Its Receptors (CD44, RHAMM) Regulate the Activities of Inflammation and Cancer. *Front Immunol* **6**, 201, doi:10.3389/fimmu.2015.00201 (2015).
51 Vigetti, D., Viola, M., Karousou, E., De Luca, G. & Passi, A. Metabolic control of hyaluronan synthases. *Matrix Biol* **35**, 8-13, doi:10.1016/j.matbio.2013.10.002 (2014).
52 Campbell, S. *et al.* Glutamine deprivation triggers NAGK-dependent hexosamine salvage. *Elife* **10**, doi:10.7554/eLife.62644 (2021).
53 Jayashankar, V. & Edinger, A. L. Macropinocytosis confers resistance to therapies targeting cancer anabolism. *Nature Communications* **11**, 1121, doi:10.1038/s41467-020-14928-3 (2020).
54 DuFort, C. C., DelGiorno, K. E. & Hingorani, S. R. Mounting Pressure in the Microenvironment: Fluids, Solids, and Cells in Pancreatic Ductal Adenocarcinoma. *Gastroenterology* **150**, 1545-1557 e1542, doi:10.1053/j.gastro.2016.03.040 (2016).
55 DuFort, C. C. *et al.* Interstitial Pressure in Pancreatic Ductal Adenocarcinoma Is Dominated by a Gel-Fluid Phase. *Biophys J* **110**, 2106-2119, doi:10.1016/j.bpj.2016.03.040 (2016).

56 Jacobetz, M. A. *et al.* Hyaluronan impairs vascular function and drug delivery in a mouse model of pancreatic cancer. *Gut* **62**, 112-120, doi:10.1136/gutjnl-2012-302529 (2013).
57 Olive, K. P. *et al.* Inhibition of Hedgehog signaling enhances delivery of chemotherapy in a mouse model of pancreatic cancer. *Science* **324**, 1457-1461, doi:10.1126/science.1171362 (2009).
58 Van Cutsem, E. *et al.* Randomized Phase III Trial of Pegvorhyaluronidase Alfa With Nab-Paclitaxel Plus Gemcitabine for Patients With Hyaluronan-High Metastatic Pancreatic Adenocarcinoma. *J Clin Oncol*, JCO2000590, doi:10.1200/JCO.20.00590 (2020).
59 Helms, E., Onate, M. K. & Sherman, M. H. Fibroblast Heterogeneity in the Pancreatic Tumor Microenvironment. *Cancer Discov* **10**, 648-656, doi:10.1158/2159-8290.CD-19-1353 (2020).
60 Lee, J. J. *et al.* Stromal response to Hedgehog signaling restrains pancreatic cancer progression. *Proc Natl Acad Sci U S A* **111**, E3091-3100, doi:10.1073/pnas.1411679111 (2014).
61 Özdemir, B. C. *et al.* Depletion of Carcinoma-Associated Fibroblasts and Fibrosis Induces Immunosuppression and Accelerates Pancreas Cancer with Reduced Survival. *Cancer Cell* **28**, 831-833, doi:10.1016/j.ccell.2015.11.002 (2015).
62 Rhim, A. D. *et al.* Stromal elements act to restrain, rather than support, pancreatic ductal adenocarcinoma. *Cancer Cell* **25**, 735-747, doi:10.1016/j.ccr.2014.04.021 (2014).
63 Hwang, R. F. *et al.* Cancer-associated stromal fibroblasts promote pancreatic tumor progression. *Cancer research* **68**, 918-926, doi:10.1158/0008-5472.CAN-07-5714 (2008).
64 Commisso, C., Flinn, R. J. & Bar-Sagi, D. Determining the macropinocytic index of cells through a quantitative image-based assay. *Nature Protocols* **9**, 182-192, doi:10.1038/nprot.2014.004 (2014).
65 Kothapalli, D. *et al.* Hyaluronan and CD44 antagonize mitogen-dependent cyclin D1 expression in mesenchymal cells. *J Cell Biol* **176**, 535-544, doi:10.1083/jcb.200611058 (2007).
66 Li, C.-W. *et al.* Glycosylation and stabilization of programmed death ligand-1 suppresses T-cell activity. *Nature Communications* **7**, 12632, doi:10.1038/ncomms12632 (2016).
67 Freeman, G. J. *et al.* Engagement of the PD-1 immunoinhibitory receptor by a novel B7 family member leads to negative regulation of lymphocyte activation. *J Exp Med* **192**, 1027-1034, doi:10.1084/jem.192.7.1027 (2000).
68 Chen, L. & Han, X. Anti-PD-1/PD-L1 therapy of human cancer: past, present, and future. *J Clin Invest* **125**, 3384-3391, doi:10.1172/jci80011 (2015).
69 Sharma, P. & Allison, J. P. Immune checkpoint targeting in cancer therapy: toward combination strategies with curative potential. *Cell* **161**, 205-214, doi:10.1016/j.cell.2015.03.030 (2015).
70 Topalian, S. L., Taube, J. M., Anders, R. A. & Pardoll, D. M. Mechanism-driven biomarkers to guide immune checkpoint blockade in cancer therapy. *Nat Rev Cancer* **16**, 275-287, doi:10.1038/nrc.2016.36 (2016).
71 Brahmer, J. R. *et al.* Safety and activity of anti-PD-L1 antibody in patients with advanced cancer. *N Engl J Med* **366**, 2455-2465, doi:10.1056/NEJMoa1200694 (2012).
72 Herbst, R. S. *et al.* Predictive correlates of response to the anti-PD-L1 antibody MPDL3280A in cancer patients. *Nature* **515**, 563-567, doi:10.1038/nature14011 (2014).
73 Liu, L. *et al.* Combination therapy for pancreatic cancer: anti-PD-(L)1-based strategy. *Journal of Experimental & Clinical Cancer Research* **41**, 56, doi:10.1186/s13046-022-02273-w (2022).
74 Weiss, G. J. *et al.* Phase Ib/II study of gemcitabine, nab-paclitaxel, and pembrolizumab in metastatic pancreatic adenocarcinoma. *Invest New Drugs* **36**, 96-102, doi:10.1007/s10637-017-0525-1 (2018).

75 Wainberg, Z. A. *et al.* Open-label, Phase I Study of Nivolumab Combined with nab-Paclitaxel Plus Gemcitabine in Advanced Pancreatic Cancer. *Clin Cancer Res* **26**, 4814-4822, doi:10.1158/1078-0432.Ccr-20-0099 (2020).
76 Jayaprakash, N. G. & Surolia, A. Role of glycosylation in nucleating protein folding and stability. *Biochem J* **474**, 2333-2347, doi:10.1042/bcj20170111 (2017).
77 Li, C. W. *et al.* Eradication of Triple-Negative Breast Cancer Cells by Targeting Glycosylated PD-L1. *Cancer Cell* **33**, 187-201.e110, doi:10.1016/j.ccell.2018.01.009 (2018).
78 Lee, H. H. *et al.* Removal of N-Linked Glycosylation Enhances PD-L1 Detection and Predicts Anti-PD-1/PD-L1 Therapeutic Efficacy. *Cancer Cell* **36**, 168-178.e164, doi:10.1016/j.ccell.2019.06.008 (2019).
79 Kim, P. K. *et al.* Hyaluronic acid fuels pancreatic cancer cell growth. *eLife* **10**, e62645, doi:10.7554/eLife.62645 (2021).
80 Zhang, Y. *et al.* Myeloid cells are required for PD-1/PD-L1 checkpoint activation and the establishment of an immunosuppressive environment in pancreatic cancer. *Gut* **66**, 124-136, doi:10.1136/gutjnl-2016-312078 (2017).
81 Ran, F. A. *et al.* Genome engineering using the CRISPR-Cas9 system. *Nat Protoc* **8**, 2281-2308, doi:10.1038/nprot.2013.143 (2013).

# Chapter 4

# Conclusion and Future Directions

## 4.1 Conclusion

Our works contribute to the growing field of elucidating the role of the hexosamine biosynthetic pathway in pancreatic cancer and the complex role of the tumor microenvironment as a nutrient source that supports pancreatic cancer metabolism. Below, we highlight the key findings of each chapter and their relevance. Finally, we discuss future directions that can further the field and potentially point to novel strategies against pancreatic cancer.

## 4.2 Identification of hyaluronic acid as a novel source of fuel for pancreatic cancer cells

In Chapter 2, our work builds on our previous work and other findings that implicate the HBP as a potential metabolic vulnerability in pancreatic cancer[1-4]. We employed CRIPSR-Cas9 to specifically target GFAT1, and observed that HBP fidelity was required in vitro but not in vivo in both subcutaneous and orthotopic models. This led us to hypothesize that the tumor microenvironment was providing the means to bypass GFAT1.

To address the scavenging hypothesis, we subjected GFAT1 null clones to denatured conditioned media from CAFs and wild type PDA cells and observed a rescue in viability. This led us to look for a molecule(s) without tertiary structure, such as metabolite(s). Because GlcNAc is a known metabolite that can bypass GFAT1 via the GlcNAc salvage pathway, we hypothesized that hyaluronic acid (HA), a GlcNAc-containing glycosaminoglycan that is found in abundance in the tumor microenvironment, could act as a nutrient that can refill the HBP. Specifically, we demonstrated that the very low molecular weight version of hyaluronic acid, or

oligo-HA (o-HA) refills the HBP via NAGK, the enzyme that mediates the GlcNAc salvage pathway.

Our work reveals a novel role of HA as a nutrient source that fuels pancreatic cancer metabolism beyond its previously known structural and signaling roles[5,6]. Our work contributes to the growing body of works that have identified various components of the tumor microenvironment as nutrient sources that regulate cancer metabolism[7-11].

HA is clinically relevant for several reasons. Due to its highly hydrophilic nature, HA retains water to create the supraphysiological intratumoral pressure that leads to vasculature collapse. This limits nutrient, oxygen, and drug delivery[12]. Indeed, previous studies demonstrated that treating PDA with hyaluronidase to break down HA increased vascularization and improved drug delivery to the tumor[13,14]. However, a phase III clinical trial that combined pegylated hyaluronidase with nab-paclitaxel plus gemcitabine showed no improvement in overall patient survival[15].

Our work offers a potential explanation for the discrepancy between the clinical response to pegylated hyaluronidase and the preclinical data. Other studies point to both the pro- and anti-tumor effects of HA. For example, HA matrix itself may be necessary to restrain tumor, similar to what was observed in the CAF depletion studies[16]. On the other hand, HA degradation led to extracellular matrix remodeling that resulted in increased cytotoxic T cells infiltration. Our work shows that HA degradation may support pancreatic cancer metabolism. Elucidating the seemingly conflicting, context-dependent nature of HA is critical to determine the optimal way to exploit this unique feature of pancreatic tumor.

### 4.3 Exploring the HBP as a target to sensitize pancreatic cancer to anti-PD(L)1 therapy

In chapter 3, we performed preliminary experiments to address our hypothesis that inhibition of cell-intrinsic hexosamine biosynthetic pathway can sensitize pancreatic cancer to

anti-PD(L)1 therapy. This is based on a previous finding utilizing DON, a glutamine analog that targets glutamine-utilizing enzymes such as GFAT1, which led to anti-PD1 therapy sensitization in mice[17]. Another group found that PD-L1 is highly *N*-glycosylated, and removing the glycosylation moieties through enzymatic digestion improved binding to anti-PD-L1 antibody[18]. Because the hexosamine biosynthesis pathway is the only de novo pathway for generating UDP-GlcNAc, a crucial precursor for *N*-glycosylation, we hypothesized that targeting GFAT1 could be another way to de-glycosylate PD-L1 to improve its binding to anti-PD-L1.

Although the project is still in its early stage, we have described future experiments in detail to test the hypothesis in the most direct, time-efficient manner in Chapter 3. If our hypothesis is supported, we will have demonstrated a novel strategy to turn pancreatic tumor, which is notoriously "cold" and insensitive immune checkpoint blockade, to "hot," immunologically sensitive tumor.

### 4.4 Future directions

Our work and a recent finding from another group implicate NAGK, the enzyme that mediates the GlcNAc salvage pathway, as a potential therapeutic target[19,20]. Glutamine limitation in pancreatic cancer suppressed de novo HBP but increased GlcNAc availability for salvage. *NAGK* expression was elevated in human tumors, and NAGK deficiency significantly blunted GlcNAc salvage in cells and tumor growth in a xenograft, subcutaneous mouse model[20]. Based on these findings, it is possible that pancreatic cancer cells rely on NAGK since they are rapidly dividing and reside in the nutrient-limiting, tumor microenvironment. Furthermore, while GFAT1 is required for embryonic development in mice, NAGK knockout mice are viable, which suggests a wider therapeutic window.

To test whether NAGK is a potential therapeutic target, we would knock out NAGK in syngeneic murine cells, and perform subcutaneous and/or orthotopic implantations in mice.

Concurrently, we would perform colony formation assay and proliferation assay between the parental cells and NAGK knockout clones in a glutamine-limiting condition to test the importance of NAGK. These experiments would serve as proof-of-concept regarding NAGK as a potential therapeutic target. If true, we expect to observe significant reduction in survival, proliferation, and tumor growth.

We can further mechanistically delineate how very low molecular weight or oligo-HA (o-HA) fuels the HBP by targeting the HA receptors, CD44 and RHAMM[21]. Knocking down either or both of these genes in GFAT1 null clones, and then testing whether HA or WT PDA CM can still rescue could answer as well as pose several interesting questions. If the rescue is significantly decreased, then we know the HA intake by PDA cells is likely via receptor-mediated endocytosis[22]. Considering that receptor-mediated endocytosis of HA is mostly associated with high molecular weight HA and not o-HA, this could reveal an affinity for o-HA that was previously unknown or underappreciated[23].

Although our work in Chapter 2 mainly focused on HA, there are other members of the glycosaminoglycans apart from HA that contain GlcNAc and GalNAc, namely heparan sulfate (HS) and chondroitin sulfate (CS), respectively[24]. We could measure the HS and CS level in the CM, exogenously supplement them to GFAT1 null clones to observe if any rescue occurs, and measure their expression in our tumor studies to determine whether HS and CS can act as novel nutrient sources in our system.

Based on current literature, o-HA could potentially be degraded into its glucuronic acid and GlcNAc building blocks in the lysosomes via β-D-glucuronidase and β-N-acetyl-D-hexosaminidase[25]. This implicates an unknown lysosomal GlcNAc transporter or another process through which GlcNAc released in the lysosome is available to fuel the HBP, which occurs in the cytoplasm. To address this, we would conduct a positive CRISPR screen. The selective pressure would be the exogenous o-HA supplementation to GFAT1 null clones that

are grown without GlcNAc. It would be important to first establish the right concentration of o-HA that would result in only a small population of cells surviving. The negative control would be GFAT1 null clones grown without GlcNAc. The surviving cells would be collected, their plasmids PCR-amplified and sequenced using next-generation sequencing to identify their cDNA or target gene. This screen would be the first step to identifying a potential lysosomal GlcNAc transporter or another mechanism for HA fueling the HBP. If HS or CS can rescue GFAT1 null clones, the same screening strategy could be used as a starting point to elucidate the mechanism.

Another future direction could test whether macrophage could provide the means to refuel the HBP to rescue GFAT1 null cells. Macrophages are major cell populations found in the tumor microenvironment, and they provide potential metabolic support to fuel PDA metabolism[10]. To study the potential crosstalk between macrophages and PDA cells, we would generate the following subtypes of macrophages: tumor-educated macrophages (TEMs), a classically activate phenotype (M1), and alternatively activated phenotype (M2). We would culture murine bone-marrow-derived macrophages in PDA CM, treat them with lipopolysaccharide or interleukin 4 to generate TEM, M1, and M2, respectively. CM from TEM, M1, and M2 would be tested to see if they can rescue GFAT1 null cells. If any rescue is observed, we could freeze-thaw or boil the CM to test whether the rescue is mediated by metabolites. If so, we already have the metabolic profiling of these different CM obtained via liquid chromatography-coupled tandem mass spectrometry metabolomics[10]. Along with the CM experiments, we could co-culture murine macrophage cells RAW264.7 with WT or GFAT1 null cells to test if any rescue occurs. These experiments could reveal novel ways through which macrophages regulate HBP in cancer cells.

## References


1 Ying, H. *et al.* Oncogenic Kras maintains pancreatic tumors through regulation of anabolic glucose metabolism. *Cell* **149**, 656-670, doi:10.1016/j.cell.2012.01.058 (2012).

2 Guillaumond, F. *et al.* Strengthened glycolysis under hypoxia supports tumor symbiosis and hexosamine biosynthesis in pancreatic adenocarcinoma. *Proc Natl Acad Sci U S A* **110**, 3919-3924, doi:10.1073/pnas.1219555110 (2013).

3 Lucena, M. C. *et al.* Epithelial Mesenchymal Transition Induces Aberrant Glycosylation through Hexosamine Biosynthetic Pathway Activation. *J Biol Chem* **291**, 12917-12929, doi:10.1074/jbc.M116.729236 (2016).

4 Walter, L. A. *et al.* Inhibiting the Hexosamine Biosynthetic Pathway Lowers O-GlcNAcylation Levels and Sensitizes Cancer to Environmental Stress. *Biochemistry* **59**, 3169-3179, doi:10.1021/acs.biochem.9b00560 (2020).

5 Toole, B. P. Hyaluronan: from extracellular glue to pericellular cue. *Nat Rev Cancer* **4**, 528-539, doi:10.1038/nrc1391 (2004).

6 Vigetti, D., Viola, M., Karousou, E., De Luca, G. & Passi, A. Metabolic control of hyaluronan synthases. *Matrix Biol* **35**, 8-13, doi:10.1016/j.matbio.2013.10.002 (2014).

7 Commisso, C. *et al.* Macropinocytosis of protein is an amino acid supply route in Ras-transformed cells. *Nature* **497**, 633-637, doi:10.1038/nature12138 (2013).

8 Kamphorst, J. J. *et al.* Human pancreatic cancer tumors are nutrient poor and tumor cells actively scavenge extracellular protein. *Cancer Res* **75**, 544-553, doi:10.1158/0008-5472.Can-14-2211 (2015).

9 Davidson, S. M. *et al.* Direct evidence for cancer-cell-autonomous extracellular protein catabolism in pancreatic tumors. *Nat Med* **23**, 235-241, doi:10.1038/nm.4256 (2017).

10 Halbrook, C. J. *et al.* Macrophage-Released Pyrimidines Inhibit Gemcitabine Therapy in Pancreatic Cancer. *Cell Metab* **29**, 1390-1399.e1396, doi:10.1016/j.cmet.2019.02.001 (2019).

11 Zhu, Z. *et al.* Tumour-reprogrammed stromal BCAT1 fuels branched-chain ketoacid dependency in stromal-rich PDAC tumours. *Nat Metab* **2**, 775-792, doi:10.1038/s42255-020-0226-5 (2020).

12 Olive, K. P. *et al.* Inhibition of Hedgehog signaling enhances delivery of chemotherapy in a mouse model of pancreatic cancer. *Science* **324**, 1457-1461, doi:10.1126/science.1171362 (2009).

13 Jacobetz, M. A. *et al.* Hyaluronan impairs vascular function and drug delivery in a mouse model of pancreatic cancer. *Gut* **62**, 112-120, doi:10.1136/gutjnl-2012-302529 (2013).

14 Provenzano, P. P. *et al.* Enzymatic targeting of the stroma ablates physical barriers to treatment of pancreatic ductal adenocarcinoma. *Cancer Cell* **21**, 418-429, doi:10.1016/j.ccr.2012.01.007 (2012).

15 Van Cutsem, E. *et al.* Randomized Phase III Trial of Pegvorhyaluronidase Alfa With Nab-Paclitaxel Plus Gemcitabine for Patients With Hyaluronan-High Metastatic Pancreatic Adenocarcinoma. *J Clin Oncol* **38**, 3185-3194, doi:10.1200/jco.20.00590 (2020).

16 Özdemir, B. C. *et al.* Depletion of Carcinoma-Associated Fibroblasts and Fibrosis Induces Immunosuppression and Accelerates Pancreas Cancer with Reduced Survival. *Cancer Cell* **28**, 831-833, doi:10.1016/j.ccell.2015.11.002 (2015).

17 Sharma, P. & Allison, J. P. Immune checkpoint targeting in cancer therapy: toward combination strategies with curative potential. *Cell* **161**, 205-214, doi:10.1016/j.cell.2015.03.030 (2015).

18 Lee, H. H. *et al.* Removal of N-Linked Glycosylation Enhances PD-L1 Detection and Predicts Anti-PD-1/PD-L1 Therapeutic Efficacy. *Cancer Cell* **36**, 168-178.e164, doi:10.1016/j.ccell.2019.06.008 (2019).
19 Kim, P. K. *et al.* Hyaluronic acid fuels pancreatic cancer cell growth. *eLife* **10**, e62645, doi:10.7554/eLife.62645 (2021).
20 Campbell, S. *et al.* Glutamine deprivation triggers NAGK-dependent hexosamine salvage. *eLife* **10**, e62644, doi:10.7554/eLife.62644 (2021).
21 Toole, B. P. Hyaluronan and its binding proteins, the hyaladherins. *Curr Opin Cell Biol* **2**, 839-844, doi:10.1016/0955-0674(90)90081-o (1990).
22 Qhattal, H. S. & Liu, X. Characterization of CD44-mediated cancer cell uptake and intracellular distribution of hyaluronan-grafted liposomes. *Mol Pharm* **8**, 1233-1246, doi:10.1021/mp2000428 (2011).
23 Michalczyk, M., Humeniuk, E., Adamczuk, G. & Korga-Plewko, A. Hyaluronic Acid as a Modern Approach in Anticancer Therapy-Review. *Int J Mol Sci* **24**, doi:10.3390/ijms24010103 (2022).
24 Khan, S. A., Mason, R. W., Kobayashi, H., Yamaguchi, S. & Tomatsu, S. Advances in glycosaminoglycan detection. *Mol Genet Metab* **130**, 101-109, doi:10.1016/j.ymgme.2020.03.004 (2020).
25 Ronny, R. & Mark, E. M. in *Molecular Regulation of Endocytosis* (ed Ceresa Brian) Ch. 14 (IntechOpen, 2012).